

Aus der Klinik für Radiologie
der Medizinischen Fakultät Charité – Universitätsmedizin Berlin

DISSERTATION

Evaluation of prostatic lesions by simultaneous
[⁶⁸Ga]Ga-PSMA-11 PET/MRI

Bewertung von prostatistischen Läsionen durch simultane
[⁶⁸Ga]Ga-PSMA-11 PET/MRT

zur Erlangung des akademischen Grades
Doctor of Philosophy (Ph.D.)

vorgelegt der Medizinischen Fakultät
Charité – Universitätsmedizin Berlin

von

Jing Zhao

aus Hubei, Volksrepublik China

Datum der Promotion: 30.11.2023

Table of contents

List of tables	v
List of figures	vi
List of abbreviations	vii
Abstract (English)	1
Zusammenfassung	3
1. Introduction	5
1.1 Male reproductive system introduction	5
1.2 Prostate gland	5
1.3 Common prostate conditions	6
1.4 Background of prostate cancer	7
1.4.1 Epidemiology of prostate cancer	7
1.4.2 Etiology and risk factors of prostate cancer	7
1.4.3 Symptoms of prostate cancer	8
1.5 Diagnosis of prostate cancer	9
1.5.1 Screening for prostate cancer	9
1.5.2 Diagnosing prostate cancer	9
1.5.3 Determining the aggressiveness of prostate cancer	11
1.5.4 Detecting the spread of prostate cancer	11
1.6 Aim of the research	13
2. Methods	14
2.1 Patients	14
2.2 Imaging acquisition protocol	14
2.3 Imaging analysis	15

2.3.1 LBR of SUVmax	15
2.3.2 Comparison between PI-RADS 2.0 and 2.1	16
2.3.3 Dynamic contrast-enhanced MRI	16
2.3.4 Radiomics analysis	17
2.4 Statistical analysis	17
2.4.1 LBR of SUVmax	17
2.4.2 Comparison between PI-RADS 2.0 and 2.1	17
2.4.3 Dynamic contrast-enhanced MRI	18
2.4.4 Radiomics analysis	18
3. Results	19
3.1 LBR of SUVmax	19
3.1.1 Patient cohort	19
3.1.2 Imaging analysis	19
3.2 Comparison between PI-RADS 2.0 and 2.1	19
3.2.1 Patient cohort	19
3.2.2 Imaging analysis	20
3.3 Dynamic contrast-enhanced MRI	21
3.3.1 Patient cohort	21
3.3.2 Imaging analysis	21
3.4 Radiomics analysis	24
3.4.1 Patient cohort	24
3.4.2 Imaging analysis	25
4. Discussion	27
4.1 Short summary of results	27

4.2 Interpretation of results	27
4.2.1 LBR of SUVmax	27
4.2.2 Comparison between PI-RADS 2.0 and 2.1	27
4.2.3 Dynamic contrast-enhanced MRI	28
4.2.4 Radiomics analysis	29
4.3 Embedding the results into the current state of research	30
4.4 Strengths and weaknesses of the study	32
4.5 Implications for practice and future research	33
5. Conclusion	33
Reference list	34
Statutory declaration	41
Declaration of own contribution to the publications	42
Publications	44
Excerpt from Journal Summary List--1	44
Zhao J, Hamm B, Brenner W, Makowski MR: Lesion-to-background ratio threshold value of SUVmax of simultaneous [⁶⁸ Ga]Ga-PSMA-11 PET/MRI imaging in patients with prostate cancer. Insights into Imaging 2020;11:137.	45
Excerpt from Journal Summary List--2	57
Zhao J, Mangarova DB, Brangsch J, Kader A, Hamm B, Brenner W, Makowski MR: Correlation between Intraprostatic PSMA Uptake and MRI PI-RADS of [⁶⁸ Ga]Ga-PSMA-11 PET/MRI in Patients with Prostate Cancer: Comparison of PI-RADS Version 2.0 and PI-RADS Version 2.1. CANCERS 2020;12:3523.	58
Excerpt from Journal Summary List--3	72
Zhao J, Kader A, Mangarova DB, Brangsch J, Brenner W, Hamm B, Makowski MR: Dynamic Contrast-Enhanced MRI of Prostate Lesions of Simultaneous [⁶⁸ Ga]Ga-PSMA-11 PET/MRI: Comparison between Intraprostatic Lesions and Correlation between Perfusion Parameters. CANCERS 2021;13:1404.	73

Curriculum Vitae	86
Publication list	87
Acknowledgement	89

List of tables

Table 1. MRI scanning parameters.....	15
Table 2. Benign and malignant lesions comparison.....	22
Table 3. Pearson correlation analysis.....	22

List of figures

Figure 1: ROC curve.	19
Figure 2: TZ with typical BPH nodules.	20
Figure 3: TZ with an atypical nodule.	21
Figure 4: TZ with a PI-RADS 1 change.	23
Figure 5: TZ with a PI-RADS 5 lesion.	24
Figure 6: Metastasis at right ischium.	25
Figure 7: Metastasis at right scapula.	26

List of abbreviations

ACR	American College of Radiology
ADC	Apparent diffusion coefficient
ADT	Androgen deprivation therapy
AT	Arrival time
AUC	Area under curve
BPH	Benign prostatic hyperplasia
CI	Confidence interval
CT	Computed tomography
DCE	Dynamic contrast-enhanced
DRE	Digital rectal examination
DWI	Diffusion-weighted imaging
EES	Extracellular and extravascular space
ESUR	European Society of Urogenital Radiology
FDG	Fluorodeoxyglucose
FOV	Field-of-view
Ga	Gallium
GS	Gleason score
iAUC	Initial area under curve
IQR	Interquartile range
LBM	Lean body mass
LBR	Lesion-to-background ratio
MDP	Methyl diphosphonate

MI	Molecular imaging
MRI	Magnetic resonance imaging
mpMRI	Multiparametric magnetic resonance imaging
OSEM	Ordered subset expectation-maximization
PCa	Prostate cancer
PEI	Peak enhancement intensity
PET/CT	Positron emission tomography / computed tomography
PET/MRI	Positron emission tomography / magnetic resonance imaging
PI-RADS	Prostate Imaging Reporting and Data System
PSA	Prostate-specific antigen
PSMA	Prostate-specific membrane antigen
PZ	Peripheral zone
ROC	Receiver operating characteristic
ROI	Region of interest
RP	Radical prostatectomy
SPECT	Single-photon emission computed tomography
SUV	Standardized uptake value
Tc	Technetium
TE	Echo time
TR	Repetition time
TRUS	Transrectal ultrasound
TTP	Time to peak
T2WI	T2-weighted imaging
TZ	Transitional zone

W-in Wash-in slope

W-out Wash-out slope

Abstract (English)

Prostate cancer (PCa) is a malignant disease that has a negative impact on the quality of life of older men. Due to its clinical features, which include difficult detection, spread, and recurrence, the need for more accurate and better imaging diagnostic grows. In recent years, there has been a great deal of researches into multi-modality imaging, ^{68}Ga prostate-specific membrane antigen (^{68}Ga]Ga-PSMA-11) positron emission tomography/ magnetic resonance imaging (PET/MRI). In terms of diagnostic accuracy, standard definition, and diagnostic stability, the existing ^{68}Ga]Ga-PSMA-11 PET/MRI requires significant improvement. The diagnosis of prostate lesions can be optimized.

The aim of this dissertation is to analyze imaging characteristics on ^{68}Ga]Ga-PSMA-11 PET/MRI, by evaluating and quantifying lesions of PCa.

This dissertation is based on four sub-projects. The research is based on retrospective study design. Multi-modality and molecular imaging techniques, ^{68}Ga]Ga-PSMA-11 PET/MRI were applied. Scanner 3.0 T PET/MRI system (SIEMENS MAGNETOM Biograph mMR, Erlangen, Germany) was used. First, I evaluated the compatibility, consistency and diagnostic threshold SUVmax of PET and MRI in ^{68}Ga]Ga-PSMA-11 PET/MRI. Thirty-two patients and 170 lesions were investigated in this sub-project. Second, a comparison of the diagnostic criteria of the new and old versions of Prostate Imaging Reporting and Data System (PI-RADS) was performed. Forty-six patients and 215 lesions were investigated in this sub-project. Third, the dynamic changes of dynamic contrast-enhanced (DCE)-MRI in the lesions were analyzed with quantitative analysis. Thirty-nine patients and 154 lesions were investigated in this sub-project. Fourth, radiomics analysis of PCa was studied. As it is an ongoing project, in this dissertation two cases are presented as examples.

I have obtained that when the lesion-to-background ratio (LBR) is 2.5, the coincidence of the two modalities (PET and MRI) is the highest. The new version of PI-RADS offers more detailed diagnostic criteria, allowing for greater diagnostic repeatability, and the kappa value was raised from 0.723 to 0.853. DCE parameters provide more information on lesions' characteristics. It showed that the malignant lesion had more abundant blood vessels, which made the time for the contrast agent to flow into the lesion shorter than that of the benign lesion. There is also a close relationship between perfusion parameters. Radiomics analysis was presented by two cases.

Diagnostic criteria improvement and lesion information refinement are beneficial in clarifying the nature of lesions, optimizing diagnostic methods, and reasonably evaluating treatment alternatives, consequently enhancing the accuracy and diagnostic efficiency of image-guided therapies.

Zusammenfassung

Prostatakrebs ist eine bösartige Tumorerkrankung, welche die Lebensqualität von älteren Männern mindert. Aufgrund seiner klinischen Merkmale, zu denen die schwierige Diagnose, die Ausbreitung und das Rezidivieren von PCa, wächst der Bedarf an genauerer und besserer bildgebender Diagnostik. In den letzten Jahren wurde im Bereich der multimodalen Bildgebung intensiv an der multimodalen Bildgebung, der ^{68}Ga -Positronenemissionstomographie/Magnetresonanztomographie (PET/MRT) mit prostataspezifischem Membranantigen (^{68}Ga]Ga-PSMA-11), geforscht. In Bezug auf die diagnostische Genauigkeit, die Standarddefinition und die diagnostische Stabilität muss das bestehende ^{68}Ga]Ga-PSMA-11 PET/MRT erheblich verbessert werden. Die Diagnose von Prostataläsionen kann optimiert werden.

Ziel dieser Dissertation ist die Analyse der Bildgebungseigenschaften von ^{68}Ga]Ga-PSMA-11 PET/MRT, indem PCa-Läsionen bewertet und quantifiziert werden.

Diese Dissertation umfasst vier Teilprojekte. Die Forschung basiert auf einem retrospektiven Studiendesign, wobei multimodale und molekulare Bildgebungsverfahren, ^{68}Ga]Ga-PSMA-11 PET/MRT, in einem 3.0 T PET/MRI-Scanner (SIEMENS MAGNETOM Biograph mMR, Erlangen, Deutschland) ausgewertet wurden. Zunächst wurde die Kompatibilität, Konsistenz und den diagnostischen Schwellenwert SUVmax von PET und MRT bei ^{68}Ga]Ga-PSMA-11 PET/MRT bewertet. 32 Patienten und 170 Läsionen wurden in diesem Teilprojekt untersucht. Außerdem wurde ein Vergleich der Diagnosekriterien zwischen der neuen und der alten Version des Prostate Imaging Reporting and Data System (PI-RADS) durchgeführt, wobei 46 Patienten und 215 Läsionen eingeschlossen wurden. Als Drittes wurden die dynamischen Veränderungen der dynamischen Kontrastverstärkung (DCE)-MRT in den Läsionen mit einer quantitativen Analyse untersucht. Hierbei wurden 39 Patienten und 154 Läsionen analysiert. Schließlich wurde im letzten Teilprojekt, die radiomische Analyse von PCa erforscht. Da es sich um ein laufendes Projekt handelt, werden in dieser Dissertation zwei Fallbeispiele vorgestellt.

Es wurde festgestellt, dass die Übereinstimmung der beiden Modalitäten, PET und MRT, am höchsten ist, wenn das Läsions-Hintergrund-Verhältnis (LBR) 2,5 beträgt. Die neue Version von PI-RADS bietet detailliertere Diagnosekriterien und ermöglicht eine höhere diagnostische Wiederholbarkeit von 0,723 bis 0,853 (kappa value). Die

DCE-Parameter liefern mehr Informationen über die Merkmale der Läsionen. Es zeigte sich, dass bösartige Läsionen über mehr Blutgefäße verfügen, wodurch die Zirkulationszeit des Kontrastmittels in die Läsion kürzer war als bei gutartigen Läsionen. Zudem zeigte sich ein enger Zusammenhang der Perfusionsparameter. Die radiomische Analyse wurde anhand von zwei Fällen vorgestellt.

Die Verbesserung der Diagnosekriterien und die Präzisierung der Informationen über die Läsion tragen dazu bei, die Art der Läsion zu erkennen, die Diagnosemethoden zu optimieren und die Behandlungsalternativen adäquat zu bewerten, wodurch die diagnostische Effizienz der bildgestützten Therapien erhöht werden.

1. Introduction

1.1 Male reproductive system introduction

All of the anatomical organs involved in sexual reproduction make up what is known as the reproductive system, which is a biological system. The reproductive system is composed of several non-living substances, including fluids, hormones, and pheromones, all of which are essential[1]. It is the collective name for the organs in the human reproductive system that create children and secrete sex hormones to maintain sex traits in humans.

The male reproductive system is comprised of internal and external genitalia. Internal genitalia include the reproductive glands, the ducts of seminal discharge, and the accessory glands. External genitalia include the scrotum and the penis.

1.2 Prostate gland

Prostate gland is the biggest accessory sexual gland found in pelvic cavity, situated between the bladder and the penis[2]. It is positioned anterior to the rectum. Urethra goes through from bladder to penis over the inner section of prostate, allowing urine to flow freely out of body. With the levator ani muscle inferolateral to the gland, prostate gland is positioned underneath the bladder neck and above the external urethral sphincter. An important anatomical feature is the location of the rectum ampulla behind the prostate, which is utilized in the digital rectal examination (DRE) for inspecting the prostate.

Typically, almost seventy percent of the prostate is glandular in nature, while the remainder consists of fibro-muscular tissue. A thin fibrous capsule surrounds the prostate gland. However, it is not a true capsule but rather resembles the thin connective tissue seen in big blood veins called the adventitia. Due to the fact that the urethra and ejaculatory ducts run through the prostate, the prostate has traditionally been classified into anatomical lobes.

As stated in McNeal et al., "The prostate gland contains three major glandular regions—the peripheral zone, the central zone, and the transition zone—which differ

histologically and biologically” ([3], p. 613). Central zone, which encompasses ejaculatory ducts, accounts for approximately one-quarter of the normal prostate volume[2]. Central glandular duct discharges at an angle into the prostatic urethra, preventing urine reflux. The transitional zone (TZ) is positioned in the urethra's central region, surrounds it, and accounts for about 5% to 10% of typical prostate volume. The peripheral zone (PZ) accounts for approximately 65% of the gland volume and is placed in the rear. The fibromuscular stroma is found anteriorly in the gland and merges with the tissue of the urogenital diaphragm."

1.3 Common prostate conditions

In clinical realm, common prostate conditions comprise prostatitis, enlarged prostate, and prostate cancer. Prostatitis is a disorder characterized by inflammation of the prostate gland[4]. Prostatitis can manifest at any age[5]. However, it usually occurs between thirty and fifty. Prostatitis is broadly categorized into two main types, as outlined in the review by Domingue and Hellstrom[6]: chronic prostatitis and acute prostatitis. Chronic prostatitis, the most prevalent form, is characterized by recurrent symptoms that last for months at a time. On the other hand, acute prostatitis is often caused by germs from the urethra infiltrating the prostate and causing inflammation. While it is generally rare, it can pose a serious threat if symptoms are severe and sudden. In such cases, prompt treatment is imperative.

The appearance of an enlarged prostate indicates that the gland has grown in size. In the majority of men, the prostate tends to increase in size as they age. It is common to hear the term benign prostatic hyperplasia (BPH) to refer to enlarging of prostate[7]. The exact cause of an enlarged prostate is still unknown. Changes in the cells of the testicles, as well as factors associated with age, may have an impact on both the development of the gland and the quantities of testosterone produced. BPH is the most prevalent senile alteration seen in prostate imaging. In the past, it has long been the focus of differential diagnosis between BPH and prostate cancer (PCa) foci.

PCa is epithelial cancer that originates in the prostate gland and spreads throughout the body, which is one of the most often diagnosed kinds of malignant diseases in males. Further information about PCa is provided below.

1.4 Background of prostate cancer

1.4.1 Epidemiology of prostate cancer

According to data from the Global Cancer Statistics 2020 encapsulated by Sung et al.[8], PCa will account for 7.3% of all cancers, including both male and female, in 2020, in terms of new cases registered worldwide. In terms of incidence, it is the 2nd most common male malignancy, accounting for 14.1 % of all malignancies, trailing only lung carcinoma (14.3%). According to the American Cancer Society, PCa is 3.8% of total cancer fatalities in both genders, ranking it eighth in overall mortality. It also accounts for 6.8% of all cancer deaths in males, ranking it fifth in overall mortality. This tendency is linked to the advancement of screening and diagnosis tools for PCa. PCa grows relatively slowly and may not show signs for decades. This has resulted in PCa being more frequent in older men.

1.4.2 Etiology and risk factors of prostate cancer

The tangible origin of PCa remains largely unknown. But several factors raise the exposure to this disease. These include age, ethnicity, family history, and obesity.

Advanced age is the primary risk factor for PCa. It is usually happened in men over 50-year-old and is the most prevalent in males over the age of 70. Life expectancy has grown as medical conditions and technology have improved. Additionally, usage of prostate-specific antigen (PSA) screening is growing, and more older men are detected with PCa. Scardino[9] observed that over one-third of men over the age of 50 die of causes other than PCa, and that histological evidence of PCa is discovered at necropsy.

PCa prevalence varies significantly between ethnic groupings. According to Wu et al.[10], this significant disparity is related to socioeconomic situations and biological characteristics. Some studies suggest that genetic susceptibility may be a factor in biological characteristics. A chromosomal 8q24 mutation has been related to a rising danger of PCa in African American males [11-14].

According to Gallagher et al.[15], around one-fifth of individuals with PCa have a family history, which may be explained by similar patterns of exposure to certain environmental carcinogens and shared lifestyle choices, among other variables. Genetic

factors are associated with an elevated risk of PCa, accounting for around 5% of the disease risk.

In the majority of obese men, the metabolism and circulation levels of sex steroid hormones, which are acknowledged to be prostate growth and cancer-related, have changed[16]. As a result, obesity is associated with metastatic and aggressive PCa[17,18]. Large body mass index (BMI) is also related to more aggressive diseases, as well as less favorable outcomes[19].

1.4.3 Symptoms of prostate cancer

In PCa's early stages, it does not exhibit clear symptoms and indications. Advanced PCa might present signs and symptoms. Basic invasion of normal prostate tissue and metastatic invasion of lymph nodes, soft tissues, and bone structures are the primary symptoms of PCa[20].

According to the Prostate Cancer 2020 guidelines, primary tumor invasion causes difficulty peeing, reduced urine stream power, blood in the urine or sperm, substantial weight loss, and erectile dysfunction[21]. Because of the increasing pressure exerted by the enlarged prostate gland on the urethra, patients may experience growing difficulty urinating, which is frequently the first symptom that they notice. When a tumor compresses the rectum, it can result in difficulty passing stools or intestinal obstruction; when a tumor compresses the vas deferens, it can result in an inability to ejaculate; and when a tumor compresses the nerves, it can result in pain in the perineum that can radiate to the sciatic nerve.

In addition to spreading to nearby organs such as the bladder, PCa metastases can spread to the osseous and other organs via the blood or lymphatic system. PCa that has migrated to the bones can cause bone pain and fractures[22]. It is possible that PCa will spread to the bladder, seminal vesicles, and vascular nerve bundles, causing haematuria, haematochezia, and impotence in the process. Metastases to the pelvic lymph nodes can result in edema in both lower limbs on either side of the body. PCa patients frequently develop bone metastases, which can result in bone discomfort, pathological fractures, and paraplegia. PCa can also spread to the bone marrow, resulting in anemia or a low blood count in some cases. Even if PCa has spread to other

systems, it may still respond to treatment and be under control, but it is uncertain that it will be cured.

1.5 Diagnosis of prostate cancer

1.5.1 Screening for prostate cancer

PSA is an antigen associated with the prostate gland and a single-chain glycoprotein secreted, as demonstrated by Balk et al.[23]. Normally only very low PSA levels are present in the blood, and pathological alterations or traumas to prostate can lead to an elevated serum PSA level. Benign prostate disease can also lead to an increase in serum PSA[24]. Serum PSA levels are raised in the majority of patients with PCa. Therefore, PSA is routinely used as PCa serum marker and is widely used for detection, risk management, monitoring and prognostic evaluation of PCa.

Doctors utilize DRE to examine the prostate since it is a very easy procedure. After putting on gloves or finger gloves, the doctor applies some lubricant to the index finger and the anal area, then inserts the index finger into the rectum for the examination. Because the prostate is an inside organ, doctor will not be able to see it immediately during the procedure but can feel it by pressing against it. It is used in a preliminary screening of PCa and is quite painless[24]. Having a prostate that is bigger than normal for the patient's age might indicate that he has a problem with an enlarged prostate. This might be an indication of PCa if it is firm or lumpy in the prostate.

1.5.2 Diagnosing prostate cancer

Transrectal ultrasound (TRUS) scans are used to produce an image of a specific region of the body by using high-frequency sound waves. A prostate ultrasound scan can detect changes in patient's prostate, including abnormal growths, that might otherwise go undetected. Ultrasound scanners detect tissue using sound waves and transform them into a visual picture on a computer screen. It is possible that the patient will have a biopsy of his prostate gland performed at the same time as your PCa screening. It is called TRUS-guided biopsy[26].

Magnetic resonance imaging (MRI) is used for noninvasive evaluation. As Weinreb et al. reported, “Advances in technology (both in software and hardware) have led to the development of multiparametric MRI (mpMRI), which combines anatomic T2-weighted (T2W) with functional and physiologic assessment, including diffusion-weighted imaging (DWI) and its derivative apparent-diffusion coefficient (ADC) maps, dynamic contrast-enhanced (DCE) MRI, and sometimes other techniques such as in-vivo MR proton spectroscopy” ([27], p. 2). MpMRI scan creates a comprehensive image of prostate and surrounding tissues using magnets. As mentioned in the same paper, “The Prostate Imaging – Reporting and Data System Version 2 (PI-RADS™ v2) is the product of an international collaboration of the American College of Radiology (ACR), European Society of Urogenital Radiology (ESUR), and AdMetech Foundation” (Weinreb et al.[27], p. 1). Categories are assigned to area of prostate from 1-5, which implies a gradual rise in the likelihood of experiencing clinically significant malignancies. This method is widely utilized worldwide and has developed into a standard protocol. PI-RADS V2.1 was introduced by Turkbey et al.[28] in 2019. A comparison of the old and new versions is one of the studies in this dissertation. MpMRI can be used to assist pinpoint potential cancerous regions in the prostate and to estimate the rate at which cancer may develop. It reveals whether the disease has progressed beyond the prostate or to other regions of the pelvic. If a prostate biopsy is necessary, doctors can use the scan images to determine which areas of the prostate to sample. “The use of mpMRI-targeted biopsy is increasing the detection of clinically significant prostate cancer in both biopsy-naive and previous negative biopsy settings,” as described in Stabile et al.([29], p. 2).

Prostate biopsy is a procedure that utilizes tiny needles to obtain small samples of prostate tissue, which is usually performed while TRUS. The tissue is evaluated for signs of malignancy subsequently. If cancer is detected, the biopsy findings will indicate the disease’s aggressiveness. In other words, it is a proclivity for spreading outside the prostate. Doctors often collect 10 to 12 small pieces of tissue from various regions of the prostate in standard biopsy for PCa diagnosis[30,31]. Nowadays, with the development of mpMRI, MRI-targeted biopsy is also a choice for prostate biopsy. Men who had a positive mpMRI result received MRI-targeted biopsy under real-time ultrasonographic supervision, aligning target MRI image with prostate real-time ultrasound imaging while biopsy. It can be accomplished with visual records or with the help of software, thus it is also called MRI-ultrasonographic fusion biopsy[32,33].

1.5.3 Determining the aggressiveness of prostate cancer

The Gleason score (GS) is a widely utilized tool in clinical practice to assess the grading of PCa cells. The current version, introduced in 2014[34], is the prevailing standard. After a biopsy establishes the existence of cancer, the next step is to ascertain the cancer cells' aggressiveness. In a laboratory, doctors analyze samples of cancer cells to evaluate the extent of their deviation from healthy cells. A higher score indicates a more aggressive malignancy with a greater tendency for rapid spread. Given the potential variation in severity within prostate tumors, the Gleason score assesses samples of prostate cancer cells on a scale of 3 to 5. It involves summing up the scores of the first and second dominant patterns, resulting in a range from 6 to 10. Higher scores denote a more aggressive and poorly differentiated form of cancer.

Clinicians have acknowledged the need for a more precise method to categorize malignancy classes than the Gleason score, given various considerations. As a result, a Grade Group System comprising five grades was developed to offer a more comprehensive and simplified understanding of how PCa behaves and responds to treatment. This gives a single score from 1 to 5 based on increasing Gleason scores[35]. Grade Group 1 represents the least aggressive form, while Grade Group 5 signifies the most aggressive. This represents a significant advancement in the diagnosis of PCa. Currently, a biopsy pathology report typically includes both the Gleason score and the Grade Group, providing clinicians with a comprehensive view of the disease's characteristics.

1.5.4 Detecting the spread of prostate cancer

After patients have been diagnosed with PCa, further TNM staging is required to specify a treatment plan. The following methods can help determine the systemic spread of metastases.

Bone scintigraphy can assist determine whether cancer has spread to the bones, and it has been widely used in the evaluation of bone metastases with multi cancers[36]. When PCa spreads to other regions, it often starts in the bones. Patient is injected with a little dose of low-dose radioactive agent, technetium ^{99m}-methyl diphosphonate (^{99m}Tc-MDP), that achieves in injured regions of ossein all over body in

this scanning. As stated in Papathanassiou et al., "Single-photon emission computed tomography (SPECT) combined with computed tomography (CT) provides both structural and functional information. SPECT/CT has been proven useful for interpreting radionuclide bone scan results in patients with bone malignancies" ([37], p. 474). Because ^{99m}Tc -MDP bone scintigraphy is widely available and inexpensive, it has been applied to assess PCa bone metastases for decades. However, it has a low specificity for this illness when compared to other imaging techniques, due to the radiotracer's accumulation in inflammatory, traumatic, and degenerative lesions. Other disadvantages of bone scintigraphy are low spatial resolution and insufficient image quality. Therefore, traditional bone scintigraphy will be taken the place by positron emission tomography (PET)/ CT when evaluating bone metastases, if a PET/CT scanner is applicable[38].

As illustrated by Jones et al., "Instrumentation for PET imaging has experienced tremendous improvements in performance over the past 60 years since it was first conceived as a medical imaging modality" ([39], p. 2). The scan is conducted using a tracer that contains radioactive tracers. This sort of tracer is injected into the vein of patients' arm. Different tracers are used for different examination purposes. The tracer is subsequently incorporated into certain organs and tissues. When a PET scanner detects the tracers, they give important information to the doctors about the condition of patient's organs and tissues. Certain tissues and diseases have a high level of chemical activity. Areas with more chemical activity concentrate more tracers. Such areas on PET scans show up as radioactive concentrations. Standardized uptake value maximum (SUVmax) is often used as a quantifier of PET images, which is commonly used in the analysis of fluorodeoxyglucose (FDG)-PET images, as well as other PET agents. SUVmax is the ratio of the radiopharmaceutical concentration in a volume of a region of interest (ROI) expressed "in microcuries of injected agent per volume to concentration in the body if uniformly distributed (determined by a standard body phantom)," as defined in Waxman et al. ([40], p. 1). There are no units for SUV. Depending on how the SUV is normalized, there are some different formulas for SUV, like "body weight, lean body mass (LBM), or body surface area," as defined in Tao Chan([41], p. 130). SUV normalized by body weight is the most commonly used, which is used in this study.

Prostate-specific membrane antigens (PSMA) has piqued the enthusiasm of researchers in recent years as potential particular targets for PCa imaging. In conventional PET scans, the most often used tracer is FDG, , which detects glucose

metabolism. In the case of PCa, however, FDG is not particularly effective in detecting PCa cells. PSMA is a transmembrane glycoprotein that has been linked to tumor growth and recurrence, and it is found in high levels in PCa cells, where it is overexpressed[42,43]. ^{68}Ga is generated from $^{68}\text{Ge} / ^{68}\text{Ga}$ radionuclide generator systems that are not dependent on the presence of a cyclotron. As established in Sterzing et al., “using the novel ^{68}Ga -labelled PSMA ligand Glu-urea-Lys(Ahx)-HBED-CC (^{68}Ga]-Ga-PSMA-11), which presents outstanding affinity to PSMA, a highly selective approach of imaging PCa, lymph node metastases and distant metastases is available” ([44], p. 35).

PET/CT and PET/MRI are currently widely used in evaluation of tumor diseases worldwide. Eiber et al.[45] illustrated that ^{68}Ga]-Ga-PSMA-11 PET/CT shows a much wider range of detection within the clinically relevant scope of low PSA levels than in other imaging modalities. Compare to MRI, CT offers advantages in terms of relatively low cost, fast scanning speed, and short examination time. However, its spatial resolution for pelvic scanning is not as satisfying as MRI. PET/MRI combines MRI with PET. It supplies high soft-tissue contrast, which allows for comprehensive multi-modality examination. By incorporating functional MR, it is also possible to go beyond anatomical correlation. The possibility of genuinely simultaneous operation enables multiple MR sequences to be acquired during a PET scan without the need for additional examination time. Hybrid PET/MRI with simultaneous collection of PET and MRI data enables the combination of functional and molecular information.

1.6 Aim of the research

^{68}Ga]-Ga-PSMA-11 PET/MRI is universally applied in diagnosis and assessment of PCa, and its continued use in the future is generally anticipated[46,47]. Besides providing a comprehensive evaluation of lesion distribution and monitoring patients' results, it also allows for the treatment prognosis[48].

The aim of this dissertation is to analyze imaging characteristics of ^{68}Ga]-Ga-PSMA-11 PET/MRI, by evaluating and quantifying lesions of PCa.

2. Methods

2.1 Patients

All cohort studies were approved by the local ethics review board (EA1/060/16), and the requirement for informed consent for this retrospective analysis was waived. Criteria for selecting the participants were as follows. Criteria for inclusion: (1) individuals with PCa proved by biopsy; (2) individuals received [⁶⁸Ga]Ga-PSMA-11 PET/MRI in our department; (3) it was possible to get the essential information. Criteria for exclusion: (i) For sub-projects 1 to 3, individuals who had had a radical prostatectomy (RP) prior to scanning were eliminated; (ii) The required data could not be gathered. For sub-project 4 radiomics analysis, intraprostatic lesions and metastasis were investigated, and (i) was not obligatory for metastasis cases.

All patients were confirmed to have PCa by systematic biopsy prior to [⁶⁸Ga]Ga-PSMA-11 PET/MRI scanning. Biopsy techniques included 12-core prostate biopsy and 14-core prostate biopsy. The needle biopsy technique introduced by Hodge et al. has become the gold standard method for diagnosing prostate cancers[49].

2.2 Imaging acquisition protocol

PET tracer is intravenously injected into patients. Injection dose activity: 1.8-2.2 MBq (0.049-0.060 mCi) /bodyweight kg. Thirty minutes before the beginning of PET acquisition, patients are administered furosemide to reduce the halo artifact produced by scattering over-correction, which is linked with increased renal and urinary tracer involvement on PET. The examined patient needs to urinate just before the acquisition. There were no adverse effects seen following the administration of [⁶⁸Ga]Ga-PSMA-11. Every patient's imaging protocol was carried out according to the identical methodology.

Scanner 3.0 T PET/MRI system (SIEMENS MAGNETOM Biograph mMR, Erlangen, Germany) was used. The process for acquiring the data was separated into two phases. First, a PET/MRI scan of the body is done from the apex to the middle of the thigh, with each bed receiving 3 minutes of PET collection and 24 cm of coverage. Second, a dedicated MRI scan of the pelvis was taken, followed by the reconstruction of PET data.

Table 1 summarizes the statistics of the MRI scan, and it is cited from published work by Zhao et al.([50], p. 9, CC BY 4.0). "Reconstruction was conducted with an ordered subset expectation maximization algorithm (OSEM), with 3 iterations/21 subsets, based on an x-matrix acquisition with a 4-mm Gaussian filter and relative scatter scaling. Attenuation correction was performed using the non-enhanced MRI data," stated Zhao et al.([51], p. 3). "Contrast-enhanced agent gadobutrol (Gadovist®, Bayer Pharma AG, Berlin, Germany) is intravenously administered at a clinical dose of 0.1 mmol/kg bodyweight. Following the acquisition of precontrast data, a total of 60 contrast-enhanced data were obtained, with the start of the first postcontrast acquisition corresponding with the start of the contrast injection," as mentioned in published work by Zhao et al.([52], p. 8).

Table 1. MRI scanning parameters.

Sequence	TR/TE (msec)	FOV (mm)	Flip angle (degrees)	Section thickness (mm)	Voxel size (mm)
T2WI HASTE Axial	1400.0/95.0	400	160	5.0	1.3×1.3×5.0
T1WI FS VIBE	1600.0/96.0	350	160	4.0	1.1×1.1×4.0
T2WI Axial	5500.0/103.0	180	150	3.0	0.5×0.5×3.0
T2WI Sagittal	1600.0/96.0	350	160	4.0	1.1×1.1×4.0
T2WI Coronal	4500.0/102	200	173	3.0	0.4×0.4×3.0
DWI	11600.0/70.0	280		3.0	2.5×2.5×3.0
T1WI FS TWIST Dynamic	7.41/3.30	260	12	3.5	1.4×1.4×3.5
T1WI STARVIBE	3.71/1.77	360	9	1.2	1.1×1.1×1.2

2.3 Imaging analysis

2.3.1 LBR of SUVmax

Without access to PET images, all MRI images were evaluated by a radiologist based on PI-RADS 2.0[27]. Focal lesions with a PI-RADS scoring of 2 or 3 were classified as MRI negative, whereas those with a scoring of 4 or 5 were classified as MRI positive. PI-RADS score of 1 was excluded from this investigation due to the fact that, according to PI-RADS 2.0, the score of 1 indicates normal prostate tissue. T2WI was utilized to correlate the anatomic location of [⁶⁸Ga]Ga-PSMA-11 PET. [⁶⁸Ga]Ga-PSMA-11 PET was reviewed by a nuclear medicine physician who was

unaware of the MRI findings. An aberrant signal on MRI or avid PSMA uptake on PET scans delineated an ROI. SUVmax is determined by ROI. In [⁶⁸Ga]Ga-PSMA-11 PET, avid localized lesion in prostate with concentration more than the normal prostate uptake that was not ascribed to physiological radio-tracer bio-distribution was regarded as positive. Lesions that have equivalent or lighter concentrations as background were considered negative. As stated in Zhao et al., "LBR is defined as a ratio of lesion SUVmax to background SUVmax" ([51], p. 3).

2.3.2 Comparison between PI-RADS 2.0 and 2.1

Two doctors independently assessed the images and clinical data. Both evaluators read MRI images by PI-RADS 2.0 and 2.1[28,53-55]. An aberrant signal on MRI or avid PSMA uptake on PET scans delineated an ROI. After that, the findings of both versions to determine inter-reader repeatability were examined. PI-RADS versions 2.0 and 2.1 were used to analyze mpMRI images, respectively. SUVmax was used to analyze [⁶⁸Ga]Ga-PSMA-11 PET images depending on the ROI.

2.3.3 Dynamic contrast-enhanced MRI

ROIs were manually defined and identified on MRI scans as areas having an aberrant signal. MRI images were evaluated using PI-RADS 2.1[28]. PI-RADS 1-3 lesions are categorized as benign, whilst PI-RADS 4-5 lesions are diagnosed as malignant. SUVmax is defined as the T2WI finding, using the ROI. All of the pictures were read by the same dual-trained physician.

Syngo.via MR Tissue 4D was used to produce all of the perfusion parameters, "Perfusion parameters, including arrival time (AT), time to peak (TTP), wash-in slope (W-in), wash-out slope (W-out), peak enhancement intensity (PEI), and initial area under the 60-sec curve (iAUC)," as mentioned in Zhao et al.([52], pp. 8-9). They were derived from the time-intensity curves. X-axis indicates time, while Y-axis indicates the increase based on the baseline. SUVmax between 2.0 and 3.0 have previously been proposed as appropriate cutoff levels for reducing false-positive interpretations of weakly PSMA positive uptake[56,57]. In this project, a SUVmax 3.0 threshold was used. The definitions for the aforementioned parameters are cited from my previously published work([52], p.9). "AT: point in time when contrast enhancement starts; TTP: time from arrival time to end of wash-in; W-in: slope of the fitted line between AT and end of wash-in; W-out: slope of the fitted line between start of wash-out and end of measurement; PEI: value of

concentration when the contrast enhancement reaches the highest concentration; iAUC: initial area under curve in 60 sec.”

2.3.4 Radiomics analysis

First, focal lesion selection was achieved using dedicated post-processing software Syngo.via (Siemens Healthcare, Erlangen, Germany). Syngo.via can automatically calculate lesion's SUVmax and volume. The volume calculation is based on voxel size. Lesion inclusion criteria were: 1) The lesion was present on both twice scans; 2) The lesion should have a clear border with adjacent tissue; 3) Lesions showing PSMA avidity and having a volume of at least 1.0cm³. Exclusion criteria was: Lesions, which are smaller than 1.0cm³, can not be captured by image matrix resolution are therefore excluded. The borders of the volume of interest (VOI) were defined using a threshold SUVmax > 3.0[56,57]. A cutoff of SUVmax > 3.0 was selected in this study to minimize false-positive interpretations of slightly PSMA-positive findings. The tumor boundaries were then automatically contoured. T2WI was used for anatomical correlation for [68Ga]Ga-PSMA-11 PET. Each included lesion was analyzed in the same location in both before and after treatment imaging.

2.4 Statistical analysis

Descriptive statistics are used to describe demographics and clinical features of patients. Normally distributed data are reported as mean ± SD, while non-normally distributed data are reported as medians (interquartile range, IQR Q1, Q3). Data analysis was conducted using SPSS 25 (IBM Corp, Armonk, NY, USA). A p-value <0.05 was considered statistically significant.

2.4.1 LBR of SUVmax

Ranging from 2 to 5, prostate lesions were divided into 4 categories based on PI-RADS scores and then LBR for each category were calculated. I employed receiver operating characteristic (ROC) and area under curve (AUC) calculations to determine the optimal LBR cutoff point[51].

2.4.2 Comparison between PI-RADS 2.0 and 2.1

Regarding PI-RADS 2.0 and 2.1, I studied the same set of lesions. With kappa(k) value, the inter-reader agreement was examined respectively. “Kappa statistic values

are : less than 0.0, 0.00-0.20, 0.21-0.40, 0.41-0.60, 0.61-0.80 and 0.81-1.00, indicating strength of agreement : poor , slight, fair, moderate, substantial and almost-perfect, respectively” (Landis & Koch[58], p.165).

2.4.3 Dynamic contrast-enhanced MRI

The DCE-MRI parameters between prostate benign and malignant lesions were compared by Mann–Whitney U test. Correlations between each parameter were calculated by Pearson correlation.

2.4.4 Radiomics analysis

Radiomics features were extracted from PET images. Texture analysis was performed using 3D slicer 4.10 (<http://www.slicer.org/>), an open-source python platform[59]. The VOI was segmented by setting a threshold SUVmax >3.0. The tumor boundaries were then automatically contoured. This ensured that the VOI for radiomics analysis and semiquantitative analysis for the same lesion was identical due to the use of the same cutoff value.

The following radiomics features—entropy, variance, and mean—were selected for analysis due to their extensive study and reporting in other publications[60-62]. Each texture feature describes a specific relationship of pixels with their neighbors. The definitions of features are: Entropy: entropy specifies the uncertainty/randomness of image values. It measures the average amount of information required to encode the image values; Variance: variance is the mean of the squared distances of each intensity value from the mean value; Mean: average gray-level intensity within the VOI.

3. Results

3.1 LBR of SUVmax

3.1.1 Patient cohort

Thirty-two patients are investigated in this sub-project. Characteristics of patients are presented as follow: Age: 70 ± 7 ; PSA level: 11.45 (5.67, 24.36) (ng/mL); Biopsy Gleason score (n): 3+3 (4), 3+4 (7), 4+3(5), 4+4(9), 4+5(2), 5+4(3), 5+5(2).

3.1.2 Imaging analysis

“A total of 170 focal prostate lesions were detected. PI-RADS score was 2 in 70 lesions (70/170) with LBR of 1.5 (0.9, 2.4); 3 in 16 lesions (16/170) with LBR of 2.5 (1.6, 3.4); 4 in 46 lesions (46/170) with LBR of 3.7 (2.6, 4.8); and 5 in 38 lesions (38/170) with LBR of 6.7 (3.5, 12.7),” as reported in Zhao et al.([51], p. 4). The ROC for [⁶⁸Ga]Ga-PSMA-11 PET and lesion validation results are shown in **Figure 1**.

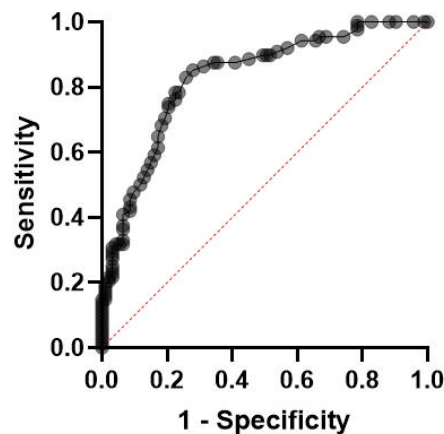


Figure 1: ROC curve. ROC curve generated with a generalized linear model of LBR for [⁶⁸Ga]Ga-PSMA PET. With the generalized linear model estimate, AUC for [⁶⁸Ga]Ga-PSMA PET was 0.83, 95% CI (0.77, 0.89), with an optimal LBR threshold of 2.5, 85.2% sensitivity, 72.0% specificity, $p < 0.001$. The presented figure is cited from previously published work by Zhao et al.([51], p. 4, CC BY 4.0).

3.2 Comparison between PI-RADS 2.0 and 2.1

3.2.1 Patient cohort

Forty-six patients are investigated in this sub-project. Characteristics of patients are presented as follow: Age: 75 ± 7 ; PSA level: 12.48 (4.33, 26.48) (ng/mL); Biopsy Gleason score (n): 3+3 (10), 3+4 (9), 4+3(7), 4+4(10), 4+5(3), 5+4(5), 5+5(2).

3.2.2 Imaging analysis

A total of 215 focal prostate lesions were studied. "Regarding the inter-reader agreement of the PI-RADS assessment category between the two readers, the kappa value was 0.723, substantial for version 2.0; and 0.853, almost perfect for version 2.1," as reported in Zhao et al.([50], p. 3). **Figure 2** illustrates "typical nodules", and **Figure 3** illustrates an atypical nodule with DWI 5, which increases PI-RADS evaluation from 2 to 3.

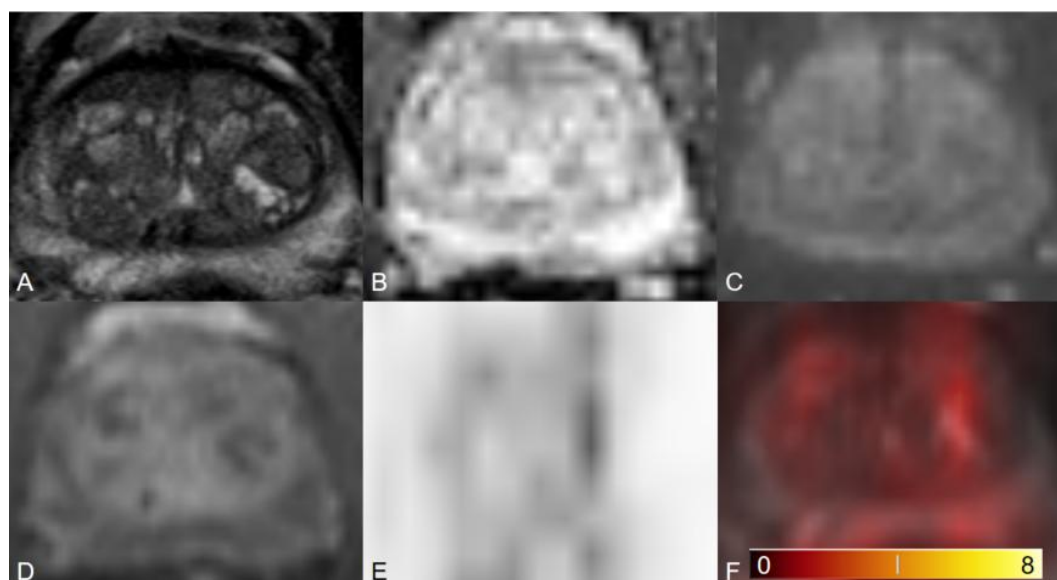


Figure 2: TZ with typical BPH nodules. (A) Axial T2WI shows completely encapsulated "typical" nodules. (B) ADC map image presents no focal lesion with hypointense signal below the background. (C) DWI ($b = 1000 \text{ s/mm}^2$) shows no lesion with a markedly hyperintense signal above the background. (D) Early dynamic contrast-enhanced image presents no positive enhancement within the typical BPH nodules. T2WI = 1, DWI = 1, DCE = negative, PI-RADS assessment category = 1. (E) PET image shows inhomogeneous [^{68}Ga]Ga-PSMA-11 uptake. (F)[^{68}Ga]Ga-PSMA-11 PET/MRI fusion. The presented figure is cited from previously published work by Zhao et al.([50], p. 5, CC BY 4.0).

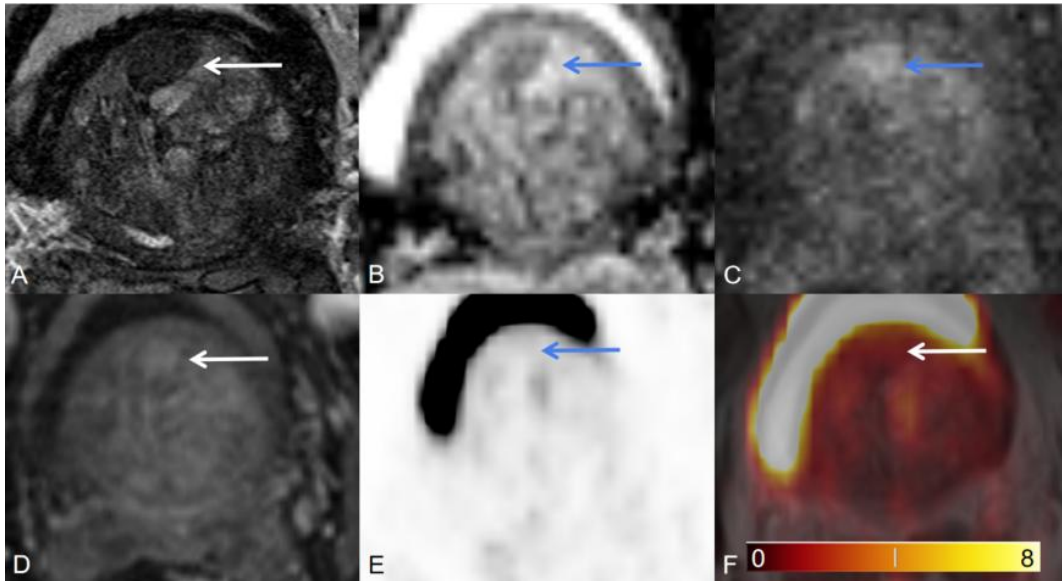


Figure 3: TZ with an atypical nodule. (A) Axial T2WI shows a homogeneous T2 hypointense, mostly encapsulated nodule. (B) ADC map image presents a focal lesion with a markedly hypointense signal below the background corresponding to the lesion seen in (A). (C) DWI ($b = 1000 \text{ s/mm}^2$) shows a focal lesion with a markedly hyperintense signal above the background corresponding to the lesion seen in (A,B). (D) Early dynamic contrast-enhanced image presents avid enhancement within the nodule. T2WI = 2, DWI = 5, DCE = positive, PI-RADS assessment category = 3. (E) PET image shows no $[^{68}\text{Ga}]\text{Ga-PSMA-11}$ avid uptake. (F) $[^{68}\text{Ga}]\text{Ga-PSMA-11}$ PET/MRI fusion. The presented figure is cited from previously published work by Zhao et al. ([50], p. 5, CC BY 4.0).

3.3 Dynamic contrast-enhanced MRI

3.3.1 Patient cohort

Thirty-nine patients are investigated in this sub-project. Characteristics of patients are presented as follow: Age: 69 ± 9 ; PSA level: $8.70(5.18, 18.83)$ (ng/mL); Biopsy Gleason score (n): 3+3 (8), 3+4 (8), 4+3(8), 4+4(7), 4+5(2), 5+4(3), 5+5(3).

3.3.2 Imaging analysis

A total of 154 focal prostate lesions were studied. Comparing benign and malignant lesions, TTP and SUVmax are significantly different ($p < 0.05$). Other parameters did not indicate significant difference, presented in **Table 2**. There is a moderate to strong

correlation between the perfusion parameters, presented in **Table 3**. The presented tables are cited from previously published work by Zhao et al. ([52], pp. 3-4, CC BY 4.0).

Table 2. Benign and malignant lesions comparison.

Parameter	Benign lesions			Malignant lesions			P Value
	Median	Q1	Q3	Median	Q1	Q3	
SUVmax	2.3	1.5	3.7	7.0	4.2	11.5	p<0.05*
AT(min)	0.47	0.40	0.57	0.47	0.39	0.56	p>0.05
TTP(min)	1.09	0.84	1.32	0.95	0.75	1.22	p<0.05*
W-in	0.13	0.07	0.18	0.12	0.08	0.22	p>0.05
W-out	0.01	0.01	0.02	0.01	0.01	0.02	p>0.05
PEI	0.21	0.15	0.28	0.20	0.15	0.26	p>0.05
iAUC	0.08	0.05	0.11	0.08	0.05	0.12	p>0.05

* p < 0.05.

Table 3. Pearson correlation analysis.

	AT	TTP	W-in	W-out	PEI	iAUC
AT	1	-0.17*	0.18*	-0.05	-0.004	0.18*
TTP	-	1	-0.45**	0.71**	0.17*	-0.31**
W-in	-	-	1	-0.30**	0.57**	0.95**
W-out	-	-	-	1	0.41**	-0.18*
PEI	-	-	-	-	1	0.70**
iAUC	-	-	-	-	-	1

* p < 0.05, ** p < 0.01

[⁶⁸Ga]Ga-PSMA-11 imaging is used to supplement mpMRI in order to characterize worrisome lesions for target biopsy[63]. Lesions' multi-modality quantitative assessment

adds therapeutic significance to this research. DCE parameters reflect the microvascular configuration of lesions, while SUVmax represents the concentration of PSMA in lesions. A fusion of data enables a thorough assessment of tumor status and the selection of an optimal treatment plan. These characteristics give extensive information on the aggressiveness of tumors located in various areas, **Figures 4 and 5**.

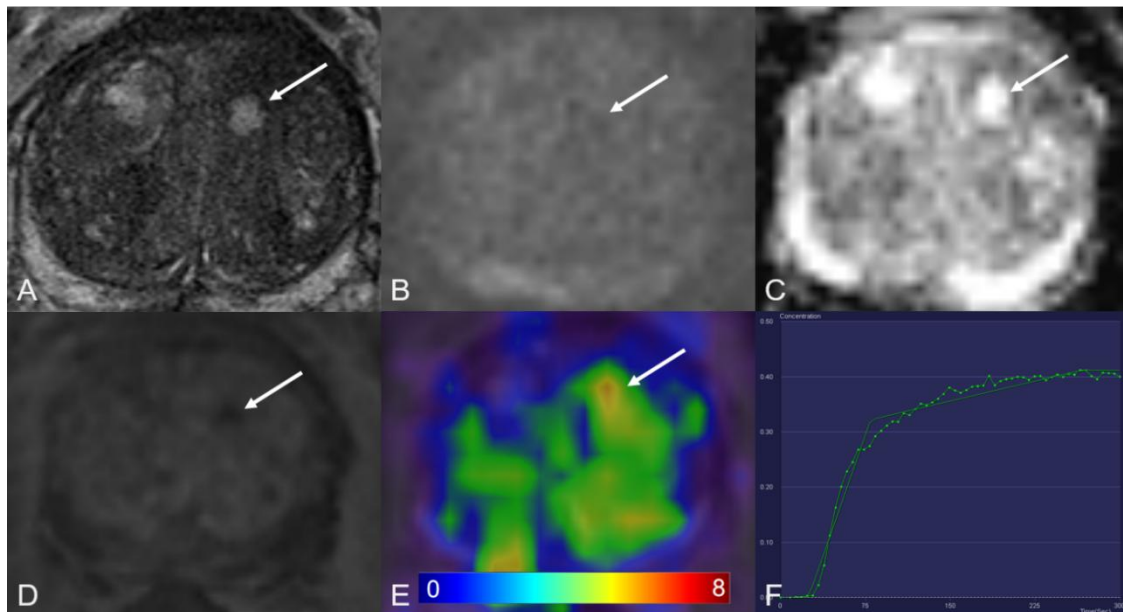


Figure 4: TZ with a PI-RADS 1 change. (A) Axial T2WI shows typical BPH change. (B) DWI ($b = 1000 \text{ s/mm}^2$) shows no lesion with a marked hyperintense signal above the background. (C) ADC map image presents no diffusion restriction. (D) Early dynamic contrast-enhanced image presents no enhancement within the typical BPH nodule. (E) $[^{68}\text{Ga}]\text{Ga-PSMA-11}$ PET/MRI fusion image shows moderate $[^{68}\text{Ga}]\text{Ga-PSMA-11}$ uptake, with SUVmax of 6.3. (F) DCE-MRI time-intensity curve demonstrates persistent increase enhancement. AT: 0.39min; TTP: 1.09min; W-in: 0.16; W-out: 0.02; PEI: 0.25; iAUC: 0.10. The presented figure is cited from previously published work by Zhao et al. ([52], p. 5, CC BY 4.0).

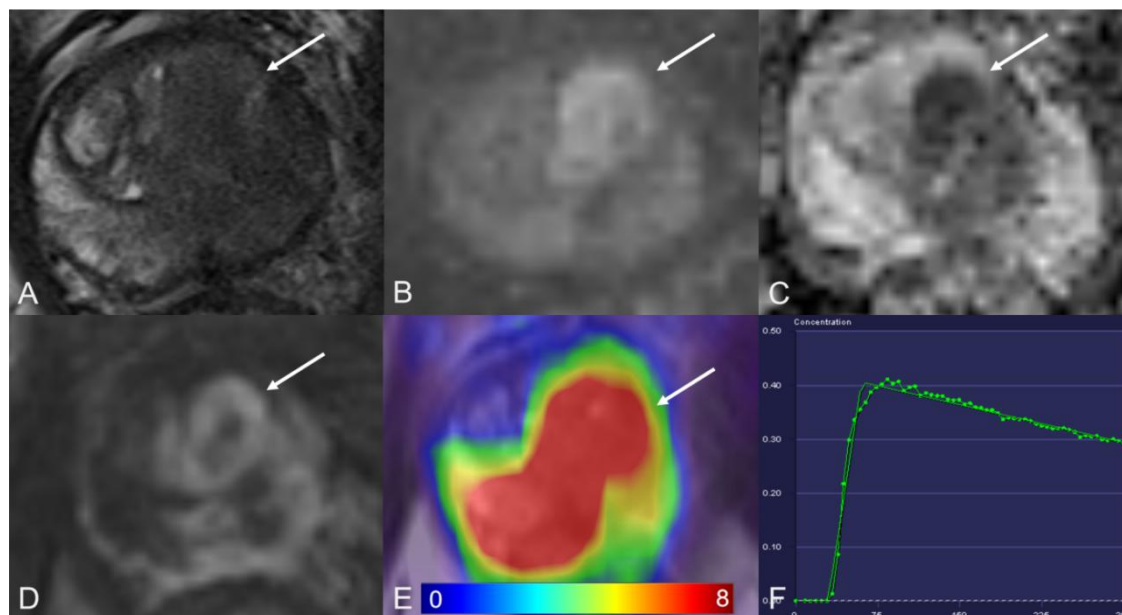


Figure 5: TZ with a PI-RADS 5 lesion. (A) Axial T2WI shows homogeneous hypointense. (B) DWI ($b = 1000 \text{ s/mm}^2$) shows a marked hyperintense signal above the background. (C) ADC map image presents a lesion with hypointense signal below the background. (D) Early dynamic contrast-enhanced image presents positive enhancement within the lesion. (E) $[^{68}\text{Ga}]\text{Ga-PSMA-11}$ PET/MRI fusion image shows avid $[^{68}\text{Ga}]\text{Ga-PSMA-11}$ uptake, with SUVmax of 29.2. (F) DCE-MRI time-intensity curve demonstrates a decline after initial up-slope enhancement. AT: 0.47min; TTP: 0.50min; W-in: 0.80; W-out: -0.03; PEI: 0.41; iAUC: 0.31. The presented figure is cited from previously published work by Zhao et al. ([52], p. 5, CC BY 4.0).

3.4 Radiomics analysis

3.4.1 Patient cohort

In this sub-project, I compared lesion's radiomics data from two examinations before and after treatment of the same patient. As this sub-project is an ongoing project, in this dissertation, I presented two cases as examples. Characteristics of patients are presented as follow.

Case 1: a 65-year-old patient. Gleason score: 4+3. PSA at 1st examination: 3.75 ng/mL. PSA at 2nd examination: 3.49 ng/mL. Treatment: Lu-177-PSMA-617. Interval between the two examinations: 91 days.

Case 2: a 73-year-old patient. Gleason score: 4+5. PSA at 1st examination: 12.00 ng/mL. PSA at 2nd examination: 26.00 ng/mL. Treatment: Androgen deprivation therapy (ADT). The interval between the two examinations: 399 days.

3.4.2 Imaging analysis

Figure 6 is case 1 with metastasis at the right ischium.

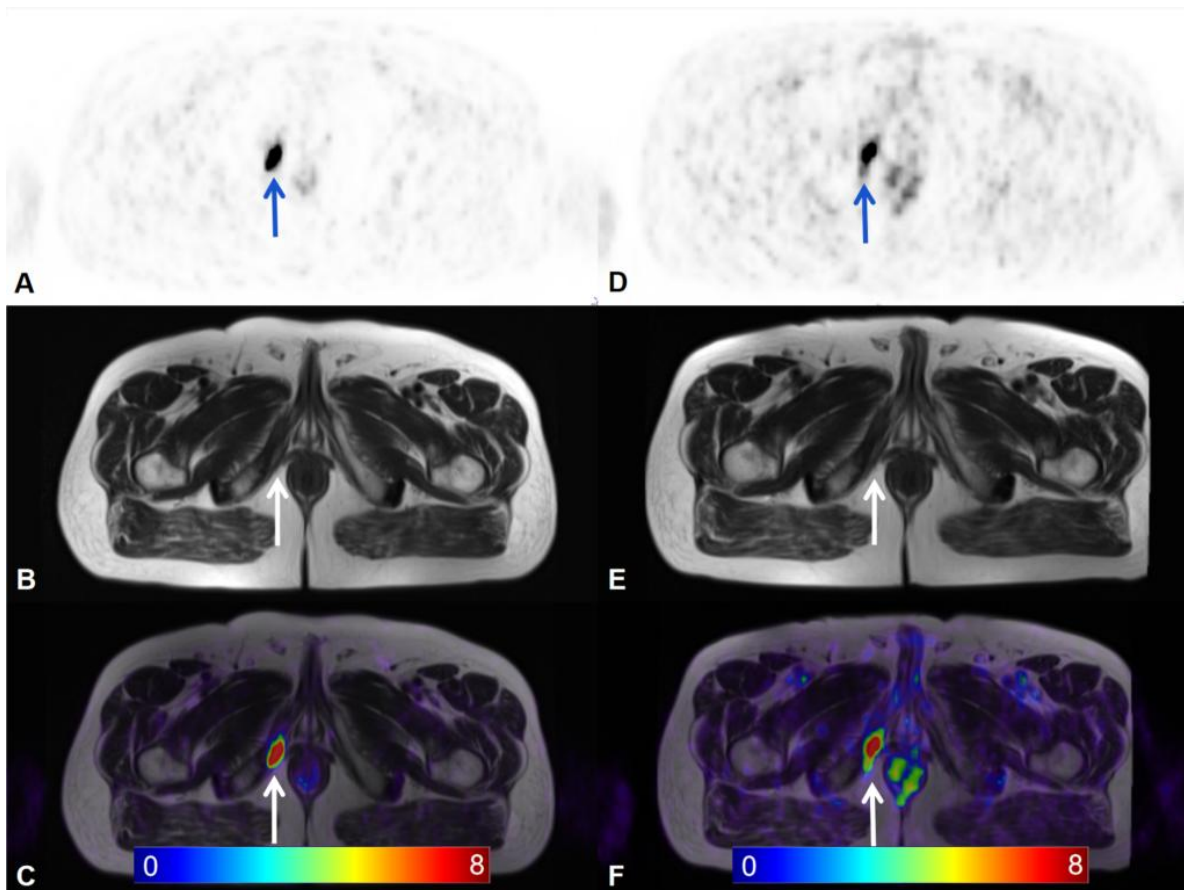


Figure 6: Metastasis at right ischium. The left column (A, B, and C) presents the results of the first examination, and the right column (D, E, and F) presents the results of the second examination. Location of metastasis: right ischium. From top to bottom: PET, T2WI HASTE, PET/MRI fusion. Results of the first and second examinations are as follows: SUVmax: 24.1, 14.9; Volume(cm^3): 2.55, 2.79. PET radiomics features: entropy: 5.94, 5.54; variance: 26.89, 11.35; mean: 8.60, 6.38. The arrow indicates the target lesion, while the other area of high uptake shows physiological rectal uptake.

Figure 7 is a case 2 with metastasis at the right scapula (indicated by arrow).

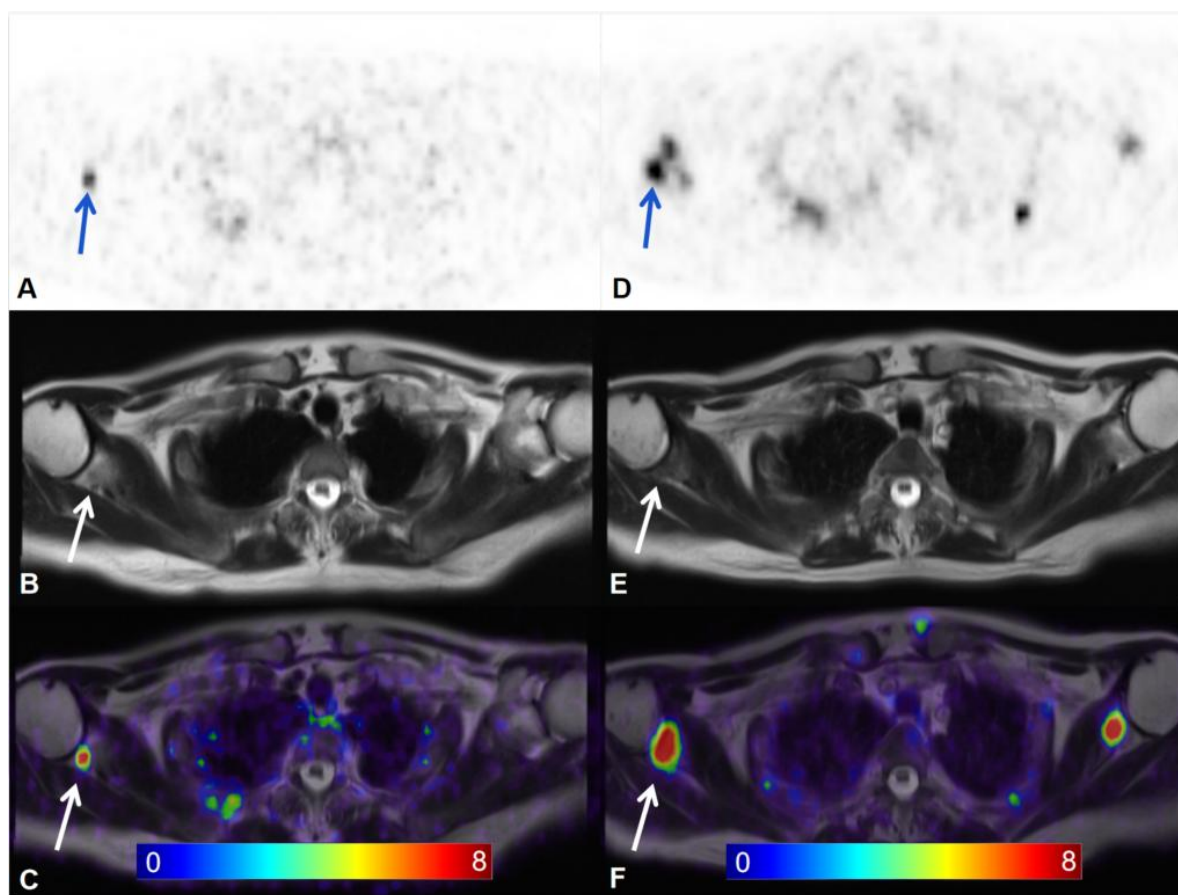


Figure 7: Metastasis at right scapula. The left column (A, B, and C) presents the results of the first examination and the right column (D, E, and F) presents the results of the second examination. Location of metastasis: right scapula. From top to bottom: PET, T2WI HASTE, PET/MRI fusion. Results of the first and second examinations are as follows: SUVmax: 7.8, 11.9; Volume (cm³): 0.64, 12.70. PET radiomics features: entropy: 4.06, 6.74; variance: 2.18, 3.98; mean: 5.13, 5.45. The arrow indicates the target lesion, while other areas of high uptake indicate new metastatic lesions.

4. Discussion

4.1 Short summary of results

I investigated the SUVmax threshold value for the LBR, the comparison of PI-RADS versions of old and new versions, DCE-MRI parameters in detail, and the changes in the radiomics features reflecting the lesions' change. The clinical applications of my results aid in the diagnostic criteria improvement and lesion information refinement of prostate.

4.2 Interpretation of results

4.2.1 LBR of SUVmax

In sub-project 1, threshold value of LBR of SUVmax was investigated. According to the observations, [⁶⁸Ga]Ga-PSMA-11 PET has greater sensitivity for distinguishing foci. Some foci which are negative on MRI have greater SUVmax than the adjacent SUVmax. It has the potential to result in low specificity. A higher threshold value is required in lieu of tissue background. I calculated LBR, a relative ratio, to enhance the clinical applicability of analysis. In this research, in [⁶⁸Ga]Ga-PSMA-11 PET scan, a threshold LBR of 2.5 was observed to be more clinically and research applicable for classifying lesions into positive and negative. The accuracy of imaging diagnosis is important in diagnosing prostate focal lesions.

PSMA may concentrate to varying degrees in both benign and malignant lesions[64,65], and we cannot rule out the possibility that lesions exhibiting uptake are malignant in every instance. Conversely, lesions that do not exhibit avid concentration are not always benign. Using the prostate normal tissue's SUVmax as a cutoff point for determining whether a focus on PET examination is positive or negative results in rather poor specificity. It is essential to establish another cutoff point for distinguishing benign from malignant lesions in order to optimize diagnostic effectiveness.

4.2.2 Comparison between PI-RADS 2.0 and 2.1

In sub-project 2, in order to make the interpretation criteria more clear, many adjustments are built to PI-RADS version 2.1, which Turkbey et al.[28] epitomized. The modifications are categorized into three sections: the acquisition of imaging data,

clarification of interpretation criteria, and biparametric MRI. Certain revisions alter lesion categories, whilst others give explicit descriptions of existing groups, in order to enhance diagnostic consistency of interpretation across doctors and institutes.

First, T2WI is the main sequence that determines the TZ. In version 2.0, typical BPH nodules were accredited a T2WI 2. These lesions are classified as 2 on the PI-RADS evaluation scale. In version 2.1, a "typical nodule" is a focal nodule that appears normal or a circular, fully encapsulated nodule. As age-related BPH is improbable to represent PCa, in the new version, BPH alone is deemed physiological revision, and is accredited T2WI 1. In addition to BPH, it is widely recognized that BPH can exhibit a significant absorption of PSMA on PET[66-69]. **Figure 2** is an example.

Second, the determination of the total evaluation group in TZ has been revised. In comparison to PI-RADS V2.0, the modification in assessing the PI-RADS measurement category as a whole places a greater emphasis on TZ lesions T2WI 2. In TZ, T2WI of a lesion is equal to 2. When DWI is 1-3, the overall PI-RADS is maintained at 2. When DWI is 4-5, the overall score is 3. Certain lesions that were formerly allocated as PI-RADS 2 are now classified as 3. **Figure 3** is an example.

Third, the criteria of DWI ratings 2-3 is revised. According to version 2.0, characterization of DWI finds scores 2-3 is ambiguous. Because of differences in personal experience, ambiguity, and variable perceptions of physicians' judgment, making a diagnosis can be difficult. Furthermore, observations needed to meet both the ADC and the DWI criteria, not a single sequence set in version 2.1. The new version affords a more comprehensive and consistent explanation of DWI results than the previous version[50].

Fourth, the difference between positive and negative DCE is clarified. The features in version 2.0 that correspond to DCE negative, as well as extensive multi-focal enhancement evaluation were indeterminate. In version 2.1, the definition of negative DCE is revised. This modification is anticipated to eliminate reader-to-reader inconsistencies in DCE-MRI interpretation. DCE is the secondary sequence that determines PZ lesions. This revision has the potential to improve diagnostic reproducibility[50].

4.2.3 Dynamic contrast-enhanced MRI

In sub-project 3, DCE-MRI has been explored in several clinical researches. It is used for non-invasive detection of different diseases. Contrast agent is injected into

blood flow to track changes in MRI signal intensity within the target tissue. This technique provides both anatomical detail information and functional change information of the target tissue. DCE is used to describe the function of the tissue, mainly reflected in perfusion-related research. As epitomized in Khalifa et al., “Kinetics (spatial and temporal distributions) of the contrast agent transit depend heavily on tissue perfusion, vessel permeability, and volume of the extracellular and extravascular space (EES)” ([70], p. 1). Perfusion information can be detected by MRI signal intensity variation. In this project, I used perfusion parameters reflected by dynamic curves to analyze prostate lesions.

Perfusion parameters were compared between benign and malignant foci in this study. The time that it takes for contrast enhancement to reach its maximum, is referred to TTP. TTP was shown to be statistically significantly different. Lower TTP indicates that time required to arrive at the climax is shorter. The fact that blood vessels are more numerous in the associated lesions may therefore be explained. Microvascular dissemination is an important indicator of neovascularization, as it is responsible for local development and tumor metastasis[71,72]. A wide variety of malignant neoplasms were studied by Chang et al.[43] , and it was shown that PSMA was consistently found in the blood vessels of these cancerous tumors. Microvascular structures are commonly more abundant in more malignant lesions[73,74]. DCE-MRI is a well-established imaging biomarker of tumor microvessels. Using a PET/MRI scanner, two modalities can be performed at the same time, allowing for further in-depth comparison and combination of two markers.

4.2.4 Radiomics analysis

Radiomics analysis is a promising study area of PCa. “The application of radiomics approaches in prostate cancer has not only enabled automatic localization of the disease but also provided a non-invasive solution to assess tumor biology,” encapsulated in Sun et al.([75], p. 4). Quantitative information is extracted from medical imaging data, which is the primary emphasis of radiomics. Radiomics techniques in PCa have permitted the automated localization of the illness, as well as they have also offered a non-invasive option for assessing tumor biology[76].

In sub-project 4, I investigated patients with PCa who underwent repeat scanning before and after treatment in our department. SUVmax was calculated. Radiomics features - entropy, variance and mean were extracted from PET images and compared between twice examinations. By comparing the features' data from the two scans, I was able to observe changes in the texture of lesions. In this part, I presented images and data from two patients as examples. In **Figure 6**, I present a patient with metastasis at the right ischium. After Lu-177-PSMA-617 treatment, there is a decrease in SUVmax of the lesion. **Figure 7** presents a patient with metastasis at the right scapula (indicated by arrow). Although the patient underwent ADT treatment, there is a progression of bone metastasis. Its volume significantly increased. SUVmax increased. At the same time, the images reveal several new metastatic lesions.

4.3 Embedding the results into the current state of research

Multi-modality imaging refers to the combination of equipment that operates in two imaging modalities into one unit. Anatomical imaging techniques, as well as functional image techniques, have seen significant advancements. Combining sequences from multiple modalities may offer substantial diagnostic benefits and requires the use of sophisticated image fusion algorithms to collect structural and functional information. Clinical and preclinical studies have demonstrated the potential for multi-modality imaging to improve non-invasive tissue characterization[77]. With advances in medical science and diagnosis technology, there have been tremendous breakthroughs in diagnosing and assessing PCa[78]. Molecular imaging (MI) is becoming the mainstream of imaging development[79]. MI techniques have reached a fascinating new level of specificity for diagnosing a wide range of diseases. With the advantage of precise localization and quantification of tumors and metastases, PET radiopharmaceuticals have made an essential contribution to this development. The methods I applied in this dissertation combine the advantages of both multi-modality imaging and MI. PET and MRI are two modalities, and [⁶⁸Ga]Ga-PSMA-11 PET is molecular imaging.

My study accentuated that [⁶⁸Ga]Ga-PSMA-11 PET may detect PCa, whereas MRI can be used to provide accurate anatomic guidance. Researchers conducted a meta-analysis of [⁶⁸Ga]Ga-PSMA-11 PET precision[80]. This study discovered that it has 0.74 sensitivity and specificity. When it comes to identifying lymph node and bone

metastases, Hirmas et al.[81] demonstrated exceptional accuracy. It achieved a much better rate of concordance of 90%, compared to 75% for bone scans, 73% for MRI, and 60% for CT. [⁶⁸Ga]Ga-PSMA-11 PET scan has a wide scanning range and high sensitivity, and it is widely utilized for effective staging as well as post-treatment effectiveness assessment. Increasing the use of [⁶⁸Ga]Ga-PSMA-11 is advantageous. It reduces the time required to diagnose metastatic lesions and benefits clinical decision-making. There have been several efforts to use a multi-modality method[82].

Imaging diagnostic criteria are changeable in response to technological advancements and the development of physicians' expertise in order to achieve further improvement. The evaluation of diagnostic criteria for the prostate diagnosis was improved in 2019. PI-RADS V2.1 was introduced by Turkbey et al.[28]. The new version proposes some changes. These modifications clarify diagnostic specifications and thus improve diagnostic repeatability between doctors and institutes. Previous literature has addressed the issue of variability. PI-RADS V2.0 was evaluated in a multi-center research[83]. It concluded that positive predictive value of version 2.0 was insufficient and diversified significantly between institutes. PI-RADS V2.1 makes improvements. PI-RADS V2.1 is easier to understand while lowering diagnostic indeterminacy. In my study, I investigated the differences and similarities between the two versions. The new guidance seeks to increase reproducibility among readers by offering a more detailed explanation of diagnostic criteria.

In my project, DCE-MRI is used to allow for the visualization of foci in prostate with various levels of enhancement, as well as the collection of characterization of lesions. DCE-MRI characteristics associated with prostate lesions were examined. By comparing the tissue's MRI signal intensity, DCE imaging may be used to determine perfusion condition, vessels supply, and vascularity. DCE-MRI, by virtue of its ability to quantify microvascular characteristics, provides critical detail to the characterization of lesions[84]. DCE-MRI is a highly effective diagnostic technique for identifying localized lesions of PCa, and it increases test accuracy for detecting and evaluating prostatic tumor lesions[85]. Chen et al.[86] revealed that wash-out slope correlates significantly with the Gleason score and provides accurate diagnostic findings for assessing the aggressiveness of PCa. In males with PCa, microvessel density has been linked with staging, recurrence, metastatic, and prognosis[87-89]. PCa can be identified utilizing contrast-enhanced MRI methods due to its increased microvasculature[90]. The increase

of the perfusion signal may be measured using semi-quantitative analysis[70,91]. The curve analysis technique has the advantage of being simple to measure. Parameters used in model-based calculations are complicated, giving more details on vascular physiology[92].

In the current work, I assessed the potential value of PET radiomics analysis to detect bone metastasis of follow-up after treatment. About radiomics analysis on prostate cancer, Lu et al.[93] assessed patients who underwent two mpMRI scans within two weeks and studied the reproducibility of quantitative imaging features among sequential scans. They found that quantitative imaging features are reproducible across sequential prostate mpMRI acquisition at a preset level of filters. Some other researchers have already reported significant results on prostate cancer. Woznicki et al.[94] combined radiomics analysis with PI-RADS and clinical parameters, concluding quantitative image data represent potential biomarkers. PET texture analysis can be used to assess radiomics features of lesions. A comparison of radiomics features extracted from [⁶⁸Ga]Ga-PSMA-11 PET/MRI scans obtained pre- and post-treatment allows assessing the change of individual lesions. Radiomics features can provide more information and data to evaluate the lesion changes comprehensively.

4.4 Strengths and weaknesses of the study

The strengths of this dissertation include: first, it followed the main lines of research in imaging studies and developed a clear experimental plan; second, it used qualitative and quantitative research methods and produced clear results; third, it included sub-experiments to comprehensively and comprehensively analyze the imaging characteristics of prostate cancer lesions from multiple perspectives; fourth, the results of this dissertation were published in three original publications on top journals and were recognized by peer review.

I aware that my research may have two weaknesses. First, the results are somewhat constrained due to the study's retrospective nature and single-center design. In order to enhance the usefulness and breadth of the outcomes, more validation should be undertaken in prospective multi-center research to gather additional patient data and deeper experimental results. Second, this is a descriptive visual study of imaging data. Because of the features of the patient cohort, all patients have their PCa verified through

routine biopsy prior to [⁶⁸Ga]Ga-PSMA-11 PET/MRI scanning. The majority PCa patients are elderly males who have an underlying illness or geriatric condition, which precludes histological testing. Gross histopathology examinations are frequently impractical owing to patient ethics and reality.

4.5 Implications for practice and future research

My experiments used the most prevalent analytical method for imaging studies. The combination of findings provides ideas and methods for future improvements. Further research should be undertaken to explore novel molecular probes and new advanced imaging technology. Creation of novel specific receptor ligands, targeting probes, and antibodies are expected to improve the performance of MI and diagnosis of PCa. And new imaging techniques can lead to the feasibility of more imaging modalities or sequences. We can target new molecular probes or imaging techniques for image characterization in the future. And a cross-sectional or longitudinal comparison with the results of the present study will give a more comprehensive analysis of the disease.

5. Conclusion

In my synopsis, LBR of SUVmax, comparison between PI-RADS 2.0 and 2.1, DCE-MRI parameters and radiomics analysis have been presented, in the context of diagnosing and evaluating prostate lesions.

PET/MRI combines MRI with PET. It supplies molecular information and high soft-tissue contrast, which allows for further multi-modality examination, and by including functional MRI, it is also feasible to go beyond anatomical correlation. From the standpoint of enhancing the accuracy of imaging diagnosis, physicians need better diagnostic criteria and more data information in order to more precisely identify the characteristic of disease for increasing the effectiveness of diagnostic procedures. Diagnostic criteria improvement and lesion information refinement are beneficial in clarifying the nature of lesions, optimizing diagnostic methods, and reasonably evaluating treatment alternatives, consequently enhancing the accuracy and diagnostic efficiency of image-guided therapies.

Reference list

- 1 Abd-Alazeez M, Ramachandran N, Dikaios N, Ahmed HU, Emberton M, Kirkham A, Arya M, Taylor S, Halligan S, Punwani S: Multiparametric MRI for detection of radiorecurrent prostate cancer: Added value of apparent diffusion coefficient maps and dynamic contrast-enhanced images. *PROSTATE CANCER P D* 2015;18:128-136.
- 2 Lee CH, Akin-Olugbade O, Kirschenbaum A: Overview of prostate anatomy, histology, and pathology. *Endocrinol Metab Clin North Am* 2011;40:565-575.
- 3 McNeal JE: Normal histology of the prostate. *AM J SURG PATHOL* 1988;12:619-633.
- 4 Krieger JN, Nyberg LJ, Nickel JC: NIH consensus definition and classification of prostatitis. *JAMA* 1999;282:236-237.
- 5 Sharp VJ, Takacs EB, Powell CR: Prostatitis: Diagnosis and treatment. *AM FAM PHYSICIAN* 2010;82:397-406.
- 6 Domingue GS, Hellstrom WJ: Prostatitis. *CLIN MICROBIOL REV* 1998;11:604-613.
- 7 Thorpe A, Neal D: Benign prostatic hyperplasia. *LANCET* 2003;361:1359-1367.
- 8 Sung H, Ferlay J, Siegel RL, Laversanne M, Soerjomataram I, Jemal A, Bray F: Global Cancer Statistics 2020: GLOBOCAN Estimates of Incidence and Mortality Worldwide for 36 Cancers in 185 Countries. *CA Cancer J Clin* 2021;71:209-249.
- 9 Scardino PT: Early detection of prostate cancer. *Urol Clin North Am* 1989;16:635-655.
- 10 Wu I, Modlin CS: Disparities in prostate cancer in African American men: What primary care physicians can do. *Cleve Clin J Med* 2012;79:313-320.
- 11 Okobia MN, Zmuda JM, Ferrell RE, Patrick AL, Bunker CH: Chromosome 8q24 variants are associated with prostate cancer risk in a high risk population of African ancestry. *PROSTATE* 2011;71:1054-1063.
- 12 Haiman CA, Chen GK, Blot WJ, Strom SS, Berndt SI, Kittles RA, Rybicki BA, Isaacs WB, Ingles SA, Stanford JL, Diver WR, Witte JS, Chanock SJ, Kolb S, Signorello LB, Yamamura Y, Neslund-Dudas C, Thun MJ, Murphy A, Casey G, Sheng X, Wan P, Pooler LC, Monroe KR, Waters KM, Le Marchand L, Kolonel LN, Stram DO, Henderson BE: Characterizing genetic risk at known prostate cancer susceptibility loci in African Americans. *PLOS GENET* 2011;7:e1001387.
- 13 Freedman ML, Haiman CA, Patterson N, McDonald GJ, Tandon A, Waliszewska A, Penney K, Steen RG, Ardlie K, John EM, Oakley-Girvan I, Whittemore AS, Cooney KA, Ingles SA, Altshuler D, Henderson BE, Reich D: Admixture mapping identifies 8q24 as a prostate cancer risk locus in African-American men. *Proc Natl Acad Sci U S A* 2006;103:14068-14073.
- 14 Chang BL, Isaacs SD, Wiley KE, Gillanders EM, Zheng SL, Meyers DA, Walsh PC, Trent JM, Xu J, Isaacs WB: Genome-wide screen for prostate cancer susceptibility genes in men with clinically significant disease. *PROSTATE* 2005;64:356-361.
- 15 Gallagher RP, Fleshner N: Prostate cancer: 3. Individual risk factors. *CMAJ* 1998;159:807-813.
- 16 Allott EH, Masko EM, Freedland SJ: Obesity and prostate cancer: Weighing the evidence. *EUR UROL* 2013;63:800-809.

- 17 Demark-Wahnefried W, Moyad MA: Dietary intervention in the management of prostate cancer. *CURR OPIN UROL* 2007;17:168-174.
- 18 Greenwald P: Clinical trials in cancer prevention: Current results and perspectives for the future. *J NUTR* 2004;134:3507S-3512S.
- 19 Freedland SJ, Aronson WJ: Obesity and prostate cancer. *UROLOGY* 2005;65:433-439.
- 20 Mohler JL, Antonarakis ES, Armstrong AJ, D'Amico AV, Davis BJ, Dorff T, Eastham JA, Enke CA, Farrington TA, Higano CS, Horwitz EM, Hurwitz M, Ippolito JE, Kane CJ, Kuettel MR, Lang JM, McKenney J, Netto G, Penson DF, Plimack ER, Pow-Sang JM, Pugh TJ, Richey S, Roach M, Rosenfeld S, Schaeffer E, Shabsigh A, Small EJ, Spratt DE, Srinivas S, Tward J, Sheehy DA, Freedman-Cass DA: Prostate Cancer, Version 2.2019, NCCN Clinical Practice Guidelines in Oncology. *J NATL COMPR CANC NE* 2019;17:479-505.
- 21 Mottet N, van den Bergh R, Briers E, Van den Broeck T, Cumberbatch MG, De Santis M, Fanti S, Fossati N, Gandaglia G, Gillessen S, Grivas N, Grummet J, Henry AM, van der Kwast TH, Lam TB, Lardas M, Liew M, Mason MD, Moris L, Oprea-Lager DE, van der Poel HG, Rouvière O, Schoots IG, Tilki D, Wiegel T, Willemse PM, Cornford P: EAU-EANM-ESTRO-ESUR-SIOG Guidelines on Prostate Cancer-2020 Update. Part 1: Screening, Diagnosis, and Local Treatment with Curative Intent. *EUR UROL* 2021;79:243-262.
- 22 Logothetis CJ, Lin SH: Osteoblasts in prostate cancer metastasis to bone. *NAT REV CANCER* 2005;5:21-28.
- 23 Balk SP, Ko Y, Bubley GJ: Biology of Prostate-Specific antigen. *J CLIN ONCOL* 2003;21:383-391.
- 24 Lilja H, Ulmert D, Vickers AJ: Prostate-specific antigen and prostate cancer: Prediction, detection and monitoring. *NAT REV CANCER* 2008;8:268-278.
- 25 Naji L, Randhawa H, Sohani Z, Dennis B, Lautenbach D, Kavanagh O, Bawor M, Banfield L, Profetto J: Digital rectal examination for prostate cancer screening in primary care: A systematic review and Meta-Analysis. *ANN FAM MED* 2018;16:149-154.
- 26 Harvey CJ, Pilcher J, Richenberg J, Patel U, Frauscher F: Applications of transrectal ultrasound in prostate cancer. *Br J Radiol* 2012;85 Spec No 1:S3-S17.
- 27 Weinreb JC, Barentsz JO, Choyke PL, Cornud F, Haider MA, Macura KJ, Margolis D, Schnall MD, Shtern F, Tempany CM, Thoeny HC, Verma S: PI-RADS Prostate Imaging – Reporting and Data System: 2015, Version 2. *EUR UROL* 2016;69:16-40.
- 28 Turkbey B, Rosenkrantz AB, Haider MA, Padhani AR, Villeirs G, Macura KJ, Tempany CM, Choyke PL, Cornud F, Margolis DJ, Thoeny HC, Verma S, Barentsz J, Weinreb JC: Prostate Imaging Reporting and Data System Version 2.1: 2019 Update of Prostate Imaging Reporting and Data System Version 2. *EUR UROL* 2019;76:340-351.
- 29 Stabile A, Giganti F, Rosenkrantz AB, Taneja SS, Villeirs G, Gill IS, Allen C, Emberton M, Moore CM, Kasivisvanathan V: Multiparametric MRI for prostate cancer diagnosis: Current status and future directions. *NAT REV UROL* 2020;17:41-61.
- 30 Elabbady AA, Khedr MM: Extended 12-Core prostate biopsy increases both the detection of prostate cancer and the accuracy of gleason score. *EUR UROL* 2006;49:49-53.
- 31 Eskicorapci SY, Baydar DE, Akbal C, Sofikerim M, Günay M, Ekici S, Ozen H: An extended 10-Core transrectal ultrasonography guided prostate biopsy protocol improves the detection of prostate cancer. *EUR UROL* 2004;45:444-449.

- 32 Kasivisvanathan V, Jichi F, Klotz L, Villers A, Taneja SS, Punwani S, Freeman A, Emberton M, Moore CM: A multicentre randomised controlled trial assessing whether MRI-targeted biopsy is non-inferior to standard transrectal ultrasound guided biopsy for the diagnosis of clinically significant prostate cancer in men without prior biopsy: A study protocol. *BMJ OPEN* 2017;7:e17863.
- 33 Kasivisvanathan V, Stabile A, Neves JB, Giganti F, Valerio M, Shanmugabavan Y, Clement KD, Sarkar D, Philippou Y, Thurtle D, Deeks J, Emberton M, Takwoingi Y, Moore CM: Magnetic resonance imaging-targeted biopsy versus systematic biopsy in the detection of prostate cancer: A systematic review and meta-analysis. *EUR UROL* 2019;76:284-303.
- 34 Epstein JI, Egevad L, Amin MB, Delahunt B, Srigley JR, Humphrey PA: The 2014 international society of urological pathology (ISUP) consensus conference on gleason grading of prostatic carcinoma: Definition of grading patterns and proposal for a new grading system. *AM J SURG PATHOL* 2016;40:244-252.
- 35 Berney DM, Beltran L, Fisher G, North BV, Greenberg D, Møller H, Soosay G, Scardino P, Cuzick J, On BOTT: Validation of a contemporary prostate cancer grading system using prostate cancer death as outcome. *BRIT J CANCER* 2016;114:1078-1083.
- 36 Even-Sapir E, Metser U, Mishani E, Lievshitz G, Lerman H, Leibovitch I: The detection of bone metastases in patients with high-risk prostate cancer: 99mTc-MDP Planar bone scintigraphy, single- and multi-field-of-view SPECT, 18F-fluoride PET, and 18F-fluoride PET/CT. *J NUCL MED* 2006;47:287-297.
- 37 Papatthanassiou D, Bruna-Muraille C, Jouannaud C, Gagneux-Lemoussu L, Eschard JP, Liehn JC: Single-photon emission computed tomography combined with computed tomography (SPECT/CT) in bone diseases. *JOINT BONE SPINE* 2009;76:474-480.
- 38 Langsteger W, Rezaee A, Pirich C, Beheshti M: 18F-NaF-PET/CT and 99mTc-MDP bone scintigraphy in the detection of bone metastases in prostate cancer. *SEMIN NUCL MED* 2016;46:491-501.
- 39 Jones T, Townsend D: History and future technical innovation in positron emission tomography. *J Med Imaging (Bellingham)* 2017;4:11013.
- 40 Waxman A, Ozawa Y: 2 - Nuclear Medicine Imaging in Thoracic Surgery; in Lewis MI, McKenna RJ, Falk JA, Chaux GE (eds): *Medical Management of the Thoracic Surgery Patient*. Philadelphia, W.B. Saunders, 2010, pp 30-59.
- 41 Chan T: Computerized method for automatic evaluation of lean body mass from PET/CT: Comparison with predictive equations. *J NUCL MED* 2012;53:130-137.
- 42 Ghosh A, Heston WDW: Tumor target prostate specific membrane antigen (PSMA) and its regulation in prostate cancer. *J CELL BIOCHEM* 2004;91:528-539.
- 43 Chang SS, Reuter VE, Heston WD, Bander NH, Grauer LS, Gaudin PB: Five different anti-prostate-specific membrane antigen (PSMA) antibodies confirm PSMA expression in tumor-associated neovasculature. *CANCER RES* 1999;59:3192-3198.
- 44 Sterzing F, Kratochwil C, Fiedler H, Katayama S, Habl G, Kopka K, Afshar-Oromieh A, Debus J, Haberkorn U, Giesel FL: ⁶⁸Ga-PSMA-11 PET/CT: A new technique with high potential for the radiotherapeutic management of prostate cancer patients. *EUR J NUCL MED MOL I* 2016;43:34-41.
- 45 Eiber M, Maurer T, Souvatzoglou M, Beer AJ, Ruffani A, Haller B, Graner FP, Kubler H, Haberkorn U, Eisenhut M, Wester HJ, Gschwend JE, Schwaiger M: Evaluation of hybrid ⁶⁸Ga-PSMA ligand

- PET/CT in 248 patients with biochemical recurrence after radical prostatectomy. *J NUCL MED* 2015;56:668-674.
- 46 Wallitt KL, Khan SR, Dubash S, Tam HH, Khan S, Barwick TD: Clinical PET imaging in prostate cancer. *RADIOGRAPHICS* 2017;37:1512-1536.
- 47 Lindenberg L, Choyke P, Dahut W: Prostate cancer imaging with novel PET tracers. *CURR UROL REP* 2016;17:18.
- 48 Afshar-Oromieh A, Haberkorn U, Schlemmer HP, Fenchel M, Eder M, Eisenhut M, Hadaschik BA, Kopp-Schneider A, Röthke M: Comparison of PET/CT and PET/MRI hybrid systems using a ^{68}Ga -labelled PSMA ligand for the diagnosis of recurrent prostate cancer: Initial experience. *EUR J NUCL MED MOL I* 2014;41:887-897.
- 49 Hodge KK, McNeal JE, Terris MK, Stamey TA: Random systematic versus directed ultrasound guided transrectal core biopsies of the prostate. *J Urol* 1989;142:71-74, 74-75.
- 50 Zhao J, Mangarova DB, Brangsch J, Kader A, Hamm B, Brenner W, Makowski MR: Correlation between Intraprostatic PSMA Uptake and MRI PI-RADS of [^{68}Ga]Ga-PSMA-11 PET/MRI in Patients with Prostate Cancer: Comparison of PI-RADS Version 2.0 and PI-RADS Version 2.1. *CANCERS* 2020;12:3523.
- 51 Zhao J, Hamm B, Brenner W, Makowski MR: Lesion-to-background ratio threshold value of SUVmax of simultaneous [^{68}Ga]Ga-PSMA-11 PET/MRI imaging in patients with prostate cancer. *Insights into Imaging* 2020;11:137.
- 52 Zhao J, Kader A, Mangarova DB, Brangsch J, Brenner W, Hamm B, Makowski MR: Dynamic Contrast-Enhanced MRI of Prostate Lesions of Simultaneous [^{68}Ga]Ga-PSMA-11 PET/MRI: Comparison between Intraprostatic Lesions and Correlation between Perfusion Parameters. *CANCERS* 2021;13:1404.
- 53 Hamm B, Asbach P: Magnetic resonance imaging of the prostate in the PI-RADS era. 2018:99-115.
- 54 Rosenkrantz AB, Babb JS, Taneja SS, Ream JM: Proposed Adjustments to PI-RADS Version 2 Decision Rules: Impact on Prostate Cancer Detection. *RADIOLOGY* 2017;283:119-129.
- 55 Barrett T, Rajesh A, Rosenkrantz AB, Choyke PL, Turkbey B: PI-RADS version 2.1: One small step for prostate MRI. *CLIN RADIOL* 2019;74:841-852.
- 56 Giesel FL, Fiedler H, Stefanova M, Sterzing F, Rius M, Kopka K, Moltz JH, Afshar-Oromieh A, Choyke PL, Haberkorn U, Kratochwil C: PSMA PET/CT with Glu-urea-Lys-(Ahx)-[^{68}Ga (HBED-CC)] versus 3D CT volumetric lymph node assessment in recurrent prostate cancer. *EUR J NUCL MED MOL I* 2015;42:1794-1800.
- 57 Woythal N, Arsenic R, Kempkensteffen C, Miller K, Janssen J, Huang K, Makowski MR, Brenner W, Prasad V: Immunohistochemical validation of PSMA expression measured by ^{68}Ga -PSMA PET/CT in primary prostate cancer. *J NUCL MED* 2018;59:238-243.
- 58 Landis JR, Koch GG: The measurement of observer agreement for categorical data. *BIOMETRICS* 1977;33:159-174.
- 59 Fedorov A, Beichel R, Kalpathy-Cramer J, Finet J, Fillion-Robin J, Pujol S, Bauer C, Jennings D, Fennessy F, Sonka M, Buatti J, Aylward S, Miller JV, Pieper S, Kikinis R: 3D Slicer as an image computing platform for the Quantitative Imaging Network. *MAGN RESON IMAGING* 2012;30:1323-1341.

- 60 Stoyanova R, Takhar M, Tschudi Y, Ford JC, Solórzano G, Erho N, Balagurunathan Y, Punnen S, Davicioni E, Gillies RJ, Pollack A: Prostate cancer radiomics and the promise of radiogenomics. *TRANSL CANCER RES* 2016;5:432-447.
- 61 Stanzione A, Gambardella M, Cuocolo R, Ponsiglione A, Romeo V, Imbriaco M: Prostate MRI radiomics: A systematic review and radiomic quality score assessment. *EUR J RADIOL* 2020;129:109095.
- 62 Smith CP, Czarniecki M, Mehralivand S, Stoyanova R, Choyke PL, Harmon S, Turkbey B: Radiomics and radiogenomics of prostate cancer. *ABDOM RADIOL* 2019;44:2021-2029.
- 63 Maurer T, Eiber M, Schwaiger M, Gschwend JE: Current use of PSMA–PET in prostate cancer management. *NAT REV UROL* 2016;13:226-235.
- 64 Wright GJ, Haley C, Beckett ML, Schellhammer PF: Expression of prostate-specific membrane antigen in normal, benign, and malignant prostate tissues. *Urol Oncol* 1995;1:18-28.
- 65 Demirci E, Sahin OE, Ocak M, Akovali B, Nematyazar J, Kabasakal L: Normal distribution pattern and physiological variants of ⁶⁸Ga-PSMA-11 PET/CT imaging. *NUCL MED COMMUN* 2016;37:1169-1179.
- 66 Eiber M, Weirich G, Holzapfel K, Souvatzoglou M, Haller B, Rauscher I, Beer AJ, Wester H, Gschwend J, Schwaiger M, Maurer T: Simultaneous ⁶⁸Ga-PSMA HBED-CC PET/MRI improves the localization of primary prostate cancer. *EUR UROL* 2016;70:829-836.
- 67 Ben Jemaa A, Bouraoui Y, Sallami S, Banasr A, Nouira Y, Oueslati R: PSA-PSMA profiles and their impact on sera PSA levels and angiogenic activity in hyperplasia and human prostate cancer. *PATHOL BIOL* 2014;62:129-136.
- 68 Eiber M, Fendler WP, Rowe SP, Calais J, Hofman MS, Maurer T, Schwarzenboeck SM, Kratochwil C, Herrmann K, Giesel FL: Prostate-Specific membrane antigen ligands for imaging and therapy. *J NUCL MED* 2017;58:67S-76S.
- 69 Lapidus RG, Tiffany CW, Isaacs JT, Slusher BS: Prostate-specific membrane antigen (PSMA) enzyme activity is elevated in prostate cancer cells. *PROSTATE* 2000;45:350-354.
- 70 Khalifa F, Soliman A, El-Baz A, Abou EM, El-Diasty T, Gimel'Farb G, Ouseph R, Dwyer AC: Models and methods for analyzing DCE-MRI: A review. *MED PHYS* 2014;41:124301.
- 71 Folkman J: The role of angiogenesis in tumor growth. *SEMIN CANCER BIOL* 1992;3:65.
- 72 Borre M, Offersen BV, Nerstrøm B, Overgaard J: Microvessel density predicts survival in prostate cancer patients subjected to watchful waiting. *BRIT J CANCER* 1998;78:940-944.
- 73 Singanamalli A, Rusu M, Sparks RE, Shih NNC, Ziober A, Wang L, Tomaszewski J, Rosen M, Feldman M, Madabhushi A: Identifying in vivo DCE MRI markers associated with microvessel architecture and gleason grades of prostate cancer. *J MAGN RESON IMAGING* 2016;43:149-158.
- 74 van den Ouden D, Kranse R, Hop WC, van der Kwast TH, Schroder FH: Microvascular invasion in prostate cancer: Prognostic significance in patients treated by radical prostatectomy for clinically localized carcinoma. *UROL INT* 1998;60:17-24.
- 75 Sun Y, Reynolds HM, Parameswaran B, Wraith D, Finnegan ME, Williams S, Haworth A: Multiparametric MRI and radiomics in prostate cancer: A review. *Australas Phys Eng Sci Med* 2019;42:3-25.

- 76 Cysouw MCF, Jansen BHE, van de Brug T, Oprea-Lager DE, Pfaehler E, de Vries BM, van Moorselaar RJA, Hoekstra OS, Vis AN, Boellaard R: Machine learning-based analysis of [¹⁸F]DCFPyL PET radiomics for risk stratification in primary prostate cancer. *EUR J NUCL MED MOL I* 2021;48:340-349.
- 77 Townsend DW: Multimodality imaging of structure and function. *PHYS MED BIOL* 2008;53:R1-R39.
- 78 Ghafoor S, Burger IA, Vargas AH: Multimodality imaging of prostate cancer. *J NUCL MED* 2019;60:1350-1358.
- 79 Kader A, Brangsch J, Kaufmann JO, Zhao J, Mangarova DB, Moeckel J, Adams LC, Sack I, Taupitz M, Hamm B, Makowski MR: Molecular MR imaging of prostate cancer. *Biomedicines* 2021;9:1.
- 80 Hope TA, Goodman JZ, Allen IE, Calais J, Fendler WP, Carroll PR: Metaanalysis of ⁶⁸Ga-PSMA-11 PET accuracy for the detection of prostate cancer validated by histopathology. *J NUCL MED* 2019;60:786-793.
- 81 Hirmas N, Al-Ibraheem A, Herrmann K, Alsharif A, Muhsin H, Khader J, Al-Daghmin A, Salah S: [⁶⁸Ga]PSMA PET/CT improves initial staging and management plan of patients with High-Risk prostate cancer. *MOL IMAGING BIOL* 2019;21:574-581.
- 82 Park SY, Zacharias C, Harrison C, Fan RE, Kunder C, Hatami N, Giesel F, Ghanouni P, Daniel B, Loening AM, Sonn GA, Iagaru A: Gallium 68 PSMA-11 PET/MR Imaging in Patients with Intermediate- or High-Risk Prostate Cancer. *RADIOLOGY* 2018;288:495-505.
- 83 Westphalen AC, McCulloch CE, Anaokar JM, Arora S, Barashi NS, Barentsz JO, Bathala TK, Bittencourt LK, Booker MT, Braxton VG, Carroll PR, Casalino DD, Chang SD, Coakley FV, Dhatt R, Eberhardt SC, Foster BR, Froemming AT, Fütterer JJ, Ganeshan DM, Gertner MR, Mankowski Gettle L, Ghai S, Gupta RT, Hahn ME, Houshyar R, Kim C, Kim CK, Lall C, Margolis DJA, McRae SE, Oto A, Parsons RB, Patel NU, Pinto PA, Polascik TJ, Spilseth B, Starcevich JB, Tammisetti VS, Taneja SS, Turkbey B, Verma S, Ward JF, Warlick CA, Weinberger AR, Yu J, Zagoria RJ, Rosenkrantz AB: Variability of the positive predictive value of PI-RADS for prostate MRI across 26 centers: Experience of the society of abdominal radiology prostate cancer disease-focused panel. *RADIOLOGY* 2020;296:76-84.
- 84 Delongchamps NB, Rouanne M, Flam T, Beuvon F, Liberatore M, Zerbib M, Cornud F: Multiparametric magnetic resonance imaging for the detection and localization of prostate cancer: Combination of T2-weighted, dynamic contrast-enhanced and diffusion-weighted imaging. *BJU INT* 2011;107:1411-1418.
- 85 Hara N, Okuizumi M, Koike H, Kawaguchi M, Bilim V: Dynamic contrast-enhanced magnetic resonance imaging (DCE-MRI) is a useful modality for the precise detection and staging of early prostate cancer. *The Prostate* 2005;62:140-147.
- 86 Chen Y, Chu W, Pu Y, Chueh S, Shun C, Tseng WI: Washout gradient in dynamic contrast-enhanced MRI is associated with tumor aggressiveness of prostate cancer. *J MAGN RESON IMAGING* 2012;36:912-919.
- 87 Lissbrant IF, Stattin P, Damber JE, Bergh A: Vascular density is a predictor of cancer-specific survival in prostatic carcinoma. *PROSTATE* 1997;33:38-45.
- 88 de la Taille A, Katz AE, Bagiella E, Buttyan R, Sharir S, Olsson CA, Burchardt T, Ennis RD, Rubin MA: Microvessel density as a predictor of PSA recurrence after radical prostatectomy. A comparison of CD34 and CD31. *AM J CLIN PATHOL* 2000;113:555-562.

-
- 89 Tan CH, Hobbs BP, Wei W, Kundra V: Dynamic contrast-enhanced MRI for the detection of prostate cancer: Meta-analysis. *AJR Am J Roentgenol* 2015;204:W439-W448.
- 90 van Niekerk CG, van der Laak JAWM, Hambrock T, Huisman H, Witjes JA, Barentsz JO, de Kaa CAH: Correlation between dynamic contrast-enhanced MRI and quantitative histopathologic microvascular parameters in organ-confined prostate cancer. *EUR RADIOL* 2014;24:2597-2605.
- 91 Miller JC, Pien HH, Sahani D, Sorensen AG, Thrall JH: Imaging angiogenesis: Applications and potential for drug development. *JNCI Journal of the National Cancer Institute* 2005;97:172-187.
- 92 Yi B, Kang DK, Yoon D, Jung YS, Kim KS, Yim H, Kim TH: Is there any correlation between model-based perfusion parameters and model-free parameters of time-signal intensity curve on dynamic contrast enhanced MRI in breast cancer patients? *EUR RADIOL* 2014;24:1089-1096.
- 93 Lu H, Parra NA, Qi J, Gage K, Li Q, Fan S, Feuerlein S, Pow-Sang J, Gillies R, Choi JW, Balagurunathan Y: Repeatability of quantitative imaging features in prostate magnetic resonance imaging. *FRONT ONCOL* 2020;10:551.
- 94 Woźnicki P, Westhoff N, Huber T, Riffel P, Froelich MF, Gresser E, von Hardenberg J, Mühlberg A, Michel MS, Schoenberg SO, Nörenberg D: Multiparametric MRI for prostate cancer characterization: Combined use of radiomics model with PI-RADS and clinical parameters. *CANCERS* 2020;12:1767.

Statutory declaration

“I, Jing Zhao, by personally signing this document in lieu of an oath, hereby affirm that I prepared the submitted dissertation on the topic [Evaluation of prostatic lesions by simultaneous [⁶⁸Ga]Ga-PSMA-11 PET/MRI, Bewertung von prostatistischen Läsionen durch simultane [⁶⁸Ga]Ga-PSMA-11 PET/MRT], independently and without the support of third parties, and that I used no other sources and aids than those stated.

All parts which are based on the publications or presentations of other authors, either in letter or in spirit, are specified as such in accordance with the citing guidelines. The sections on methodology (in particular regarding practical work, laboratory regulations, statistical processing) and results (in particular regarding figures, charts and tables) are exclusively my responsibility.

Furthermore, I declare that I have correctly marked all of the data, the analyses, and the conclusions generated from data obtained in collaboration with other persons, and that I have correctly marked my own contribution and the contributions of other persons (cf. declaration of contribution). I have correctly marked all texts or parts of texts that were generated in collaboration with other persons.

My contributions to any publications to this dissertation correspond to those stated in the below joint declaration made together with the supervisor. All publications created within the scope of the dissertation comply with the guidelines of the ICMJE (International Committee of Medical Journal Editors; www.icmje.org) on authorship. In addition, I declare that I shall comply with the regulations of Charité – Universitätsmedizin Berlin on ensuring good scientific practice.

I declare that I have not yet submitted this dissertation in identical or similar form to another Faculty.

The significance of this statutory declaration and the consequences of a false statutory declaration under criminal law (Sections 156, 161 of the German Criminal Code) are known to me.”

Date

Signature

Declaration of own contribution to the publications

Jing Zhao contributed the following to the below listed publications:

Publication 1: Zhao J, Hamm B, Brenner W, Makowski MR: Lesion-to-background ratio threshold value of SUVmax of simultaneous [⁶⁸Ga]Ga-PSMA-11 PET/MRI imaging in patients with prostate cancer. *Insights into Imaging* 2020;11:137.

Contribution: Studied ideas and formulated research questions. Developed and designed methodology. Performed the experiments, acquired, analyzed, and interpreted data. Prepared all figures and tables, drafted the manuscript, made critical revisions of the manuscript, corresponded to reviewer comments, approved published version.

Publication 2: Zhao J, Mangarova DB, Brangsch J, Kader A, Hamm B, Brenner W, Makowski MR: Correlation between Intraprostatic PSMA Uptake and MRI PI-RADS of [⁶⁸Ga]Ga-PSMA-11 PET/MRI in Patients with Prostate Cancer: Comparison of PI-RADS Version 2.0 and PI-RADS Version 2.1. *CANCERS* 2020;12:3523.

Contribution: Studied ideas and formulated research questions; Developed and designed methodology; Performed the experiments, acquired, analyzed, and interpreted data; Prepared all figures and tables, drafted the manuscript, made critical revisions of the manuscript; corresponded to reviewer comments, approved published version.

Publication 3: Zhao J, Kader A, Mangarova DB, Brangsch J, Brenner W, Hamm B, Makowski MR: Dynamic Contrast-Enhanced MRI of Prostate Lesions of Simultaneous [⁶⁸Ga]Ga-PSMA-11 PET/MRI: Comparison between Intraprostatic Lesions and Correlation between Perfusion Parameters. *CANCERS* 2021;13:1404.

Contribution: Studied ideas and formulated research questions; Developed and designed methodology; Performed the experiments, acquired, analyzed, and interpreted data; Prepared all figures and tables, drafted the manuscript, made critical revisions of the manuscript; corresponded to reviewer comments, approved published version.

Signature, date and stamp of first supervising university professor / lecturer

Signature of doctoral candidate

Publications

Excerpt from Journal Summary List--1

Journal Data Filtered By: **Selected JCR Year: 2019** Selected Editions: SCIE,SSCI
 Selected Categories: **"RADIOLOGY, NUCLEAR MEDICINE and MEDICAL IMAGING"** Selected Category Scheme: WoS
Gesamtanzahl: 133 Journale

Rank	Full Journal Title	Total Cites	Journal Impact Factor	Eigenfactor Score
1	JACC-Cardiovascular Imaging	10,110	12.740	0.027550
2	MEDICAL IMAGE ANALYSIS	9,028	11.148	0.017100
3	RADIOLOGY	52,731	7.931	0.057130
4	JOURNAL OF NUCLEAR MEDICINE	26,844	7.887	0.032990
5	EUROPEAN JOURNAL OF NUCLEAR MEDICINE AND MOLECULAR IMAGING	15,787	7.081	0.023630
6	IEEE TRANSACTIONS ON MEDICAL IMAGING	21,657	6.685	0.030060
7	CLINICAL NUCLEAR MEDICINE	5,042	6.587	0.006200
8	NEUROIMAGE	102,632	5.902	0.125360
9	Photoacoustics	715	5.870	0.001760
10	INTERNATIONAL JOURNAL OF RADIATION ONCOLOGY BIOLOGY PHYSICS	44,197	5.859	0.042160
11	Circulation-Cardiovascular Imaging	5,574	5.691	0.016320
12	ULTRASOUND IN OBSTETRICS & GYNECOLOGY	13,078	5.571	0.018050
13	JOURNAL OF CARDIOVASCULAR MAGNETIC RESONANCE	5,205	5.361	0.011120
14	INVESTIGATIVE RADIOLOGY	6,136	5.156	0.008830
15	RADIOGRAPHICS	12,418	4.967	0.010750
16	ULTRASCHALL IN DER MEDIZIN	2,185	4.966	0.002530
17	RADIOTHERAPY AND ONCOLOGY	17,774	4.856	0.026510
18	European Heart Journal-Cardiovascular Imaging	6,359	4.841	0.023110
19	HUMAN BRAIN MAPPING	23,094	4.421	0.042760
20	Journal of the American College of Radiology	4,409	4.268	0.010730

Rank	Full Journal Title	Total Cites	Journal Impact Factor	Eigenfactor Score
21	EUROPEAN RADIOLOGY	20,761	4.101	0.033260
22	SEMINARS IN RADIATION ONCOLOGY	2,531	4.076	0.003540
23	JOURNAL OF MAGNETIC RESONANCE IMAGING	17,046	3.954	0.024900
24	Biomedical Optics Express	11,090	3.921	0.025030
25	COMPUTERIZED MEDICAL IMAGING AND GRAPHICS	2,656	3.750	0.002940
26	JOURNAL OF DIGITAL IMAGING	2,494	3.697	0.003790
27	MAGNETIC RESONANCE IN MEDICINE	32,159	3.635	0.029700
28	Insights into Imaging	1,948	3.579	0.003260
29	INTERNATIONAL JOURNAL OF HYPERTHERMIA	4,397	3.574	0.004880
30	SEMINARS IN NUCLEAR MEDICINE	2,194	3.544	0.002420
31	AMERICAN JOURNAL OF NEURORADIOLOGY	23,135	3.381	0.027120
32	JOURNAL OF NUCLEAR CARDIOLOGY	3,600	3.366	0.004570
33	MEDICAL PHYSICS	26,445	3.317	0.027280
34	Quantitative Imaging in Medicine and Surgery	1,335	3.226	0.002800
35	NMR IN BIOMEDICINE	7,537	3.221	0.011610
36	Clinical Neuroradiology	935	3.183	0.002710
37	KOREAN JOURNAL OF RADIOLOGY	2,967	3.179	0.004490
38	Ultrasonography	618	3.075	0.001710
39	ULTRASONICS	7,808	3.065	0.008930
40	JOURNAL OF VASCULAR AND INTERVENTIONAL RADIOLOGY	9,045	3.037	0.009790
41	AMERICAN JOURNAL OF ROENTGENOLOGY	32,209	3.013	0.024770
42	Practical Radiation Oncology	1,879	2.948	0.005780

Zhao J, Hamm B, Brenner W, Makowski MR: Lesion-to-background ratio threshold value of SUVmax of simultaneous [⁶⁸Ga]Ga-PSMA-11 PET/MRI imaging in patients with prostate cancer. *Insights into Imaging* 2020;11:137.

DOI: <https://doi.org/10.1186/s13244-020-00926-y>

ORIGINAL ARTICLE

Open Access



Lesion-to-background ratio threshold value of SUVmax of simultaneous [⁶⁸Ga]Ga-PSMA-11 PET/MRI imaging in patients with prostate cancer

Jing Zhao^{1*} , Bernd Hamm¹, Winfried Brenner² and Marcus R. Makowski^{1,3}

Abstract

Purpose: This study aimed to calculate an applicable relative ratio threshold value instead of the absolute threshold value for simultaneous ⁶⁸Ga prostate-specific membrane antigen/positron emission tomography ([⁶⁸Ga]Ga-PSMA-11 PET) in patients with prostate cancer (PCa).

Materials and methods: Our study evaluated thirty-two patients and 170 focal prostate lesions. Lesions are classified into groups according to Prostate Imaging Reporting and Data System (PI-RADS). Standardized uptake values maximum (SUVmax), corresponding lesion-to-background ratios (LBRs) of SUVmax, and LBR distributions of each group were measured based on regions of interest (ROI). We examined LBR with receiver operating characteristic analysis to determine threshold values for differentiation between multiparametric magnetic resonance imaging (mpMRI)-positive and mpMRI-negative lesions.

Results: We analyzed a total of 170 focal prostate lesions. Lesions number of PI-RADS 2 to 5 was 70, 16, 46, and 38. LBR of SUVmax of each PI-RADS scores was 1.5 (0.9, 2.4), 2.5 (1.6, 3.4), 3.7 (2.6, 4.8), and 6.7 (3.5, 12.7). Based on an optimal threshold ratio of 2.5 to be exceeded, lesions could be classified into MRI-positive lesion on [⁶⁸Ga]Ga-PSMA PET with a sensitivity of 85.2%, a specificity of 72.0%, with the corresponding area under the receiver operating characteristic curve (AUC) of 0.83, $p < 0.001$. This value matches the imaging findings better.

Conclusion: The ratio threshold value of SUVmax, LBR, has improved clinical and research applicability compared with the absolute value of SUVmax. A higher threshold value than the background's uptake can dovetail the imaging findings on MRI better. It reduces the bias from using absolute background uptake value as the threshold value.

Keywords: Prostate cancer, Multiparametric MRI, PSMA, [⁶⁸Ga]Ga-PSMA PET/MRI, SUVmax

Key points

- The ratio threshold value of SUVmax, LBR, has improved clinical and research applicability compared with the absolute value of SUVmax/

- A higher threshold value than the background's uptake can dovetail the imaging findings on MRI better.
- The specificity of [⁶⁸Ga]Ga-PSMA PET needs to be further improved.

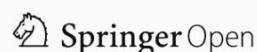
*Correspondence: jing.zhao@charite.de

¹Institute of Radiology and Nuclear Medicine, Charité – Universitätsmedizin Berlin, corporate member of Freie Universität Berlin, Humboldt-Universität zu Berlin, and Berlin Institute of Health, Charitéplatz 1, 10117 Berlin, Germany

Full list of author information is available at the end of the article

Background

Prostate cancer (PCa) is a common malignant disease in the elderly male population. Approximately 17% of patients with early prostate cancer have metastatic



© The Author(s) 2020. **Open Access** This article is licensed under a Creative Commons Attribution 4.0 International License, which permits use, sharing, adaptation, distribution and reproduction in any medium or format, as long as you give appropriate credit to the original author(s) and the source, provide a link to the Creative Commons licence, and indicate if changes were made. The images or other third party material in this article are included in the article's Creative Commons licence, unless indicated otherwise in a credit line to the material. If material is not included in the article's Creative Commons licence and your intended use is not permitted by statutory regulation or exceeds the permitted use, you will need to obtain permission directly from the copyright holder. To view a copy of this licence, visit <http://creativecommons.org/licenses/by/4.0/>.

disease. PCa is the second leading cause of cancer death in men in the western world [1].

Multiparametric magnetic resonance imaging (mpMRI) has been a clinical imaging tool for detecting primary PCa and guiding subsequent biopsy. MpMRI includes T2-weighted imaging (T2WI), diffusion-weighted imaging (DWI), apparent diffusion coefficient (ADC), and dynamic contrast-enhanced MRI (DCE-MRI). Prostate Imaging Reporting and Data System (PI-RADS) interprets results [2, 3].

PSMA is a transmembrane glycoprotein related to tumor progression and disease recurrence. PSMA over-expresses in prostate cancer cells. It is associated with PCa with higher serum prostate-specific antigen (PSA) levels and a higher Gleason score (GS) [4, 5].

Positron emission tomography (PET) images are co-registered with computed tomography (CT) scans. CT is easily acquired and widely available to provide anatomical information about the localization of PSMA-avid lesions. Previous studies suggest that [⁶⁸Ga]Ga-PSMA-11 PET/CT has a high detection rate for prostate tumors, with a sensitivity of 67–97% [6, 7]. Koerber et al. [8] and Woythal et al. [7] reported that SUVmax of PCa is higher than that of non-cancerous lesions and healthy prostate tissue. Combining [⁶⁸Ga]Ga-PSMA-11 PET and mpMRI has the potential to improve localization accuracy and diagnostic efficiency, as Zamboglou et al. proved [9]. In both studies, experts elaborated on the advantages of PET/MRI in the diagnosis of PCa.

Nevertheless, two aspects can be further optimized. First, MRI-positive lesions may show unapparent or low uptake in PET images. MRI-negative lesions may show apparent uptake in PET images. It may misdiagnose part of MRI-negative lesions as positive if we consider all apparent uptake lesions as positive in PET images. Therefore, it is necessary to increase the threshold value, which is higher than the background SUVmax.

Second, in most publications, individual research centers adopt its threshold standard to proceed with studies. The threshold standard varies from different medical centers. Hence, each study is conducted under different execution standards. Eiber et al. [10] took SUVmax higher than the background as a threshold value to prove diagnostic accuracy improvement. Woythal et al. [7] reported the best threshold value of 3.15 with sensitivity 97%, specificity 90%, and area under curve (AUC) 0.987. Donato et al. [11] described lesions as mildly avid (SUVmax < 5), moderately avid (SUVmax > 5), or intensely avid (SUVmax > 10). Hicks et al. [12] calculated a threshold of 6.7, with sensitivity 88%; specificity 96%.

However, SUVmax is affected by a specific combination of radiotracer manufacturer, systems vendor,

reconstruction techniques, uptake time, post-processing software, the time between radiotracer injection and scanning, and even the human race. Taking absolute value for research results in bias from different imaging conditions. Therefore, in our study, we used ratio value LBR to perform research.

We aimed to classify prostate lesions according to MRI morphological imaging analysis to achieve a better threshold LBR value. This LBR threshold value matches the imaging findings on MRI better. It reduces the possibility of MRI-negative lesions being misdiagnosed as positive in PET images. It reduces the bias from using absolute background uptake value as the threshold value. We also re-examined clinical follow-up information and subsequent pelvic MRI to verify whether the lesion is radiological positive or negative.

Materials and methods

Study population

This retrospective study was approved by the institutional ethics review board (EA1/060/16), and the institutional review board waived the requirement for informed consent for this retrospective analysis.

Inclusion criteria are as follows: (1) patients with biopsy-proven PCa who underwent simultaneous [⁶⁸Ga]Ga-PSMA-11 PET/MRI between January 2017 and March 2020 in our department; (2) all necessary additional information could be obtained from clinical records; (3) patients underwent pelvic MRI examination at our institution for follow-up analysis. Exclusion criteria are as follows: (1) patients who underwent prostatectomy before scanning; (2) patients whose follow-up information is not adequate.

[⁶⁸Ga]Ga-PSMA-11 PET/MRI imaging protocol

[⁶⁸Ga]Ga-PSMA-11 was synthesized using a clinical-grade ⁶⁸Ge/⁶⁸Ga radionuclide generator (Eckert & Ziegler Radiopharma GmbH, Berlin, Germany) and PSMA-HBED-CC (ABX GmbH, Radeberg, Germany) as described previously [13–15]. Patients were imaged after 83 ± 12 min after intravenous injection of a mean activity of 161.0 ± 21.4 MBq (4.4 ± 0.6 mCi) [⁶⁸Ga]Ga-PSMA-11, activity: 1.8–2.2 MBq (0.049–0.060 mCi) per kilogram bodyweight. No adverse effects were observed after the injection of [⁶⁸Ga]Ga-PSMA-11. Furosemide is injected to minimize halo artifact caused by scatter overcorrection associated with high renal and urinary tracer activity 0.5 h before the scan. Patients void urine right before the start of the examination.

Imaging was performed with a 3.0 T PET/MRI system (SIEMENS MAGNETOM Biograph mMR, Erlangen, Germany). Every patient uses the same protocol of PET and MRI scanning. The acquisition contains two parts.

First, body PET/MRI from the vertex to mid-thigh was performed with 3 min of PET acquisition in each bed position, each 24 cm. Two six-element body matrix coils placed anteriorly were used in conjunction with two posterior spine clusters to optimize the signal-to-noise ratio (SNR) in the MRI scanner. A Dixon 3D volumetric interpolated breath-hold examination (VIBE) T1-weighted MRI sequence was performed at each bed position and used for the generation of attenuation maps and anatomic allocation of the PET results. Siemens StarVIBE overcomes motion artifacts.

The second part was a dedicated MRI scan of the pelvis, followed by the reconstruction of PET data. Reconstruction was conducted with an ordered subset expectation maximization algorithm (OSEM), with 3 iterations/21 subsets, based on an x-matrix acquisition with a 4-mm Gaussian filter and relative scatter scaling. Attenuation correction was performed using the non-enhanced MRI data. Table 1 summarizes MRI imaging parameters.

Image analysis

Image analysis was performed on a Visage 7.1 Workstation (Visage Imaging GmbH, Berlin, Germany). All mpMRI images were interpreted by a board-certified radiologist with more than fifteen years without access to the PET images, following the PI-RADS criteria, version 2 [16]. The readers classified prostate focal lesions with PI-RADS scores of 2 and 3 as MRI negative, while 4 and 5 as MRI positive. The present analysis excluded PI-RADS 1 because we do not report PI-RADS 1 lesions. T2WI was used for anatomic correlation for [⁶⁸Ga]Ga-PSMA-11 PET. [⁶⁸Ga]Ga-PSMA-11 PET scans were read by a nuclear medicine specialist with more than ten years of experience, who was not aware of the MRI results. ROI was defined as a region with an abnormal signal in MRI images or avid PSMA uptake in PET images. SUVmax is measured based on ROI. Any avid focal lesion in the prostate with uptake above prostate background not attributable to physiologic radiotracer biodistribution was considered positive in [⁶⁸Ga]Ga-PSMA-11 PET.

Lesions with the same or lower uptake than background were considered negative in [⁶⁸Ga]Ga-PSMA-11 PET. Besides, background SUVmax was measured in the nearest visually defined normal tissue adjacent to a lesion as background uptake 1.0cm², a perfect circle. LBR is defined as a ratio of lesion SUVmax to background SUVmax. Readers resolved discrepancies based on a separate consensus reading. Both interpreters reviewed all imaging studies in a single session.

Statistical analysis

We classified prostate lesions into four groups according to PI-RADS from 2 to 5 and calculated the LBR of each group. Additionally, we classified LBR into four levels, including $LBR \leq 1$, $1 < LBR \leq 2$, $2 < LBR \leq 3$, $LBR > 3$, and analyzed how does LBR of each PI-RADS group distribute.

To estimate the optimal LBR threshold, we performed ROC analysis and calculation of the AUC. Youden's index defined the optimal cutoff value. Youden's index = sensitivity + specificity - 1. In order to present the threshold's effect on sensitivity and specificity, we also calculated the sensitivity and specificity corresponding to the other six thresholds, besides the optimal threshold.

Two-sided *p* values < 0.05 were considered statistically significant. All statistical analyses were performed using SPSS 25 for Windows (IBM Corp, Armonk, NY). The significance level was set to $\alpha < 0.05$. Patient demographics and clinical characteristics are summarized using descriptive statistics. Normally distributed data are reported as mean \pm SD, and non-normally distributed data are reported as medians (interquartile range, IQR Q1, Q3).

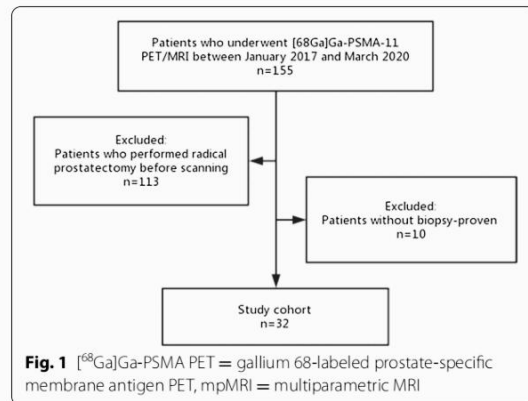
Result

Characteristics of patients

Thirty-two patients who underwent [⁶⁸Ga]Ga-PSMA-11 PET/MRI without RP were retrospectively selected from the database and included for analysis.

Table 1 Imaging parameters used for MRI

Sequence	TR/TE(msec)	FOV(mm)	Flip angle (°)	Section thickness (mm)	Voxel size (mm)
T2WI HASTE Axial	1400.0/95.0	400	160	5.0	1.3 × 1.3 × 5.0
T1WI FS VIBE	1600.0/96.0	350	160	4.0	1.1 × 1.1 × 4.0
T2WI Axial	5500.0/103.0	180	150	3.0	0.5 × 0.5 × 3.0
T2WI Sagittal	1600.0/96.0	350	160	4.0	1.1 × 1.1 × 4.0
T2WI Coronal	4500.0/102.0	200	173	3.0	0.4 × 0.4 × 3.0
DWI	11,600.0/70.0	280		3.0	2.5 × 2.5 × 3.0
T1WI FSTWIST dynamic	7.41/3.30	260	12	3.5	1.4 × 1.4 × 3.5
T1WI STARVIBE	3.71/1.77	360	9	1.2	1.1 × 1.1 × 1.2

**Table 2** Summary of patient characteristics

Parameter	Value
No. of patients	32
Age (yr.)	70 ± 7
PSA level (ng/mL)	11.45 (5.67, 24.36)
Clinical T stage	
T2a	2
T2b	2
T2c	3
T3a	8
T3b	8
T4	9
Biopsy GS	
6	4
7	
3+4	7
4+3	5
8	9
9	
4+5	2
5+4	3
10	2

The PSA level of these patients was 11.45 (5.67–24.36) ng/mL. Figure 1 shows patients' inclusion and exclusion in the flowchart. Demographics are given in Table 2.

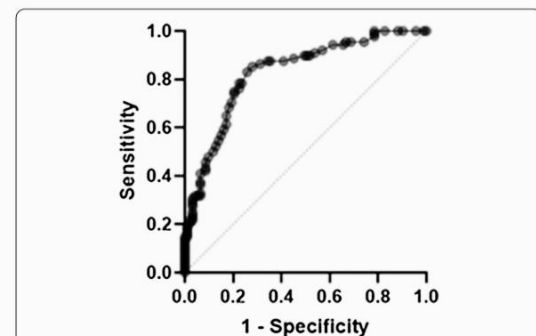
Corresponding LBR analysis

A total of 170 focal prostate lesions were detected. PI-RADS score was 2 in 70 lesions (70/170) with LBR of 1.5 (0.9, 2.4); 3 in 16 lesions (16/170) with LBR of 2.5

Table 3 LBR distribution of each PI-RADS score group

PI-RADS	LBR ≤ 1	1 < LBR ≤ 2	2 < LBR ≤ 3	LBR > 3
2	31	30	22	17
3	12	19	31	38
4	4	10	23	63
5	5	5	3	87

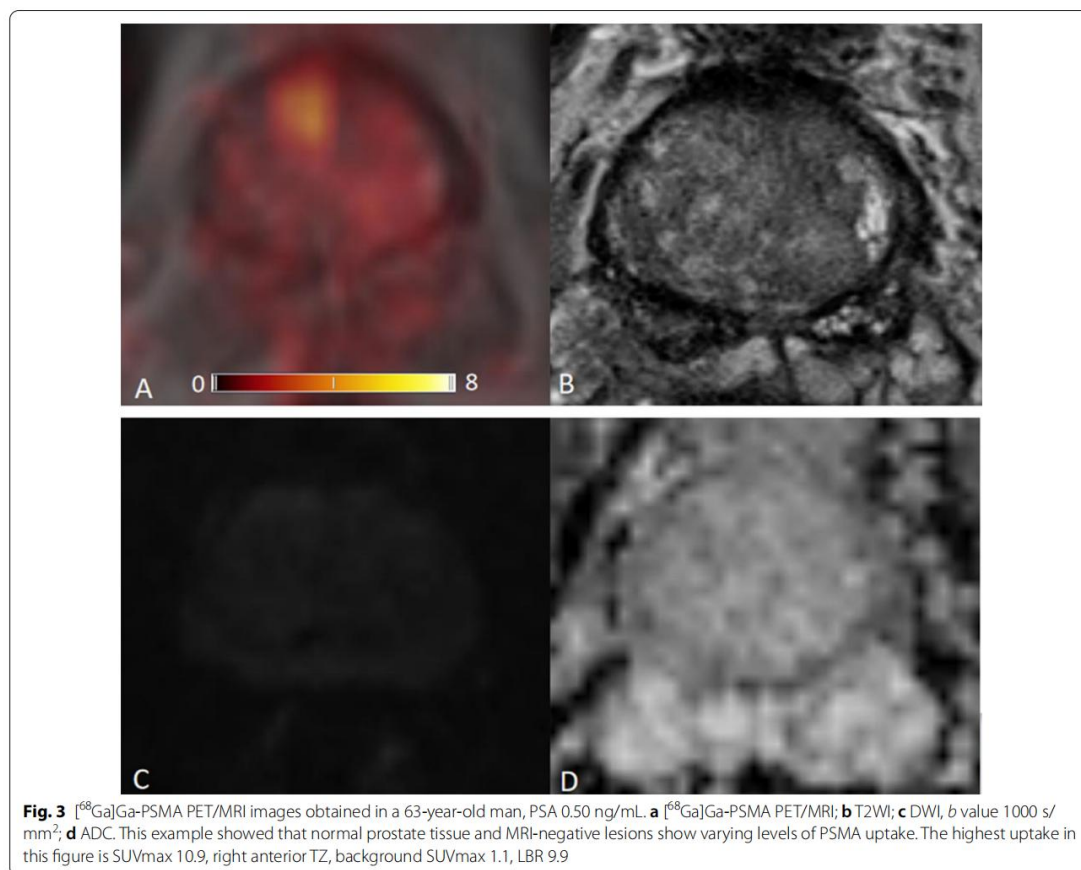
Data are described in percentage (%)

**Fig. 2** Receiver operating characteristic curves generated with a generalized linear model of LBR for ^{68}Ga]Ga-PSMA PET. With the generalized linear model estimate, AUC for ^{68}Ga]Ga-PSMA PET was 0.83, 95% CI (0.77, 0.89), 85.2% sensitivity, 72.0% specificity, $p < 0.001$

(1.6, 3.4); 4 in 46 lesions (46/170) with LBR of 3.7 (2.6, 4.8); and 5 in 38 lesions (38/170) with LBR of 6.7 (3.5, 12.7). LBR was classified into four levels, including LBR ≤ 1, 1 < LBR ≤ 2, 2 < LBR ≤ 3, and LBR > 3. Table 3 gives the distribution of each PI-RADS score group.

The ROC for ^{68}Ga]Ga-PSMA-11 PET and lesion validation results are shown in Fig. 2. The corresponding AUC for ^{68}Ga]Ga-PSMA-11 PET was 0.83, 95% confidence interval (CI) (0.77, 0.89), with an optimal LBR threshold of 2.5 (85.2% sensitivity, 72.0% specificity), $p < 0.001$. Figure 3 provides an example of MRI-negative lesions and normal prostate tissue present varying levels of PSMA uptake in ^{68}Ga]Ga-PSMA-11 PET. Figure 4 provides an example illustrating that MRI-positive lesions present apparent or unapparent radiotracer uptake in ^{68}Ga]Ga-PSMA-11 PET. Figure 5 provides an example of MRI-negative lesions, a typical encapsulated nodule with unapparent radiotracer uptake in ^{68}Ga]Ga-PSMA-11 PET. Figure 6 provides an example of MRI-positive lesions, PI-RADS 4, with apparent PSMA uptake in ^{68}Ga]Ga-PSMA-11 PET.

We also calculated the sensitivity and specificity corresponding to the other six thresholds, besides the optimal threshold, to present the threshold's effect on sensitivity, specificity, and Youden's index, summarized in Table 4.



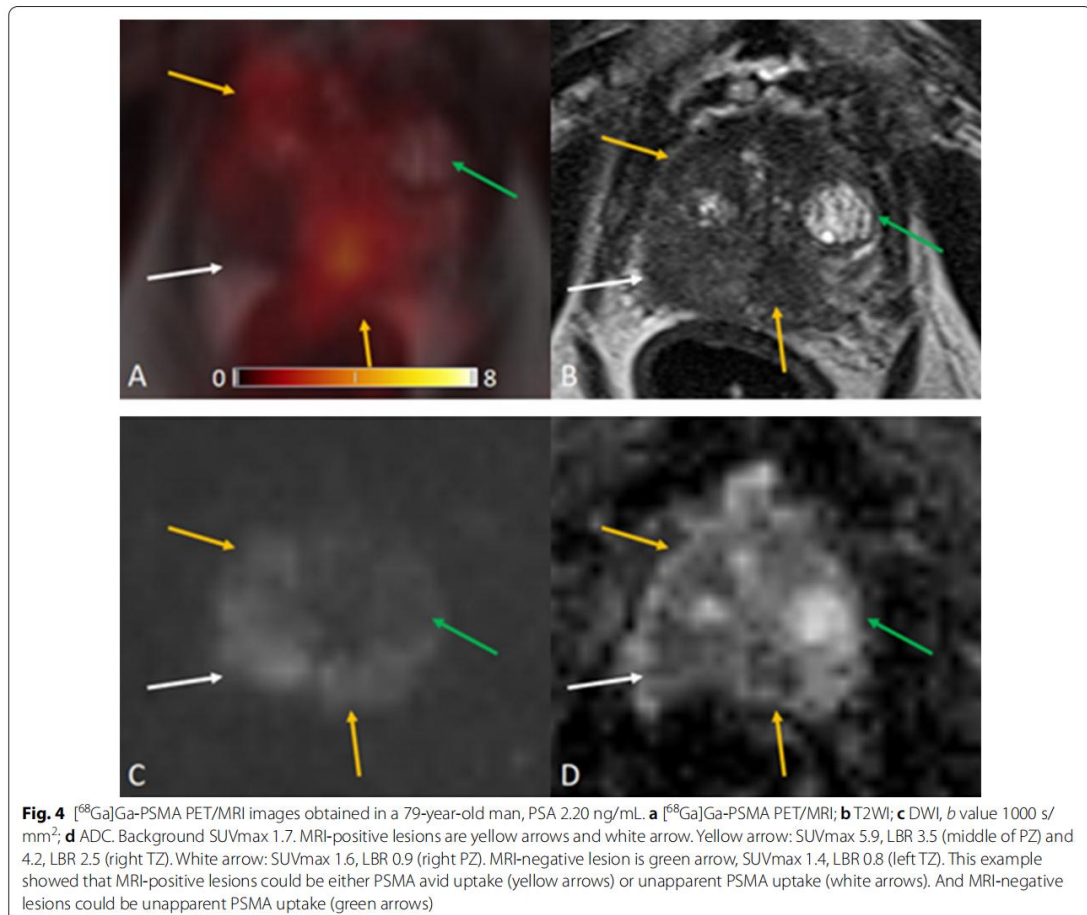
Discussion

Our study shows that [⁶⁸Ga]Ga-PSMA-11 PET presents high sensitivity of detecting prostate lesions. However, part of MRI-negative lesions show higher SUVmax than background SUVmax. It could lead to an over-diagnose of MRI-negative lesions and low specificity. A higher threshold value of [⁶⁸Ga]Ga-PSMA-11 PET is needed instead of background uptake. To improve the clinical applicability of our study, we calculated lesion-to-background ratios, a relative ratio. In our study, the threshold LBR of 2.5 achieves a better clinical and research applicability to classify positive and negative lesions of [⁶⁸Ga]Ga-PSMA-11 PET study.

We analyzed 32 patients with prostate cancer undergoing [⁶⁸Ga]Ga-PSMA-11 PET/MRI. The accuracy of imaging examinations plays a crucial role in diagnosing prostate focal lesions. In our study, LBR revealed the comparison of lesion uptake and background uptake in PET images. $LBR \leq 1$ means that lesion uptake is lower or

equal to background uptake, as well as negative in [⁶⁸Ga]Ga-PSMA-11 PET. $LBR > 1$ represents that lesion uptake is higher than background uptake, as well as positive on [⁶⁸Ga]Ga-PSMA-11 PET. The higher the ratio, the greater the tendency of a lesion to be PET positive. In the prostate, increased expression of PSMA receptors is not characteristic only of prostate cancer cells, but may also occur in normal prostate cells or non-cancerous lesions such as benign prostatic hyperplasia (BPH), as shown in Fig. 3. Our [⁶⁸Ga]Ga-PSMA-11 PET findings showed that MRI-negative focal lesions might also show a certain degree of PSMA uptake. While some of MRI-positive lesions showed unapparent or mild in PSMA PET, the majority MRI-positive lesions exhibited moderate to strong PSMA avidity, as shown in Fig. 4.

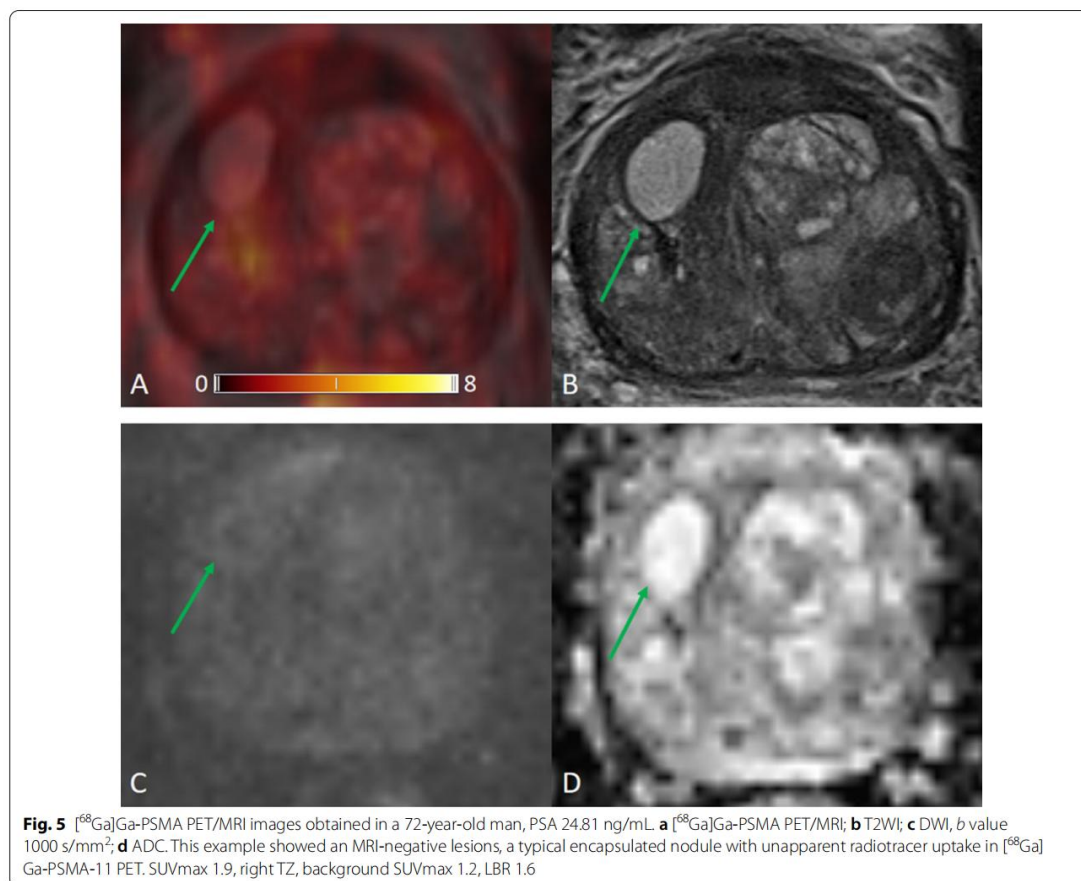
Our lesion-based LBR analysis shows that higher LBR of SUVmax tends to indicate a higher likelihood of malignancy. The higher the PI-RADS score lesions group, the more significant the proportion of $LBR > 3$. Hence, taking



prostate background SUVmax as a threshold value to identify PET positive or negative is relatively low. Our results suggest that the use of prostate background's SUVmax as a threshold value for differentiating MRI negative from MRI-positive prostate lesions can cause in a relevant number of false-positive cases. LBR is defined as a ratio of lesion SUVmax to background SUVmax. For metastasis, background SUVmax is the uptake value of nearby normal tissue, including normal bone tissue and normal soft tissue. These normal tissues usually do not show PSMA avid uptake. The background SUVmax of metastasis is relatively low. The difference between lesions and background is more pronounced. Therefore, the optimal LBR threshold of 2.5 can also be used for metastasis.

Both mpMRI and ^{68}Ga]Ga-PSMA-11 PET/CT have been widely used imaging techniques in detecting

prostate cancer. Earlier studies have revealed the usefulness of ^{68}Ga]Ga-PSMA-11 PET to detect prostate lesions patients. Hope et al. performed a meta-analysis of ^{68}Ga]Ga-PSMA-11 PET accuracy for the detection of PCa and demonstrated a sensitivity and specificity of 0.74 [17]. Hirmas et al. reported high performance for the detection of lymph node metastasis and bone metastasis. It revealed a significantly higher concordance rate of 90%, compared to the bone scan of 75%, MRI of 73%, and CT of 60% [18]. The benefit of it is a comprehensive scanning range and high sensitivity, and ^{68}Ga]Ga-PSMA-11 PET is widely used to achieve accurate staging and post-treatment efficacy evaluation. Therefore, more extensive use of ^{68}Ga]Ga-PSMA-11 PET shortens the time of prostate metastatic lesion detection and improves clinical decision-making.



MRI brings valuable superiority over $[^{68}\text{Ga}]\text{Ga-PSMA-11}$ PET/CT because of the high soft-tissue contrast and provides the advantages of functional MRI techniques, as Hoeks et al. [19] demonstrated. Some attempts have been made to provide a multimodality approach. Park et al. [20] found that $[^{68}\text{Ga}]\text{Ga-PSMA-11}$ PET can be used to identify prostate cancer, while MR imaging provides detailed anatomic guidance. Therefore, $[^{68}\text{Ga}]\text{Ga-PSMA-11}$ PET/MRI imaging provides valuable diagnostic information and may inform the need for and extent of pelvic node dissection. Domachevsky et al. [21] proved that pelvic $[^{68}\text{Ga}]\text{Ga-PSMA-11}$ PET/MRI is superior to whole-body $[^{68}\text{Ga}]\text{Ga-PSMA-11}$ PET/CT in detecting extensions of localized disease. It is mainly due to the high soft-tissue resolution of MRI, by comparing between pelvic $[^{68}\text{Ga}]\text{Ga-PSMA-11}$ PET/MRI and whole-body $[^{68}\text{Ga}]\text{Ga-PSMA-11}$ PET/CT for the initial evaluation of prostate cancer. Abd-Alazeez et al. [22] studied the added value of apparent diffusion coefficient maps

and dynamic contrast-enhanced images for the detection of radio recurrent prostate cancer and proved that MRI could evaluate recurrent or residual disease. $[^{68}\text{Ga}]\text{Ga-PSMA-11}$ PET/MRI has also been used to detect metastasis. Kranzbühler et al. [23] reported the usage of $[^{68}\text{Ga}]\text{Ga-PSMA-11}$ PET/MRI-positive peritoneal metastasis in the falciform ligament in recurrent prostate cancer. In conclusion, the development of MRI technology has dramatically improved the diagnostic accuracy of prostate cancer.

Nevertheless, PI-RADS is not perfect yet. Westphalen et al. critically evaluated the PI-RADS interpretation in 26 centers and reported that the positive predictive value of PI-RADS varied widely across centers [24]. The reason is that the efficacy of PI-RADS is generally related to the personal experience of physicians in practical application. Urologists and radiologists are still working on further optimizing the scoring system. Therefore, it is necessary to use a multimodality quantitative analysis to

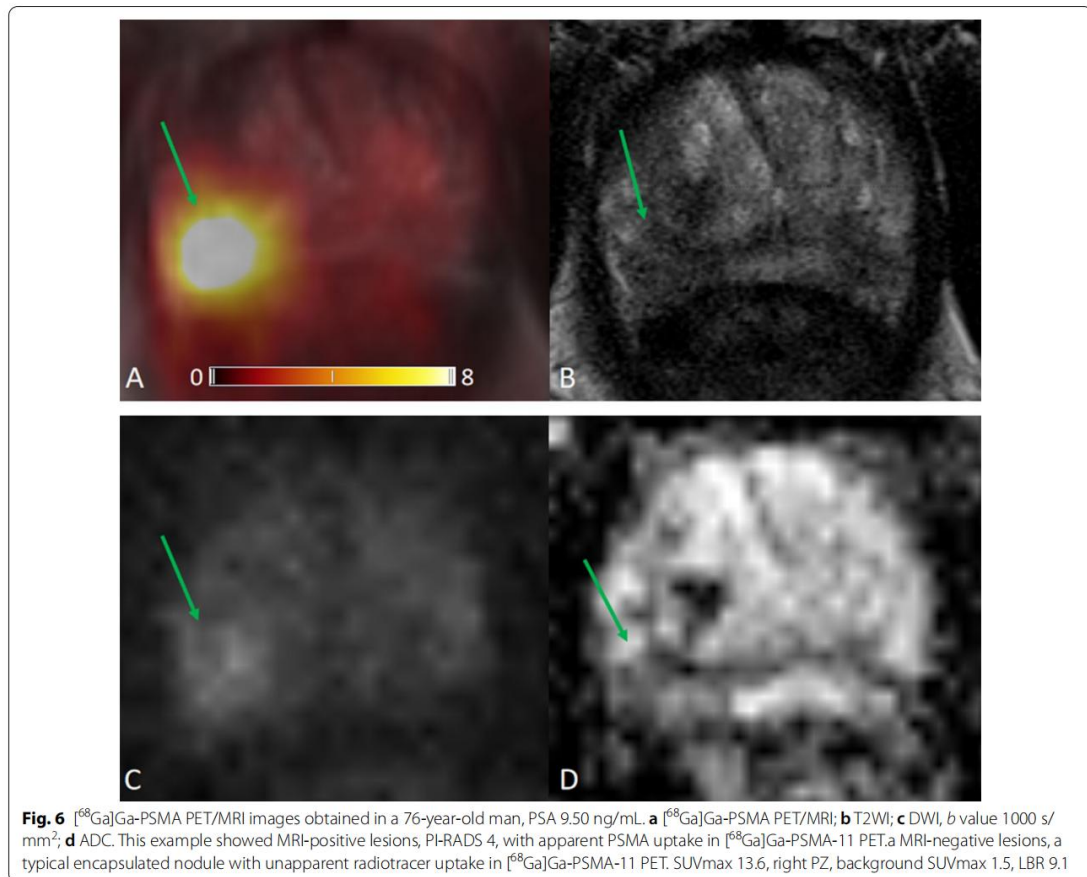


Table 4 Summary of sensitivity and specificity of thresholds

Threshold	Sensitivity	Specificity	Youden's index
1.0	95.5%	31.2%	0.267
1.5	92.0%	43.0%	0.350
2.0	88.6%	54.8%	0.434
2.5	85.2%	72.0%	0.572
3.0	73.9%	79.6%	0.535
3.5	61.4%	82.8%	0.442
4.0	50.0%	88.2%	0.382

Bold value indicates the largest Youden's index value

provide more information on diagnosis. For the interpretation of PET images, a five-point ordinal scale, Likert-scale can be utilized with a score of 1, meaning PCa was highly unlikely and a score of 5, meaning PCa was highly likely. For interpretation of PET and PET/MRI images in

PCa lesions, we may consider LBR lower than 1 as highly unlikely, LBR between 1 and 2 as unlikely, respectively, LBR between 2 and 3 as equivocal, LBR higher than 3 as likely, respectively, and LBR higher than 4 as highly likely.

Afshar-Oromieh et al. and Guberina et al. have proved ^{68}Ga Ga-PSMA-11 PET/MRI could be the ideal imaging modality for staging PCa and clarify unclear findings on PET/CT [25, 26]. Uslu-Besli et al. demonstrated that SUV and ADC values are inversely correlated in primary prostate lesions. They combined both values' usage to increase the diagnostic accuracy of hybrid PET/MRI in the detection of primary prostate lesions and lymph node metastasis [27]. Park et al. studied patients with intermediate- or high-risk cancer. They proved that ^{68}Ga Ga-PSMA-11 can be used to identify prostate cancer, while MR imaging provides detailed anatomic guidance [20]. In terms of tumor severity and evaluation of extracapsular and seminal vesicular invasion, the results of ^{68}Ga Ga-PSMA-11 PET were encouraging. These parameters

are significant considerations in treatment planning. If none of these findings exist, surgery can be performed. von Klot et al. studied that men who retain extracapsular extension may not undergo nerve-sparing surgical techniques. It leads to an increased risk of urinary incontinence and erectile dysfunction after prostatectomy [28]. These factors also have a profound impact on prognosis because both extracapsular extension and seminal vesicle invasion are associated with an increased risk of recurrence and lymph node and bone metastasis.

Because of the high sensitivity of PSMA, it is easier to detect hidden residual and recurrent focals [5, 22, 23, 25, 26, 29–32]. ^{68}Ga PSMA PET was superior to MRI in determining distant metastasis in patients with moderate- to high-risk PCa. As Roach et al. and Calais et al. demonstrated, this method becomes more widely used in clinical settings. Many patients with N0 or M0 staging, as assessed by current imaging, will more accurately stage N1 or M1 [33, 34]. The success of conventional imaging staging depends on whether the scanning range can fully cover the relevant parts. Preconditioning staging of ^{68}Ga PSMA PET may be established as it scans the whole body.

However, ^{68}Ga PSMA PET/MRI still has some drawbacks to overcome. First, hybrid PET/MRI is high-cost equipment. Many medical centers are not able to perform PET/MRI scanning before patients had RP. ^{68}Ga PSMA PET/CT is relatively affordable equipment for medical centers and an affordable examination for patients, compared to PET/MRI. Doctors take ^{68}Ga PSMA PET/CT as a regular examination for primary staging before performing radical prostatectomy. In this condition, there are more studies on ^{68}Ga PSMA PET/CT. These researches can take radical prostatectomy specimens as the reference standard to perform lesion by lesion study. Chen et al. retrospectively enrolled patients who underwent both MRI and PET/CT before radical prostatectomy and analyzed the molecular imaging PSMA expression score and the pathologic results [35].

Second, ^{68}Ga PSMA PET/MRI needs a more extended scanning protocol than ^{68}Ga PSMA-11 PET/CT. During the scanning process, the MRI device emits a harsh noise. Although technicians adopt sound insulation solutions to patients, they still cannot eliminate the interference from noise to patients. The patient needs to keep the body stable and immobile during the entire scan.

Third, although ^{68}Ga PSMA-11 has been one of the milestone discovery in the development of nuclear medicine in recent decades, which significantly improves the accuracy of prostate cancer diagnosis and assessment. Its specificity still could be further enhanced. Optimizing

the targeting specificity of molecular probes is one of the most important methods. We hope that this problem will be solved in the future.

In the end, ^{68}Ga PSMA-11 PET/MRI is widely used for staging reevaluation with recurrent prostate cancer after radical prostatectomy or to evaluate the conditions of patients who have already been treated by non-surgical therapies. Radical prostatectomy and prostate biopsies are invasive procedures with a high risk of focal hemorrhages and infection. PCa patients are mostly elderly men, with some underlying disease or age-related diseases that are not recommended to perform a pathological examination under this situation. To some extent, histopathological examination is not often feasible due to ethical and practical reasons.

Limitations

The limitation of our retrospective analysis is that ^{68}Ga PSMA-11 PET/MRI is not compared with full histopathology examination because our cohort patients are elderly male and were not feasible to perform RP. Therefore, this analysis is a descriptive radiological imaging features study.

Conclusion

The ratio threshold value of SUVmax, LBR, has improved clinical and research applicability compared with the absolute value of SUVmax. A higher threshold value than the background's uptake is capable of dovetailing the imaging findings on MRI better. The specificity of ^{68}Ga PSMA PET needs to be further improved by optimizing the targeting specificity of molecular probes.

Abbreviations

ADC: Apparent diffusion coefficient; CI: Confidence interval; CT: Computed tomography; DCE-MRI: Dynamic contrast-enhanced MRI; DWI: Diffusion-weighted imaging; FOV: Field-of-view; Ga: Gallium; GS: Gleason score; IQR: Interquartile range; mpMRI: Multiparametric magnetic resonance imaging; MRI: Magnetic resonance imaging; OSEM: Ordered subset expectation maximization algorithm; PCa: Prostate cancer; PET/CT: Positron emission tomography/computed tomography; PET/MR: Positron emission tomography/magnetic resonance; PI-RADS: Prostate Imaging Reporting and Data System; PROMISE: Prostate Cancer Molecular Imaging Standardized Evaluation; PSA: Prostate-specific antigen; PSMA: Prostate-specific membrane antigen; ROI: Region of interest; SUV: Standardized uptake value; T2WI: T2-weighted imaging; TE: Echo time; TR: Repetition time.

Acknowledgements

Jing Zhao thanks German Research Foundation (GRK2260, BIOQIC) for the support.

Authors' contributions

JZ was the major contributor in writing and organizing the manuscript. BH and MRM supervised the work and made substantial contributions to the design of the study. BW and MRM read, reviewed, and contributed with their

expertise in their different fields to the final manuscript. All authors read and approved the final manuscript.

Funding

Open Access funding enabled and organized by Projekt DEAL. The PET/MRI scanner is funded in part by the German Research Foundation (INST 335/454-1).

Availability of data and materials

The datasets analyzed and generated during this study are included in this published study.

Ethics approval and consent to participate

All procedures performed in studies involving human participants were in accordance with the ethical standards of the institutional and national research committee and with the 1964 Helsinki declaration and its later amendments or comparable ethical standards. This retrospective study was approved by the institutional ethics review board (EA1/060/16), and the institutional review board waived the requirement for informed consent for this retrospective analysis.

Consent for publication

All authors give their consent.

Competing interests

The authors declare that they have no competing interests.

Author details

¹ Institute of Radiology and Nuclear Medicine, Charité – Universitätsmedizin Berlin, corporate member of Freie Universität Berlin, Humboldt-Universität zu Berlin, and Berlin Institute of Health, Charitéplatz 1, 10117 Berlin, Germany. ² Institute of Nuclear Medicine, Charité – Universitätsmedizin Berlin, corporate member of Freie Universität Berlin, Humboldt-Universität zu Berlin, and Berlin Institute of Health, Augustenburger Platz 1, 13353 Berlin, Germany. ³ Institute of Diagnostic and Interventional Radiology, Klinikum Rechts Der Isar, Technische Universität München, Ismaninger Str. 22, 81675 Munich, Germany.

Received: 14 July 2020 Accepted: 13 October 2020

Published online: 17 December 2020

References

- Siegel RL, Miller KD, Fedewa SA et al (2017) Colorectal cancer statistics. *CA Cancer J Clin* 67(3):177–193
- Muller BG, Shih JH, Sankineni S et al (2015) Prostate cancer: interobserver agreement and accuracy with the revised prostate imaging reporting and data system at multiparametric MR imaging. *Radiology* 277(3):741–750. <https://doi.org/10.1148/radiol.2015142818>
- Rosenkrantz AB, Ginocchio LA, Cornfeld D et al (2016) Interobserver reproducibility of the PI-RADS version 2 lexicon: a multicenter study of six experienced prostate radiologists. *Radiology* 280(3):793–804. <https://doi.org/10.1148/radiol.2016152542>
- Ross JS, Sheehan CE, Fisher HAG et al (2003) Correlation of primary tumor prostate-specific membrane antigen expression with disease recurrence in prostate cancer. *Clin Cancer Res* 9(17):6357–6362
- Treglia G, Annunziata S, Pizzuto DA, Giovannella L, Prior JO, Ceriani L (2019) Detection rate of (18)F-labeled PSMA PET/CT in biochemical recurrent prostate cancer: a systematic review and a meta-analysis. *Cancers* (Basel). <https://doi.org/10.3390/cancers11050710>
- Fendler WP, Schmidt DF, Wenter V et al (2016) 68Ga-PSMA PET/CT detects the location and extent of primary prostate cancer. *J Nucl Med* 57(11):1720–1725. <https://doi.org/10.2967/jnumed.116.172627>
- Woythal N, Arsenic R, Kempensteffen C et al (2018) Immunohistochemical validation of PSMA expression measured by (68)Ga-PSMA PET/CT in primary prostate cancer. *J Nucl Med* 59(2):238–243. <https://doi.org/10.2967/jnumed.117.195172>
- Koerber SA, Utzinger MT, Kratochwil C et al (2017) (68)Ga-PSMA-11 PET/CT in newly diagnosed carcinoma of the prostate: correlation of intraprostatic PSMA uptake with several clinical parameters. *J Nucl Med* 58(12):1943–1948. <https://doi.org/10.2967/jnumed.117.190314>
- Zamboglou C, Drendel V, Jilg CA et al (2017) Comparison of (68)Ga-HBED-CC PSMA-PET/CT and multiparametric MRI for gross tumour volume detection in patients with primary prostate cancer based on slice by slice comparison with histopathology. *Theranostics* 7(1):228–237. <https://doi.org/10.7150/thno.16638>
- Eiber M, Weirich G, Holzapfel K et al (2016) Simultaneous ⁶⁸Ga-PSMA HBED-CC PET/MRI improves the localization of primary prostate cancer. *Eur Urol* 70(5):829–836. <https://doi.org/10.1016/j.eururo.2015.12.053>
- Donato P, Roberts MJ, Morton A et al (2019) Improved specificity with (68)Ga PSMA PET/CT to detect clinically significant lesions “invisible” on multiparametric MRI of the prostate: a single institution comparative analysis with radical prostatectomy histology. *Eur J Nucl Med Mol Imaging* 46(1):20–30. <https://doi.org/10.1007/s00259-018-4160-7>
- Hicks RM, Simko JP, Westphalen AC et al (2018) Diagnostic accuracy of (68)Ga-PSMA-11 PET/MRI compared with multiparametric MRI in the detection of prostate cancer. *Radiology* 289(3):730–737. <https://doi.org/10.1148/radiol.2018180788>
- Nanabala R, Anees MK, Sasikumar A, Joy A, Pillai MRA (2016) Preparation of [68 Ga]PSMA-11 for PET-CT imaging using a manual synthesis module and organic matrix based 68 Ge/68 Ga generator. *Nucl Med Biol* 43(8):463–469
- Hope TA, Aggarwal R, Chee B et al (2017) Impact of (68)Ga-PSMA-11 PET on management in patients with biochemically recurrent prostate cancer. *J Nucl Med* 58(12):1956–1961. <https://doi.org/10.2967/jnumed.117.192476>
- Afshar-Oromieh A, Malcher A, Eder M et al (2013) PET imaging with a 68 gallium-labelled PSMA ligand for the diagnosis of prostate cancer: biodistribution in humans and first evaluation of tumour lesions. *Eur J Nucl Med Mol Imaging* 40(4):486–495. <https://doi.org/10.1007/s00259-012-2298-2>
- Weinreb JC, Barentsz JO, Choyke PL et al (2016) PI-RADS prostate imaging – reporting and data system: 2015, version 2. *Eur Urol* 69(1):16–40. <https://doi.org/10.1016/j.eururo.2015.08.052>
- Hope TA, Goodman JZ, Allen IE, Calais J, Fendler WP, Carroll PR (2019) Metaanalysis of (68)Ga-PSMA-11 PET accuracy for the detection of prostate cancer validated by histopathology. *J Nucl Med* 60(6):786–793. <https://doi.org/10.2967/jnumed.118.219501>
- Hirnas N, Al-Ibraheem A, Herrmann K et al (2019) [(68)Ga]PSMA PET/CT improves initial staging and management plan of patients with high-risk prostate cancer. *Mol Imaging Biol* 21(3):574–581. <https://doi.org/10.1007/s11307-018-1278-8>
- Hoeks CM, Barentsz JO, Hambrock T et al (2011) Prostate cancer: multiparametric MR imaging for detection, localization, and staging. *Radiology* 261(1):46–66. <https://doi.org/10.1148/radiol.11091822>
- Park SY, Zacharias C, Harrison C et al (2018) Gallium-68 PSMA-11 PET/MR imaging in patients with intermediate- or high-risk prostate cancer. *Radiology* 288(2):495–505. <https://doi.org/10.1148/radiol.2018172232>
- Domachevsky L, Bernstine H, Goldberg N, Nidam M, Catalano OA, Groshar D (2020) Comparison between pelvic PSMA-PET/MR and whole-body PSMA-PET/CT for the initial evaluation of prostate cancer: a proof of concept study. *Eur Radiol* 30:328–336. <https://doi.org/10.1007/s00330-019-06353-y>
- Abd-Alazeez M, Ramachandran N, Dikaios N et al (2015) Multiparametric MRI for detection of radiorecurrent prostate cancer: added value of apparent diffusion coefficient maps and dynamic contrast-enhanced images. *Prostate Cancer Prostatic Dis* 18(2):128–136. <https://doi.org/10.1038/pcan.201455>
- Kranzbuhler B, Tran S, Zilli T, Burger IA (2017) 68Ga-PSMA PET/MR-positive peritoneal metastasis in the falciform ligament in recurrent prostate cancer. *Clin Nucl Med* 42(8):e388–e389. <https://doi.org/10.1097/RLU.0000000000001703>
- Westphalen AC, McCulloch CE, Jm Anaokar et al (2020) Variability of the positive predictive value of PI-RADS for prostate MRI across 26 centers: experience of the society of abdominal radiology prostate cancer disease-focused panel. *Radiology* 296(1):76–84
- Afshar-Oromieh A, Haberkorn U, Schlemmer HP et al (2014) Comparison of PET/CT and PET/MRI hybrid systems using a 68Ga-labelled PSMA ligand for the diagnosis of recurrent prostate cancer: initial experience.

- Eur J Nucl Med Mol Imaging 41(5):887–897. <https://doi.org/10.1007/s00259-013-2660-z>
26. Guberina N, Hetkamp P, Ruebben H et al (2019) Whole-body integrated [(68)Ga]PSMA-11-PET/MR imaging in patients with recurrent prostate cancer: comparison with whole-body PET/CT as the standard of reference. *Mol Imaging Biol*. <https://doi.org/10.1007/s11307-019-01424-4>
 27. Uslu-Besli L, Bakir B, Asa S et al (2019) Correlation of SUVmax and apparent diffusion coefficient values detected by Ga-68 PSMA PET/MRI in primary prostate lesions and their significance in lymph node metastasis: preliminary results of an on-going study. *Mol Imaging Radionucl Ther* 28(3):104–111. <https://doi.org/10.4274/mirt.galenos.2019.63825>
 28. von Klot CJ, Merseburger AS, Boker A et al (2017) (68)Ga-PSMA PET/CT imaging predicting intraprostatic tumor extent, extracapsular extension and seminal vesicle invasion prior to radical prostatectomy in patients with prostate cancer. *Nucl Med Mol Imaging* 51(4):314–322. <https://doi.org/10.1007/s13139-017-0476-7>
 29. Burger IA, Muller J, Donati OF et al (2019) (68)Ga-PSMA-11 PET/MR detects local recurrence occult on mpMRI in prostate cancer patients after HIFU. *J Nucl Med* 60(8):1118–1123. <https://doi.org/10.2967/jnumed.118.221564>
 30. Rauscher I, Duwel C, Haller B et al (2018) Efficacy, predictive factors, and prediction nomograms for (68)ga-labeled prostate-specific membrane antigen-ligand positron-emission tomography/computed tomography in early biochemical recurrent prostate cancer after radical prostatectomy. *Eur Urol* 73(5):656–661. <https://doi.org/10.1016/j.eururo.2018.01.006>
 31. Zacho HD, Nielsen JB, Dettmann K, Haberkorn U, Petersen LJ (2017) Incidental detection of thyroid metastases from renal cell carcinoma using ⁶⁸Ga-PSMA PET/CT to assess prostate cancer recurrence. *Clin Nucl Med* 42(3):221–222. <https://doi.org/10.1097/RLU.0000000000001522>
 32. Arora S, Damle NA, Parida GK et al (2018) Recurrent medullary thyroid carcinoma on ⁶⁸Ga-prostate-specific membrane antigen PET/CT: exploring new theranostic avenues. *Clin Nucl Med* 43(8):1
 33. Roach PJ, Francis R, Emmett L et al (2018) The impact of (68)Ga-PSMA PET/CT on management intent in prostate cancer: results of an Australian prospective multicenter study. *J Nucl Med* 59(1):82–88. <https://doi.org/10.2967/jnumed.117.197160>
 34. Calais J, Cao M, Nickols NG (2018) The utility of PET/CT in the planning of external radiation therapy for prostate cancer. *J Nucl Med* 59(4):557–567. <https://doi.org/10.2967/jnumed.117.196444>
 35. Chen M, Zhang Q, Zhang C et al (2019) Combination of (68)Ga-PSMA PET/CT and multiparametric MRI improves the detection of clinically significant prostate cancer: a lesion-by-lesion analysis. *J Nucl Med* 60(7):944–949. <https://doi.org/10.2967/jnumed.118.221010>

Publisher's Note

Springer Nature remains neutral with regard to jurisdictional claims in published maps and institutional affiliations.

Submit your manuscript to a SpringerOpen[®] journal and benefit from:

- Convenient online submission
- Rigorous peer review
- Open access: articles freely available online
- High visibility within the field
- Retaining the copyright to your article

Submit your next manuscript at ► [springeropen.com](https://www.springeropen.com)

Excerpt from Journal Summary List--2

Journal Data Filtered By: **Selected JCR Year: 2019** Selected Editions: SCIE,SSCI
 Selected Categories: **"ONCOLOGY"** Selected Category Scheme: WoS
Gesamtanzahl: 244 Journale

Rank	Full Journal Title	Total Cites	Journal Impact Factor	Eigenfactor Score
1	CA-A CANCER JOURNAL FOR CLINICIANS	39,917	292.278	0.093460
2	Nature Reviews Clinical Oncology	12,384	53.276	0.035980
3	NATURE REVIEWS CANCER	52,053	53.030	0.066030
4	LANCET ONCOLOGY	53,592	33.752	0.143420
5	JOURNAL OF CLINICAL ONCOLOGY	155,297	32.956	0.261940
6	Cancer Discovery	18,093	29.497	0.069280
7	CANCER CELL	41,064	26.602	0.095430
8	JAMA Oncology	13,794	24.799	0.064650
9	ANNALS OF ONCOLOGY	45,813	18.274	0.107060
10	Molecular Cancer	15,448	15.302	0.023990
11	Journal of Thoracic Oncology	18,136	13.357	0.038200
12	JNCI-Journal of the National Cancer Institute	36,018	11.577	0.045450
13	Trends in Cancer	2,351	11.093	0.010140
14	SEMINARS IN CANCER BIOLOGY	8,310	11.090	0.011730
15	Journal of Hematology & Oncology	6,732	11.059	0.015550
16	NEURO-ONCOLOGY	12,950	10.247	0.029050
17	CLINICAL CANCER RESEARCH	85,288	10.107	0.131520
18	Journal for ImmunoTherapy of Cancer	4,557	9.913	0.016030
19	CANCER RESEARCH	135,753	9.727	0.118680
20	Liver Cancer	1,131	9.720	0.002660

Rank	Full Journal Title	Total Cites	Journal Impact Factor	Eigenfactor Score
21	Journal of the National Comprehensive Cancer Network	6,912	9.316	0.020020
22	CANCER TREATMENT REVIEWS	9,427	8.885	0.017800
23	Cancer Immunology Research	6,969	8.728	0.026440
24	LEUKEMIA	25,819	8.665	0.048640
25	Blood Cancer Journal	2,800	8.023	0.010400
26	ONCOGENE	66,303	7.971	0.068320
27	Clinical and Translational Medicine	1,349	7.919	0.003280
28	npj Precision Oncology	500	7.717	0.001520
29	BIOCHIMICA ET BIOPHYSICA ACTA-REVIEWS ON CANCER	5,650	7.365	0.007800
30	CANCER LETTERS	34,162	7.360	0.044450
31	EUROPEAN JOURNAL OF CANCER	32,241	7.275	0.048170
32	Gastric Cancer	5,525	7.088	0.010730
33	JOURNAL OF EXPERIMENTAL & CLINICAL CANCER RESEARCH	9,316	7.068	0.014540
34	Therapeutic Advances in Medical Oncology	1,894	6.852	0.004260
35	Molecular Oncology	6,378	6.574	0.013820
36	CANCER AND METASTASIS REVIEWS	6,247	6.400	0.005940
37	Cancers	10,442	6.126	0.018740
38	Oncogenesis	2,775	6.119	0.007750
39	STEM CELLS	20,554	6.022	0.024110
40	npj Breast Cancer	814	6.000	0.003590
41	JOURNAL OF PATHOLOGY	16,307	5.979	0.017910



Zhao J, Mangarova DB, Brangsch J, Kader A, Hamm B, Brenner W, Makowski MR: Correlation between Intraprostatic PSMA Uptake and MRI PI-RADS of [⁶⁸Ga]Ga-PSMA-11 PET/MRI in Patients with Prostate Cancer: Comparison of PI-RADS Version 2.0 and PI-RADS Version 2.1. *CANCERS* 2020;12:3523.

DOI: <https://doi.org/10.3390/cancers12123523>

Article

Correlation between Intraprostatic PSMA Uptake and MRI PI-RADS of [⁶⁸Ga]Ga-PSMA-11 PET/MRI in Patients with Prostate Cancer: Comparison of PI-RADS Version 2.0 and PI-RADS Version 2.1

Jing Zhao ^{1,*} , Dilyana B. Mangarova ^{1,2} , Julia Brangsch ¹, Avan Kader ^{1,3} , Bernd Hamm ¹, Winfried Brenner ⁴ and Marcus R. Makowski ^{1,5}

¹ Institute of Radiology and Nuclear Medicine, Charité–Universitätsmedizin Berlin, Corporate Member of Freie Universität Berlin, Humboldt-Universität zu Berlin, and Berlin Institute of Health, Charitéplatz 1, 10117 Berlin, Germany; dilyana.mangarova@charite.de (D.B.M.); julia.brangsch@charite.de (J.B.); avan.kader@charite.de (A.K.); bernd.hamm@charite.de (B.H.); marcus.makowski@charite.de (M.R.M.)

² Department of Veterinary Medicine, Institute of Veterinary Pathology, Freie Universität Berlin, Robert-von-Ostertag-Str. 15, Building 12, 14163 Berlin, Germany

³ Department of Biology, Chemistry and Pharmacy, Institute of Biology, Freie Universität Berlin, Königin-Luise-Str. 1-3, 14195 Berlin, Germany

⁴ Department of Nuclear Medicine, Charité–Universitätsmedizin Berlin, Corporate Member of Freie Universität Berlin, Humboldt-Universität zu Berlin, and Berlin Institute of Health, Augustenburger Platz 1, 13353 Berlin, Germany; winfried.brenner@charite.de

⁵ Department of Diagnostic and Interventional Radiology, Klinikum rechts der Isar, Technische Universität München, Ismaninger Str. 22, 81675 Munich, Germany

* Correspondence: jing.zhao@charite.de

Received: 22 October 2020; Accepted: 24 November 2020; Published: 26 November 2020



Simple Summary: The newest Prostate Imaging Reporting and Data System (PI-RADS) version 2.1, was published in 2019. There are a few variations of the new standard, which will change prostate lesions' classification rules. Our study aims to analyze the pattern change of lesion positron emission tomography (PET) standardized uptake values maximum (SUVmax) distribution under PI-RADS V2.1, compared with PI-RADS V2.0. Moreover, we studied the correlation between prostate-specific membrane antigen (PSMA) SUVmax and magnetic resonance imaging (MRI) PI-RADS. So far, there is no article reporting the effect of the newest PI-RADS on [⁶⁸Ga]Ga-PSMA-11 PET/MRI. We did a thorough analysis, including two subgroups, peripheral zone, transitional zone, and 215 lesions. We analyzed the impact of each variation of PI-RADS one by one.

Abstract: Purpose: We aimed to evaluate the correlation between PSMA uptake and magnetic resonance imaging (MRI) PI-RADS of simultaneous [⁶⁸Ga]Ga-PSMA-11 PET/MRI regarding PI-RADS version 2.0 and 2.1 respectively and compared the difference between these two versions. Materials and Methods: We retrospectively analyzed a total of forty-six patients with biopsy-proven prostate cancer who underwent simultaneous [⁶⁸Ga]Ga-PSMA-11 PET/MRI. We classified the lesions regarding PI-RADS version 2.0 and 2.1, peripheral zone (PZ), and transitional zone (TZ), respectively. Based on regions of interest (ROI), standardized uptake values maximum (SUVmax), and corresponding lesion-to-background ratios (LBR) of SUVmax of each category, PI-RADS score 1 to 5, were measured. A comparison between PI-RADS version 2.0 and PI-RADS version 2.1 was performed. Results: A total of 215 focal prostate lesions were analyzed, including two subgroups, 125 TZ and 90 PZ. Data are reported as median and interquartile range (IQR). Regarding PI-RADS version 2.1, TZ SUVmax of each category were 1.5 (0.5, 1.9), 1.9 (0.8, 2.3), 3.3 (2.1, 4.6), 4.2 (3.1, 5.7), 7.3 (5.2, 9.7). PZ SUVmax of each category were 1.0 (0.8, 1.6), 2.5 (1.5, 3.2), 3.3 (1.9, 4.5), 4.3 (3.0, 5.4), 7.4 (5.0, 9.3). Regarding the inter-reader agreement of the overall PI-RADS assessment category, the kappa value was 0.723 for

version 2.0 and 0.853 for version 2.1. Conclusion: Revisions of PI-RADS version 2.1 results in variations in lesions classification. Lesions with the PI-RADS category of 3, 4, and 5 present relatively higher intraprostatic PSMA uptake, while lesions with the PI-RADS category of 1 and 2 present relatively lower and similar uptake. Version 2.1 has higher inter-reader reproducibility than version 2.0.

Keywords: prostate cancer; multiparametric MRI; PSMA; [⁶⁸Ga]Ga-PSMA-11 PET/MRI; SUVmax; PSA; molecular imaging; PI-RADS 2.1

1. Introduction

Prostate cancer (PCa) is a common malignant disease in the elderly male population [1], and a percentage of patients with early prostate cancer have metastatic disease. PCa is currently the second leading cause of cancer death in men in the western world, and men have a lifetime probability for PCa of 14%. It is important to be able to determine tumor behavior as well as the diagnosis.

Multiparametric magnetic resonance imaging (mpMRI) is a clinical imaging tool for detecting primary PCa and guiding the subsequent biopsy. MpMRI includes T2-weighted imaging (T2WI), diffusion-weighted imaging (DWI), and dynamic contrast-enhanced MRI (DCE-MRI). Prostate cancer is a type of cancer that can be extremely heterogeneous. Therefore, it is particularly important to accurately evaluate and describe the imaging features of prostate cancer lesions. The American College of Radiology, European Radiology of Uroradiology, and AdMeTech Foundation jointly released the Prostate Imaging Reporting and Data System (PI-RADS) version 2.0 in 2015. PI-RADS 2.0 was a standardized assessment of the probability of clinically significant PCa using prostate mpMRI [2,3]. PI-RADS V2.0 is widely recognized internationally among radiologists and urologists, and is widely used in daily practice and research. Many studies have confirmed the value of PI-RADS V2.0, but as expected, they also have some inconsistencies and limitations, including sub-optimal inter-reader reproducibility, relatively high false-negative rate, and decision-making rules, including the amphibolous evaluation criteria of TZ on T2WI. The detection rate of transitional zone (TZ) tumors is lower than that of peripheral zone (PZ) tumors [2,4–8]. To solve the above problems, the PI-RADS Steering Committee, applying a consensus-based process, is suggested that several modifications have been made to PI-RADS V2.0, remaining the framework for assigning scores to each sequence, and using these scores to achieve at an overall assessment category. Given the limited scope of these updates, the updated version described below is called PI-RADS V2.1. There are a few revisions in this version compared to version 2.0. Experts expect that the clinical use of PI-RADS version 2.1 will improve the variability between readers and further simplify the evaluation of PI-RADS for MRI.

Prostate-specific membrane antigen (PSMA) is a transmembrane glycoprotein related to tumor progression and disease recurrence reported as being overexpressed in prostate cancer cells. Furthermore, it is associated with PCa with higher serum prostate-specific antigen (PSA) levels and a higher Gleason score (GS) [9,10]. Positron emission tomography (PET) images are co-registered with computed tomography (CT) scans that are easily acquired and widely available to provide anatomical information for localization of PSMA-avid lesions. Previous studies suggest that [⁶⁸Ga]Ga-PSMA-11 PET/CT has a high detection rate for prostate tumors, with a sensitivity of 67% to 97%. Koerber et al. [11] and Woythal et al. [12] reported that the standardized uptake values maximum (SUVmax) of PCa is higher than that of noncancerous prostate and healthy prostate tissue. Combining [⁶⁸Ga]Ga-PSMA PET and mpMRI can improve localization accuracy and diagnostic efficiency, as Zamboglou et al. proved [13]. Eiber et al. [14] demonstrated that advances diagnostic accuracy for PCa localization both compared with mpMRI and with PET imaging alone. In the above studies, the advantages of PET/MRI in the diagnosis of PCa have been elaborated.

Our study aimed to (1) evaluate the correlation between PSMA uptake and MRI PI-RADS of the same cohort of prostate focal lesions regarding both PI-RADS version 2.0 and version 2.1, respectively, on MRI, and (2) compare the difference between these two versions.

2. Results

2.1. Characteristics of Patients

In this study, we analyzed forty-six patients in a total of 215 lesions. Few patients underwent radical prostatectomy (RP) after the scan. The staging is clinical staging based on the physical exam results, prostate biopsy, and imaging tests. Patient characteristics are compiled in Table 1.

Table 1. Summary of patient characteristics.

Characteristics	N = 46
Age at scan (years)	75 ± 7
PSA (ng/mL) at scan time	12.48 (4.33, 26.48)
Primary tumor stage (n)	
≤ cT2c	16 (35%)
≥ cT3a	30 (65%)
Primary lymph node stage (n)	
cN0	25 (54%)
cN1	21 (46%)
Biopsy Gleason score (n)	
3 + 3	10 (22%)
3 + 4	9 (19%)
4 + 3	7 (15%)
4 + 4	10 (22%)
4 + 5	3 (7%)
5 + 4	5 (11%)
5 + 5	2 (4%)
Treatment	
ADT prior to scan (n)	2 (4%)
ADT ongoing at the time of scan (n)	9 (19%)
Radiotherapy prior to scan (n)	8 (17%)

2.2. Inter-Reader Agreement

Based on the first readout, regarding the inter-reader agreement of the PI-RADS assessment category between the two readers, the kappa value was 0.723, substantial for version 2.0; and 0.853, almost perfect for version 2.1.

2.3. Lesion Analysis

Based on the second readout, two readers performed consensus reading to decide the ultimate PI-RADS score of each lesion according to PI-RADS version 2.0 and 2.1, respectively, and PET interpretation. A total of 215 focal prostate lesions were detected by mpMRI and PET, including 125 TZ and 90 PZ. TZ SUVmax and corresponding LBR of SUVmax of each category for version 2.0 and 2.1 are presented in Table 2. PZ SUVmax and corresponding LBR of SUVmax of each category for version 2.0 and 2.1 are shown in Table 3.

Table 2. TZ lesions SUVmax and corresponding LBR of SUVmax for Version 2.0 and 2.1.

PI-RADS	Version 2.0 (n)	SUVmax	LBR of SUVmax	Version 2.1 (n)	SUVmax	LBR of SUVmax	SUVmax p Value	LBR p Value
1	12	1.1 (0.4, 1.7)	1.2 (0.5, 1.9)	21	1.5 (0.5, 1.9)	1.4 (0.7, 2.1)	p = 0.02	p = 0.02
2	34	2.4 (1.3, 3.2)	2.1 (1.5, 2.9)	21	1.9 (0.8, 2.3)	1.6 (0.9, 2.4)	p = 0.02	p = 0.02
3	25	3.1 (2.1, 4.4)	2.5 (1.5, 3.5)	29	3.3 (2.1, 4.6)	2.6 (1.5, 3.6)	p = 0.73	p = 0.84
4	26	4.2 (3.1, 5.7)	3.4 (2.5, 4.8)	26	4.2 (3.1, 5.7)	3.4 (2.5, 4.8)	p = 1	p = 1
5	28	7.3 (5.2, 9.7)	6.8 (3.3, 12.8)	28	7.3 (5.2, 9.7)	6.8 (3.3, 12.8)	p = 1	p = 1

Data is presented as median, interquartile range (Q1, Q3). LBR: lesion-to-background ratio.

Table 3. PZ lesions SUVmax and corresponding LBR of SUVmax for Version 2.0 and 2.1.

PI-RADS	Version 2.0 (n)	SUVmax	LBR of SUVmax	Version 2.1 (n)	SUVmax	LBR of SUVmax	SUVmax p Value	LBR p Value
1	14	1.0 (0.8, 1.6)	1.1 (0.4, 1.8)	14	1.0 (0.8, 1.6)	1.1 (0.4, 1.8)	p = 1	p = 1
2	15	2.5 (1.3, 3.3)	2.1 (1.5, 2.9)	18	2.5 (1.5, 3.2)	2.2 (1.6, 2.9)	p = 0.81	p = 0.86
3	18	3.1 (2.0, 4.5)	2.5 (1.5, 3.5)	13	3.3 (1.9, 4.5)	2.6 (1.5, 3.6)	p = 0.85	p = 0.87
4	18	4.3 (2.9, 5.4)	3.8 (2.7, 4.4)	20	4.3 (3.0, 5.4)	3.8 (2.8, 4.8)	p = 0.92	p = 0.95
5	25	7.4 (5.0, 9.3)	6.9 (3.1, 11.9)	25	7.4 (5.0, 9.3)	6.9 (3.1, 11.9)	p = 1	p = 1

Data is presented as median, Interquartile range (Q1, Q3). LBR: Lesion-to-background ratio.

3. Discussion

PI-RADS version 2.1 has a few revisions about clarifications in interpretation criteria. Turkbey et al. expounded on this revision in detail in the review publication [15]. Revisions include three parts, image data acquisition, clarifications in interpretation criteria, and biparametric MRI. In PI-RADS V2.1 interpretation criteria, some revisions change lesion categories, while other revisions offer a more precise definition of categories to improve diagnostic consistency. In this article, we discussed the revised items in PI-RADS version 2.1 point by point. The correlation between PI-RADS and SUVmax was studied. Moreover, we analyzed these revised items' impact on ^{68}Ga]Ga-PSMA-11 PET/MRI diagnosis. We hope that urologists, radiologists, and nuclear medicine physicians can comprehend the diagnostic criteria changes so that clinical diagnosis can be further developed.

First, for the TZ, T2WI is the primary determining sequence. There is a revision in the criteria for T2WI scores of 1 and 2 in TZ. In PI-RADS V2.0, typical benign prostatic hyperplasia (BPH) nodules, including round, circumscribed, and completely or almost completely encapsulated on T2WI, were assigned a T2WI score of 2. These lesions are assigned a PI-RADS assessment category of 2. In PI-RADS V2.1, a normal-appearing TZ or a round, completely encapsulated nodules are called "typical nodules." Due to the MRI manifestations of age-related BPH, typical BPH nodules are unlikely to be PCa. In PI-RADS V2.1, findings of BPH alone are considered a normal physiological revision and are assigned a T2WI score of 1. Hence, part of T2WI of 2 lesions revise to T2WI of 1 under the new standard. It is well known that BPH can also show high uptake of PSMA on PET [14,16–18]. After a percentage of PSMA-positive BPH nodules are classified as T2WI of 1, then assigned to PI-RADS of 1, the SUVmax of PI-RADS 1 group increases, as shown in Table 2. Figure 1 shows an example of "typical nodules." Therefore, this remedy will degrade some BPH focal lesions. Doctors may not be obligatory to report such lesions.

Second, there is a revision in the determination of the overall assessment category in TZ. In PI-RADS V2.1, a mostly encapsulated nodule or a homogeneous circumscribed nodule without encapsulation is called "atypical nodules". The revision in deriving the overall PI-RADS assessment category concerns TZ lesions with a T2WI score of 2, compared to PI-RADS V2.0. In TZ, DWI score of ≥ 4 now elevates the overall PI-RADS assessment category from 2 to 3 for lesions receiving a T2WI score of 2. DWI score of ≤ 3 is assigned to PI-RADS of 2 for lesions receiving a T2WI score of 2. Some lesions that initially belonged to PI-RADS 2 are upgraded to PI-RADS 3 under the new standard. Figure 2 shows an example of an atypical nodule with DWI score of ≥ 4 , elevating the overall PI-RADS assessment category from 2 to 3. This revision requires physicians to pay more attention to the information provided by DWI.

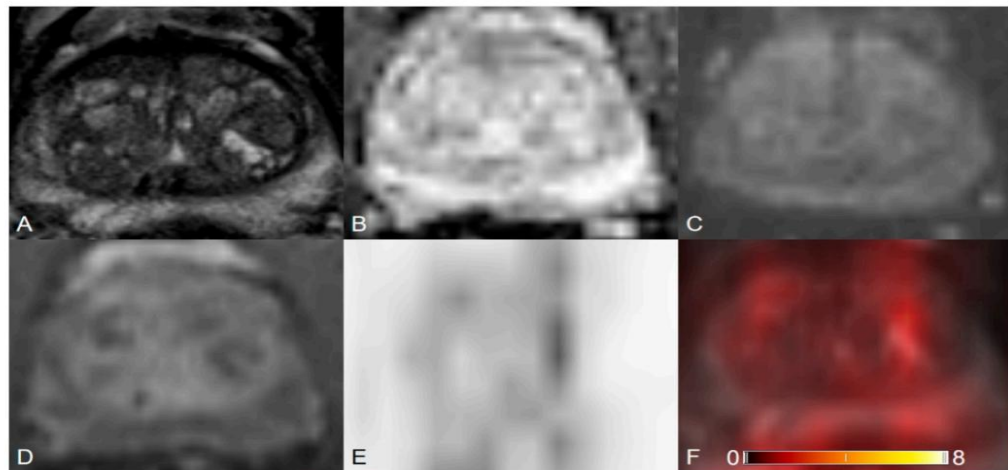


Figure 1. Transition zone with typical benign prostatic hyperplasia (BPH) changes. (A) Axial T2WI shows completely encapsulated “typical” nodules. (B) ADC map image presents no focal lesion with hypointense signal below the background. (C) DWI ($b = 1000 \text{ s/mm}^2$) shows no lesion with a markedly hyperintense signal above the background. (D) Early dynamic contrast-enhanced image presents no positive enhancement within the typical BPH nodules. T2WI = 1, DWI = 1, DCE = negative, PI-RADS assessment category = 1. (E) PET image shows inhomogeneous $[^{68}\text{Ga}]\text{Ga-PSMA-11}$ uptake. (F) $[^{68}\text{Ga}]\text{Ga-PSMA-11}$ PET/MRI fusion.

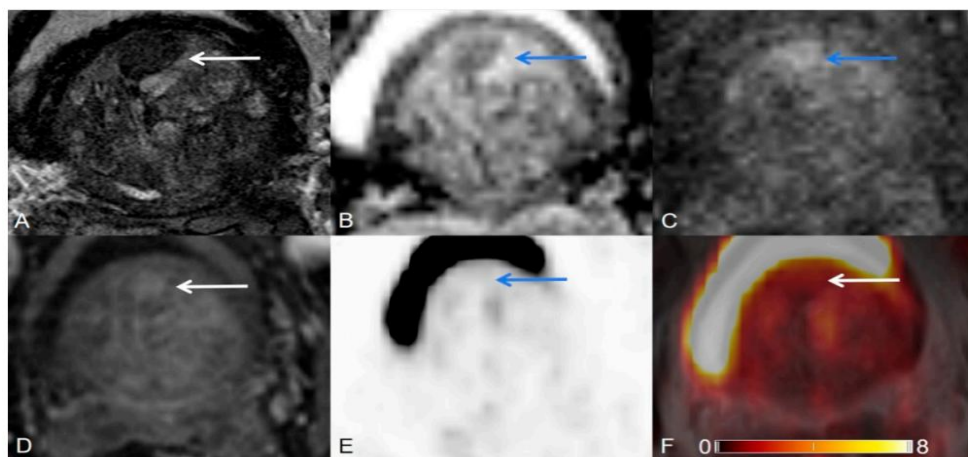


Figure 2. Transition zone with an atypical nodule. (A) Axial T2WI shows a homogeneous T2 hypointense, mostly encapsulated nodule. (B) ADC map image presents a focal lesion with a markedly hypointense signal below the background corresponding to the lesion seen in (A). (C) DWI ($b = 1000 \text{ s/mm}^2$) shows a focal lesion with a markedly hyperintense signal above the background corresponding to the lesion seen in (A,B). (D) Early dynamic contrast-enhanced image presents avid enhancement within the nodule. T2WI = 2, DWI = 5, DCE = positive, PI-RADS assessment category = 3. (E) PET image shows no $[^{68}\text{Ga}]\text{Ga-PSMA-11}$ avid uptake. (F) $[^{68}\text{Ga}]\text{Ga-PSMA-11}$ PET/MRI fusion.

Furthermore, mildly or moderately restricted diffusion is commonly encountered in mostly encapsulated and unencapsulated TZ lesions. These lesions may represent stromal hyperplasia areas and should not be upgraded based on mildly/moderately restricted diffusion [15]. Lesions with a

T2WI score of 1 or 2 should not be upgraded to a PI-RADS assessment category of 2 or 3, respectively, based on a DWI score of 3. Figure 3 shows an example of an atypical nodule with T2WI score of 2, DWI score of 3, and the overall PI-RADS assessment category remains at 2. In PI-RADS V2.1, criteria variations do not affect PI-RADS of 4 and 5 groups. In Table 2, there is no revision in PI-RADS of 4 and 5 groups. Comparing SUVmax and LBR of SUVmax under PI-RADS V2.0 and V2.1, PI-RADS of 1, 2, and 3 groups show a significant difference ($p < 0.05$) between the two versions, while PI-RADS of 4 and 5 show no significant difference ($p > 0.05$) between the two versions.

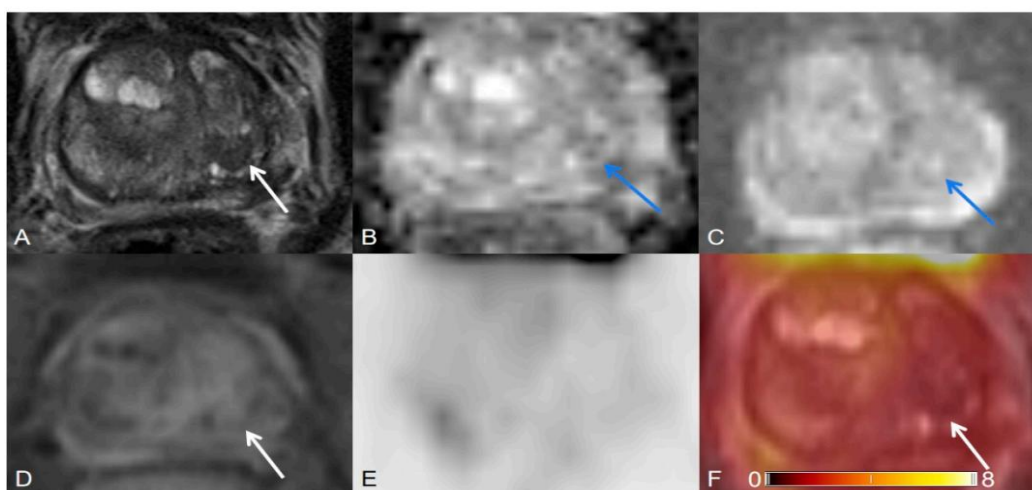


Figure 3. Transition zone with an atypical nodule. (A) Axial T2WI shows a T2 hypointense homogeneous circumscribed nodule. (B) ADC map image presents a focal lesion with a mildly hypointense signal below the background corresponding to the lesion seen in (A). (C) DWI ($b = 1000 \text{ s/mm}^2$) shows a focal lesion with a mildly hyperintense signal above the background corresponding to the lesion seen in (A, B). (D) Early dynamic contrast-enhanced image presents no early enhancement within the nodule. T2WI = 2, DWI = 3, DCE = negative, PI-RADS assessment category = 2. (E) PET image shows no $[^{68}\text{Ga}]\text{Ga-PSMA-11}$ avid uptake. (F) $[^{68}\text{Ga}]\text{Ga-PSMA-11}$ PET/MRI fusion.

Third, revision in criteria for DWI scores of 2 and 3. In PI-RADS V2.0, the description of DWI findings score of 2 and 3 is not clear. Due to differentiation in personal understanding, uncertainty and variable interpretation in physicians' judgment could cause uncertainty when making the diagnosis. Moreover, findings must conform to both apparent diffusion coefficient (ADC) and DWI criteria, but not on just one of the image sets. PI-RADS V2.1 provides a more detailed and clearer definition of DWI findings scores of 2 and 3.

Furthermore, under this new standard, findings could be positive on one of the image sets, ADC, or DWI. This criterion applies to lesions of both TZ and PZ. This revision significantly reduces the diagnosis of uncertainty. For the PZ, DWI is the primary determining sequence and dominant technique. This revision will improve the diagnostic stability of PZ lesions.

Fourth, clarification of the distinction between positive and negative enhancement on DCE. In PI-RADS V2.0, the features that represent a negative DCE score and widespread multifocal enhancement assessment are indefinite. In PI-RADS V2.1, the description for a negative score on DCE has been modified. It can be expected that this revision will reduce the differences among readers in the interpretation of DCE MRI. For the PZ lesions, DCE is the secondary determining sequence. This revision can improve diagnostic reproducibility. Table 3 listed the number of lesions under the two versions PI-RADS. It can be found that there are not so many revisions of PZ. Because for PZ, the revised standard will not make a huge revision in the classification of lesions, but it can improve

the inter-reader agreement. From the inter-reader agreement evaluation result, PI-RADS V2.1 shows better consistency between readers than PI-RADS V2.0.

Compared to PI-RADS V2.0, PI-RADS V2.1 is clearer and reduces the diagnosis uncertainty. To sum up the above points, we evaluated the correlation between PSMA uptake and MRI PI-RADS of simultaneous [⁶⁸Ga]Ga-PSMA-11 PET/MRI regarding PI-RADS version 2.0 and 2.1, respectively, and compared the difference between these two versions. We compared the inter-reader reproducibility between PI-RADS version 2.0 and version 2.1. We understand the impact of the reader experience. Generally, the experienced reader achieves a higher detection rate than the inexperienced reader, even though they follow the same PI-RADS criteria. This difference is caused by the different understanding of diagnostic criteria by each doctor. Therefore, a more accurate description of diagnostic criteria is helpful to improve the reproducibility among readers, and this is the aim of the new guideline.

Part of TZ lesions with T2WI score of 2 was upgraded to 3 because the corresponding DWI is ≥ 4 . Part of BPH decreased from PI-RADS assessment category of 2 to 1. Some PI-RADS 2 TZ lesions with avid PSMA uptake were reassigned into other groups. In PI-RADS V2.1, the number of TZ lesions in an overall score of 2 reduced. SUVmax and corresponding LBR also decreased. Although DWI and DCE criteria have revisions, the diagnosis of TZ lesions in PI-RADS 4 and 5 groups is usually very clear and has a high level of reader certainty. PI-RADS V2.1 does not have a significant effect on TZ PI-RADS 4 and 5 groups. There is no revision of SUVmax and corresponding LBR of these two groups. Considering PZ lesions, DWI and DCE are determining sequence. In PI-RADS V2.1, the revisions of DWI and DCE enhance inter-reader agreement.

The variability has been discussed in previous research. Westphalen et al. [19] performed a multi-center study across 26 centers to evaluate variability of the positive predictive value (PPV) of PI-RADS V2.0 for prostate MRI. Across all centers, the estimated PPV was 35% for a PI-RADS score greater than or equal to 3 and 49% for a PI-RADS score greater than or equal to 4. They concluded that the PPV of the PI-RADS V2.0 was low and varied widely across centers.

Some published articles also compared the detection performance of two versions and proved that PI-RADS V2.1 could be preferable for evaluating lesions and achieved a higher inter-reader agreement [20–22]. Barrett et al. [23] specifically stated in the review article that the revision of PI-RADS V2.1 is an important step in diagnosing prostate cancer. These studies have reached a common conclusion that PI-RADS V2.1 had better inter-reader reproducibility than did PI-RADS V2.0.

Imaging analysis has been an important tool for the diagnosis and staging of prostate cancer. The present study's clinical implications help radiologists, nuclear medicine physicians, and urologists understand the essential points in diagnosing and reporting prostate cancer, as well as the revisions in the new standards. Making clinical decisions about patient care is a complex process, which involves processing information and evaluating evidence, while applying critical thinking and problem-solving skills. Optimizing the scoring criteria helps doctors develop personalized treatment plans for patients. PI-RADS has already undergone several revisions. With radiologists and urologists' joint efforts, the lesion scoring details have become clearer and more precise. Ambiguous descriptions have been revised to make it easier to reach an agreement between radiologists. Multi-modality imaging, [⁶⁸Ga]Ga-PSMA-11 PET/CT, and PET/MRI examination trend toward precision medicine in recent years. It shows encouraging results and is expected to effectively improve the treatment of prostate cancer patients [24–27]. PET/MRI works based on developing a fusion of PET sequences with MRI sequences for diagnostic purposes in oncological applications. MRI evaluates soft tissue and lymph nodes involvement and bone lesions, while PET provides biological information about cancer. MRI shows superior resolution to CT and PET/CT in the T staging of primary prostate malignancies. An increasing number of researchers have reported that benign lesions and normal tissue show varying degrees of avid PSMA uptake. Therefore, revisions in the PI-RADS will also lead to changes in the correlation between SUVmax and PI-RADS.

In a word, we proved that PI-RADS version 2.1 has comparable performance in detecting prostate focal lesions compared with version 2.0. The results of this study showed that PI-RADS

V2.1 can improve the repeatability between readers and may help to improve diagnostic performance and accuracy. Therefore, it is of far-reaching significance for urologists and oncologists to make clinical decisions.

4. Materials and Methods

4.1. Patients

This retrospective study was approved by the institutional ethics review board (EA1/060/16), and the institutional review board waived the requirement for informed consent for this retrospective analysis.

Inclusion criteria: (1) patients with biopsy-proven prostate cancer who underwent [⁶⁸Ga]Ga-PSMA-11 PET/MRI between January 2017 and May 2020 in our institute; (2) all necessary additional information could be obtained from our database. Exclusion criteria: (1) patients, who underwent radical prostatectomy before scanning and no prostate left in the pelvic, were excluded; (2) additional information was not adequate. Patient inclusion and exclusion are summarized in the flowchart in Figure 4.

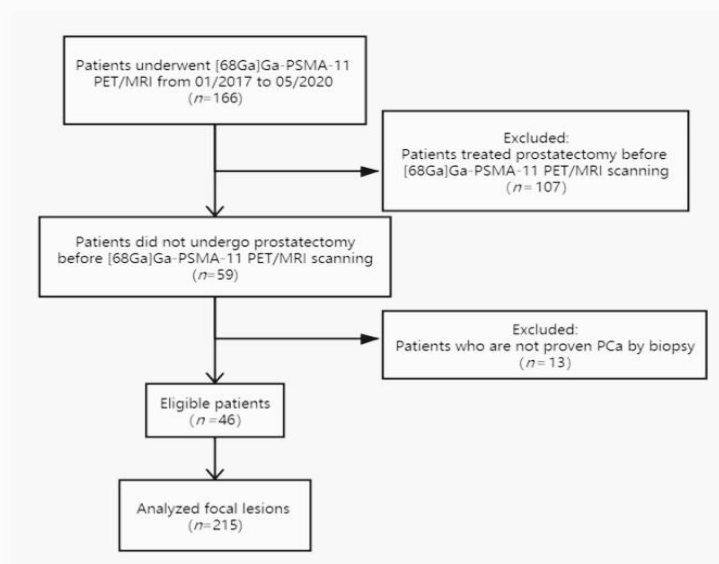


Figure 4. [⁶⁸Ga]Ga-PSMA-11 PET: gallium 68-labeled prostate-specific membrane antigen PET, mpMRI: multiparametric MRI.

4.2. [⁶⁸Ga]Ga-PSMA-11 PET/MRI Imaging Protocol

[⁶⁸Ga]Ga-PSMA-11 was synthesized using a clinical-grade ⁶⁸Ge/⁶⁸Ga radionuclide generator (Eckert & Ziegler Radiopharma GmbH, Berlin, Germany) and PSMA-HBED-CC (ABX GmbH, Radeberg, Germany) as described previously [28–30]. Patients were imaged after 85 ± 6 min after intravenous injection of a mean activity of 158.0 ± 18.4 MBq (4.3 ± 0.5 mCi) [⁶⁸Ga]Ga-PSMA-11, corresponding to activity: 1.8–2.2 MBq (0.049–0.060 mCi) per kilogram bodyweight. Furosemide is injected to minimize halo artifact caused by scatter overcorrection associated with high renal and urinary tracer activity 30 min before the start of PET acquisition. Patients were asked to void urine immediately before the start of the examination. No adverse effects were observed after [⁶⁸Ga]Ga-PSMA-11 injection.

Imaging was performed on a 3.0T PET/MRI system (SIEMENS MAGNETOM Biograph mMR, Erlangen, Germany). The acquisition was split into two parts. First, body PET/MRI cover from the vertex to mid-thigh was performed with 3 min of PET acquisition in each bed position, with coverage of

24 cm. Pre-contrast MRI sequences were acquired simultaneously using a combination of a dedicated mMR head-and-neck coil and phased-array mMR body surface coils. Siemens StarVIBE eliminates motion artifacts.

The second part was a dedicated MRI scan of the pelvis, followed by the reconstruction of PET data. MRI sequence parameters are summarized in Table 4. Reconstruction was conducted with an ordered subset expectation maximization algorithm (OSEM), with 3 iterations/21 subsets, based on an x-matrix acquisition with a 4 mm Gaussian filter and relative scatter scaling. Pre-contrast imaging data serve for attenuation correction. PET and MRI were performed using the same protocol for every patient.

Table 4. Imaging parameters used for MRI.

Sequence	TR/TE (ms)	FOV (mm)	Flip Angle (degrees)	Section Thickness (mm)	Voxel Size (mm)
T2WI HASTE Axial	1400.0/95.0	400	160	5.0	1.3 × 1.3 × 5.0
T1WI FS VIBE	1600.0/96.0	350	160	4.0	1.1 × 1.1 × 4.0
T2WI Axial	5500.0/103.0	180	150	3.0	0.5 × 0.5 × 3.0
T2WI Sagittal	1600.0/96.0	350	160	4.0	1.1 × 1.1 × 4.0
T2WI Coronal	4500.0/102.0	200	173	3.0	0.4 × 0.4 × 3.0
DWI	11,600.0/70.0	280		3.0	2.5 × 2.5 × 3.0
T1WI FS TWIST dynamic	7.41/3.30	260	12	3.5	1.4 × 1.4 × 3.5
T1WI STARVIBE	3.71/1.77	360	9	1.2	1.1 × 1.1 × 1.2

4.3. Image Analysis

Image analysis was achieved using dedicated post-processing software Syngo.via (Siemens Healthcare, Erlangen, Germany). T2WI was used for anatomic correlation for [⁶⁸Ga]Ga-PSMA-11 PET. Image analysis is comprised of twice readout. The first readout, incorporating both the MRI and PET images as well as all clinical information, were interpreted independently by two double-trained radiologists with 5 and 10 years of experience. Both readers interpreted MRI images using two versions PI-RADS, version 2.0 and 2.1. Then we compared the result of two readers of each version to evaluate inter-reader reproducibility. In the second readout, two readers performed consensus reading to determine the final PI-RADS score of each lesion according to PI-RADS version 2.0 and 2.1, respectively.

ROI were defined as regions with an abnormal signal focal lesion on MRI images or an area with PSMA avid uptake focal lesion on [⁶⁸Ga]Ga-PSMA-11 PET. Readers interpreted mpMRI images according to PI-RADS version 2.0 and version 2.1, respectively. [⁶⁸Ga]Ga-PSMA-11 PET images were interpreted by SUVmax and corresponding LBR, measured based on ROI. LBR is defined as a ratio of lesion SUVmax to background SUVmax. Using ratio value, LBR is to reduce the bias from a specific combination of radiotracer manufacturer, systems vendor, reconstruction techniques, uptake time, post-processing software, the time between radiotracer injection to scanning. Any avid focal lesion in the prostate with uptake above prostate background not attributable to physiologic radiotracer biodistribution was considered positive on [⁶⁸Ga]Ga-PSMA-11 PET. Lesions with the same or lower uptake than the background were deemed negative on [⁶⁸Ga]Ga-PSMA-11 PET. Prostate background SUVmax was measured in the nearest visually defined normal tissue adjacent to a lesion as 1.0 cm², a perfect circle.

4.4. Statistical Analysis

We classified the same cohort prostate focal lesions according to PI-RADS version 2.0 and 2.1. SUVmax and corresponding LBR were measured and compared. We divided all lesions into two subgroups, TZ and PZ. All statistical analyses were performed using SPSS 25 for Windows (IBM Corp, Armonk, NY, USA). We evaluated the inter-reader agreement of the PI-RADS assessment category for PI-RADS version 2.0 and 2.1 using the kappa(k) value. Kappa values indicate: poor 0.0,

slight 0.0–0.20, fair 0.21–0.40, moderate 0.41–0.60, substantial 0.61–0.80 and, almost-perfect 0.81–1.00 [31]. The Mann–Whitney U-test was used for data comparison between PI-RADS version 2.0 and 2.1.

The significance level was set to two-tailed $p < 0.05$. Patient demographics and clinical characteristics are summarized using descriptive statistics. Normal distributed data are reported as mean \pm standard deviation (SD), and non-normal distributed data are reported as median (interquartile range) (IQR Q1, Q3).

5. Limitations

There are some limitations to this study. First, this was a retrospective, single-center study. Therefore, the present results may need further validation in prospective multi-center studies with a larger number of patients. Second, this is a descriptive imaging analysis. Due to the characteristics of the patients' population in our institute, all patients were confirmed PCa by standard biopsy before [⁶⁸Ga]Ga-PSMA-11 PET PET/MRI scanning. MRI-ultrasound fusion-guided prostate biopsy might not be performed, or the information may not be acquirable; therefore, we were not able to study the relationship between PI-RADS scores and targeted biopsy results.

6. Conclusions

In conclusion, revisions of PI-RADS version 2.1 results in variations in lesions classification. Lesions with the PI-RADS category of 3, 4, and 5 present relatively higher intraprostatic PSMA uptake, while lesions with the PI-RADS category of 1 and 2 present relatively lower and similar uptake. PI-RADS version 2.1 has higher inter-reader reproducibility than PI-RADS version 2.0. Our result indicated that by using the updated version, radiologists and nuclear medicine doctors are more unlikely to perform an equivocal diagnosis, which could provide more useful information to urologists and oncologists for the management of lesions and clinical decisions making.

Author Contributions: Conceptualization, J.Z. and M.R.M.; methodology, J.Z.; software, J.Z.; validation, A.K., D.B.M. and J.B.; formal analysis, D.B.M.; writing—original draft preparation, J.Z.; writing—review and editing, A.K.; visualization, J.B.; supervision, M.R.M.; project administration, B.H.; funding acquisition, W.B. All authors have read and agreed to the published version of the manuscript.

Funding: The PET/MRI scanner is funded in part by the German Research Foundation (INST 335/454-1). We acknowledge support from the German Research Foundation (DFG) and the Open Access Publication Fund of Charité—Universitätsmedizin Berlin.

Acknowledgments: J.Z. thanks German Research Foundation (GRK2260, BIOQIC) for the support.

Conflicts of Interest: The authors declare that they have no conflict of interest.

Abbreviations

ADC	apparent diffusion coefficient
ADT	Androgen deprivation therapy
BPH	Benign prostatic hyperplasia
CI	Confidence interval
CT	Computed tomography
DCE-MRI	Dynamic contrast-enhanced MRI
DWI	Diffusion-weighted imaging
IQR	Interquartile range
FOV	Field-of-view
Ga	Gallium
GS	Gleason score
LBR	Lesion-to-background ratio
MRI	Magnetic resonance imaging
mpMRI	Multiparametric magnetic resonance imaging
OSEM	Ordered subset expectation maximization algorithm

PCa	Prostate cancer
PET/CT	Positron emission tomography/computed tomography
PET/MR	Positron emission tomography /magnetic resonance
PI-RADS	Prostate Imaging Reporting and Data System
PSA	Prostate-specific antigen
PSMA	Prostate-specific membrane antigen
PROMISE	Prostate Cancer Molecular Imaging Standardized Evaluation
ROI	Region of interest
RP	Radical prostatectomy
SUV	Standardized uptake value
TE	Echo time
TR	Repetition time
T2WI	T2-weighted imaging

References

1. Siegel, R.L.; Miller, K.D.; Jemal, A. Cancer statistics, 2018. *CA Cancer J. Clin.* **2018**, *60*, 277–300. [CrossRef] [PubMed]
2. Muller, B.G.; Shih, J.H.; Sankineni, S.; Marko, J.; Rais-Bahrami, S.; George, A.K.; De La Rosette, J.J.M.C.H.; Merino, M.J.; Wood, B.J.; Pinto, P.A.; et al. Prostate Cancer: Interobserver Agreement and Accuracy with the Revised Prostate Imaging Reporting and Data System at Multiparametric MR Imaging. *Radiology* **2015**, *277*, 741–750. [CrossRef] [PubMed]
3. Weinreb, J.C.; Barentsz, J.O.; Choyke, P.L.; Cornud, F.; Haider, M.A.; Macura, K.J.; Margolis, D.J.A.; Schnall, M.D.; Shtern, F.; Tempny, C.M.; et al. PI-RADS Prostate Imaging—Reporting and Data System: 2015, Version 2. *Eur. Urol.* **2016**, *69*, 16–40. [CrossRef] [PubMed]
4. Rosenkrantz, A.B.; Ginocchio, L.A.; Cornfeld, D.; Froemming, A.T.; Gupta, R.T.; Turkbey, B.; Westphalen, A.C.; Babb, J.S.; Margolis, D.J. Interobserver Reproducibility of the PI-RADS Version 2 Lexicon: A Multicenter Study of Six Experienced Prostate Radiologists. *Radiology* **2016**, *280*, 793–804. [CrossRef] [PubMed]
5. Borofsky, S.; George, A.K.; Gaur, S.; Bernardo, M.; Greer, M.; Mertan, F.V.; Taffel, M.; Moreno, V.; Merino, M.J.; Wood, B.J.; et al. What Are We Missing? False-Negative Cancers at Multiparametric MR Imaging of the Prostate. *Radiology* **2018**, *286*, 186–195. [CrossRef]
6. Rosenkrantz, A.B.; Babb, J.S.; Taneja, S.S.; Ream, J.M. Proposed Adjustments to PI-RADS Version 2 Decision Rules: Impact on Prostate Cancer Detection. *Radiology* **2017**, *283*, 119–129. [CrossRef]
7. Benndorf, M.; Hahn, F.; Krönig, M.; Jilg, C.A.; Krauss, T.; Langer, M.; Dovi-Akué, P. Diagnostic performance and reproducibility of T2w based and diffusion weighted imaging (DWI) based PI-RADSV2 lexicon descriptors for prostate MRI. *Eur. J. Radiol.* **2017**, *93*, 9–15. [CrossRef]
8. Benndorf, M.; Waibel, L.; Krönig, M.; Jilg, C.A.; Langer, M.; Krauss, T. Peripheral zone lesions of intermediary risk in multiparametric prostate MRI: Frequency and validation of the PI-RADSV2 risk stratification algorithm based on focal contrast enhancement. *Eur. J. Radiol.* **2018**, *99*, 62–67. [CrossRef]
9. Ross, J.S.; Sheehan, C.E.; Fisher, H.A.G.; Kaufman, R.P.; Kaur, P.; Gray, K.; Webb, I.; Gray, G.S.; Mosher, R.; Kallakury, B.V.S. Correlation of primary tumor prostate-specific membrane antigen expression with disease recurrence in prostate cancer. *Clin. Cancer Res.* **2003**, *9*, 6357–6362.
10. Treglia, G.; Annunziata, S.; Pizzuto, D.A.; Giovanella, L.; Prior, J.O.; Ceriani, L. Detection Rate of ¹⁸F-Labeled PSMA PET/CT in Biochemical Recurrent Prostate Cancer: A Systematic Review and a Meta-Analysis. *Cancers* **2019**, *11*, 710. [CrossRef]
11. Koerber, S.A.; Utzinger, M.T.; Kratochwil, C.; Kesch, C.; Haefner, M.F.; Katayama, S.; Mier, W.; Jagaru, A.H.; Herfarth, K.; Haberkorn, U.; et al. ⁶⁸Ga-PSMA-11 PET/CT in Newly Diagnosed Carcinoma of the Prostate: Correlation of Intraprostatic PSMA Uptake with Several Clinical Parameters. *J. Nucl. Med.* **2017**, *58*, 1943–1948. [CrossRef] [PubMed]
12. Woythal, N.; Arsenic, R.; Kempkensteffen, C.; Miller, K.; Janssen, J.-C.; Huang, K.; Makowski, M.R.; Brenner, W.; Prasad, V. Immunohistochemical Validation of PSMA Expression Measured by ⁶⁸Ga-PSMA PET/CT in Primary Prostate Cancer. *J. Nucl. Med.* **2018**, *59*, 238–243. [CrossRef]

13. Zamboglou, C.; Drendel, V.; Jilg, C.A.; Rischke, H.C.; Beck, T.I.; Schultze-Seemann, W.; Krauss, T.; Mix, M.; Schiller, F.; Wetterauer, U.; et al. Comparison of ^{68}Ga -HBED-CC PSMA-PET/CT and multiparametric MRI for gross tumour volume detection in patients with primary prostate cancer based on slice by slice comparison with histopathology. *Theranostics* **2017**, *7*, 228–237. [CrossRef]
14. Eiber, M.; Weirich, G.; Holzapfel, K.; Souvatzoglou, M.; Haller, B.; Rauscher, I.; Beer, A.J.; Wester, H.-J.; Gschwend, J.; Schwaiger, M.; et al. Simultaneous ^{68}Ga -PSMA HBED-CC PET/MRI Improves the Localization of Primary Prostate Cancer. *Eur. Urol.* **2016**, *70*, 829–836. [CrossRef]
15. Turkbey, B.; Rosenkrantz, A.B.; Haider, M.A.; Padhani, A.R.; Villeirs, G.; Macura, K.J.; Tempany, C.M.; Choyke, P.L.; Cornud, F.; Margolis, D.J.; et al. Prostate Imaging Reporting and Data System Version 2.1: 2019 Update of Prostate Imaging Reporting and Data System Version 2. *Eur. Urol.* **2019**, *76*, 340–351. [CrossRef]
16. Ben Jemaa, A.; Bouraoui, Y.; Sallami, S.; Banasr, A.; Nouira, Y.; Horchani, A.; Oueslati, R. Cellular distribution and heterogeneity of Psa and Psma expression in normal, hyperplasia and human prostate cancer. *Tunis Med.* **2013**, *91*, 458–463.
17. Eiber, M.; Fendler, W.P.; Rowe, S.P.; Calais, J.; Hofman, M.S.; Maurer, T.; Schwarzenboeck, S.M.; Kratochwil, C.; Herrmann, K.; Giesel, F.L. Prostate-Specific Membrane Antigen Ligands for Imaging and Therapy. *J. Nucl. Med.* **2017**, *58* (Suppl. 2), 67S–76S. [CrossRef]
18. Lapidus, R.G.; Tiffany, C.W.; Isaacs, J.T.; Slusher, B.S. Prostate-specific membrane antigen (PSMA) enzyme activity is elevated in prostate cancer cells. *Prostate* **2000**, *45*, 350–354. [CrossRef]
19. Westphalen, A.C.; McCulloch, C.E.; Anaokar, J.M.; Arora, S.; Barashi, N.S.; Barentsz, J.O.; Bathala, T.K.; Bittencourt, L.K.; Booker, M.T.; Braxton, V.G.; et al. Variability of the Positive Predictive Value of PI-RADS for Prostate MRI across 26 Centers: Experience of the Society of Abdominal Radiology Prostate Cancer Disease-focused Panel. *Radiology* **2020**, *296*, 76–84. [CrossRef]
20. Tamada, T.; Kido, A.; Takeuchi, M.; Yamamoto, A.; Miyaji, Y.; Kanomata, N.; Sone, T. Comparison of PI-RADS version 2 and PI-RADS version 2.1 for the detection of transition zone prostate cancer. *Eur. J. Radiol.* **2019**, *121*, 108704. [CrossRef]
21. Byun, J.; Park, K.J.; Kim, M.; Kim, J.K. Direct Comparison of PI-RADS Version 2 and 2.1 in Transition Zone Lesions for Detection of Prostate Cancer: Preliminary Experience. *J. Magn. Reson. Imaging* **2020**, *52*, 577–586. [CrossRef] [PubMed]
22. Wei, C.-G.; Zhang, Y.-Y.; Pan, P.; Chen, T.; Yu, H.-C.; Dai, G.-C.; Tu, J.; Yang, S.; Zhao, W.-L.; Shen, J. Diagnostic Accuracy and Inter-observer Agreement of PI-RADS Version 2 and Version 2.1 for the Detection of Transition Zone Prostate Cancers. *Am. J. Roentgenol.* **2020**. [CrossRef]
23. Barrett, T.; Rajesh, A.; Rosenkrantz, A.; Choyke, P.; Turkbey, B. PI-RADS version 2.1: One small step for prostate MRI. *Clin. Radiol.* **2019**, *74*, 841–852. [CrossRef]
24. Bettermann, A.S.; Zamboglou, C.; Kiefer, S.; Jilg, C.A.; Spohn, S.; Kranz-Rudolph, J.; Fassbender, T.F.; Bronsert, P.; Nicolay, N.H.; Gratzke, C.; et al. [^{68}Ga]-PSMA-11 PET/CT and multiparametric MRI for gross tumor volume delineation in a slice by slice analysis with whole mount histopathology as a reference standard—Implications for focal radiotherapy planning in primary prostate cancer. *Radiother. Oncol.* **2019**, *141*, 214–219. [CrossRef]
25. Zamboglou, C.; Wieser, G.; Hennies, S.; Rempel, I.; Kirste, S.; Soschynski, M.; Rischke, H.C.; Fechter, T.; Jilg, C.A.; Langer, M.; et al. MRI versus ^{68}Ga -PSMA PET/CT for gross tumour volume delineation in radiation treatment planning of primary prostate cancer. *Eur. J. Nucl. Med. Mol. Imaging* **2015**, *43*, 889–897. [CrossRef]
26. Garzón, J.G.; Torres, M.D.A.; Delgado-Bolton, R.C.; Ceci, F.; Ruiz, S.A.; Rincón, J.O.; Caresia-Arótzgui, A.P.; Garcia-Velloso, M.J.; Vicente, A.G. ^{68}Ga -PSMA PET/CT in prostate cancer. *Rev. Esp. Med. Nucl. Imagen. Mol.* **2018**, *37*, 130–138. [CrossRef]
27. Corfield, J.; Perera, P.M.S.; Bolton, D.; Lawrentschuk, N. ^{68}Ga -prostate specific membrane antigen (PSMA) positron emission tomography (PET) for primary staging of high-risk prostate cancer: A systematic review. *World J. Urol.* **2018**, *36*, 519–527. [CrossRef] [PubMed]
28. Nanabala, R.; Anees, M.K.; Sasikumar, A.; Joy, A.; Pillai, M. Preparation of [^{68}Ga]PSMA-11 for PET-CT imaging using a manual synthesis module and organic matrix based $^{68}\text{Ge}/^{68}\text{Ga}$ generator. *Nucl. Med. Biol.* **2016**, *43*, 463–469. [CrossRef] [PubMed]

29. Hope, T.A.; Aggarwal, R.; Chee, B.; Tao, D.; Greene, K.L.; Cooperberg, M.R.; Feng, F.; Chang, A.; Ryan, C.J.; Small, E.J.; et al. Impact of ^{68}Ga -PSMA-11 PET on Management in Patients with Biochemically Recurrent Prostate Cancer. *J. Nucl. Med.* **2017**, *58*, 1956–1961. [CrossRef]
30. Afshar-Oromieh, A.; Malcher, A.; Eder, M.; Eisenhut, M.; Linhart, H.G.; Hadaschik, B.A.; Holland-Letz, T.; Giesel, F.L.; Kratochwil, C.; Haufe, S.; et al. PET imaging with a ^{68}Ga gallium-labelled PSMA ligand for the diagnosis of prostate cancer: Biodistribution in humans and first evaluation of tumour lesions. *Eur. J. Nucl. Med. Mol. Imaging* **2013**, *40*, 486–495. [CrossRef]
31. Landis, J.R.; Koch, G.G. The Measurement of Observer Agreement for Categorical Data. *Biometrics* **1977**, *33*, 159. [CrossRef] [PubMed]

Publisher's Note: MDPI stays neutral with regard to jurisdictional claims in published maps and institutional affiliations.



© 2020 by the authors. Licensee MDPI, Basel, Switzerland. This article is an open access article distributed under the terms and conditions of the Creative Commons Attribution (CC BY) license (<http://creativecommons.org/licenses/by/4.0/>).

Excerpt from Journal Summary List--3

Journal Data Filtered By: **Selected JCR Year: 2019** Selected Editions: SCIE,SSCI
 Selected Categories: **"ONCOLOGY"** Selected Category Scheme: WoS
Gesamtanzahl: 244 Journale

Rank	Full Journal Title	Total Cites	Journal Impact Factor	Eigenfactor Score
1	CA-A CANCER JOURNAL FOR CLINICIANS	39,917	292.278	0.093460
2	Nature Reviews Clinical Oncology	12,384	53.276	0.035980
3	NATURE REVIEWS CANCER	52,053	53.030	0.066030
4	LANCET ONCOLOGY	53,592	33.752	0.143420
5	JOURNAL OF CLINICAL ONCOLOGY	155,297	32.956	0.261940
6	Cancer Discovery	18,093	29.497	0.069280
7	CANCER CELL	41,064	26.602	0.095430
8	JAMA Oncology	13,794	24.799	0.064650
9	ANNALS OF ONCOLOGY	45,813	18.274	0.107060
10	Molecular Cancer	15,448	15.302	0.023990
11	Journal of Thoracic Oncology	18,136	13.357	0.038200
12	JNCI-Journal of the National Cancer Institute	36,018	11.577	0.045450
13	Trends in Cancer	2,351	11.093	0.010140
14	SEMINARS IN CANCER BIOLOGY	8,310	11.090	0.011730
15	Journal of Hematology & Oncology	6,732	11.059	0.015550
16	NEURO-ONCOLOGY	12,950	10.247	0.029050
17	CLINICAL CANCER RESEARCH	85,288	10.107	0.131520
18	Journal for ImmunoTherapy of Cancer	4,557	9.913	0.016030
19	CANCER RESEARCH	135,753	9.727	0.118680
20	Liver Cancer	1,131	9.720	0.002660

Rank	Full Journal Title	Total Cites	Journal Impact Factor	Eigenfactor Score
21	Journal of the National Comprehensive Cancer Network	6,912	9.316	0.020020
22	CANCER TREATMENT REVIEWS	9,427	8.885	0.017800
23	Cancer Immunology Research	6,969	8.728	0.026440
24	LEUKEMIA	25,819	8.665	0.048640
25	Blood Cancer Journal	2,800	8.023	0.010400
26	ONCOGENE	66,303	7.971	0.068320
27	Clinical and Translational Medicine	1,349	7.919	0.003280
28	npj Precision Oncology	500	7.717	0.001520
29	BIOCHIMICA ET BIOPHYSICA ACTA-REVIEWS ON CANCER	5,650	7.365	0.007800
30	CANCER LETTERS	34,162	7.360	0.044450
31	EUROPEAN JOURNAL OF CANCER	32,241	7.275	0.048170
32	Gastric Cancer	5,525	7.088	0.010730
33	JOURNAL OF EXPERIMENTAL & CLINICAL CANCER RESEARCH	9,316	7.068	0.014540
34	Therapeutic Advances in Medical Oncology	1,894	6.852	0.004260
35	Molecular Oncology	6,378	6.574	0.013820
36	CANCER AND METASTASIS REVIEWS	6,247	6.400	0.005940
37	Cancers	10,442	6.126	0.018740
38	Oncogenesis	2,775	6.119	0.007750
39	STEM CELLS	20,554	6.022	0.024110
40	npj Breast Cancer	814	6.000	0.003590
41	JOURNAL OF PATHOLOGY	16,307	5.979	0.017910



Zhao J, Kader A, Mangarova DB, Brangsch J, Brenner W, Hamm B, Makowski MR: Dynamic Contrast-Enhanced MRI of Prostate Lesions of Simultaneous [⁶⁸Ga]Ga-PSMA-11 PET/MRI: Comparison between Intraprostatic Lesions and Correlation between Perfusion Parameters. *CANCERS* 2021;13:1404.

DOI: [https:// doi.org/10.3390/cancers13061404](https://doi.org/10.3390/cancers13061404)



Article

Dynamic Contrast-Enhanced MRI of Prostate Lesions of Simultaneous [⁶⁸Ga]Ga-PSMA-11 PET/MRI: Comparison between Intraprostatic Lesions and Correlation between Perfusion Parameters

Jing Zhao ^{1,*} , Avan Kader ^{1,2} , Dilyana B. Mangarova ^{1,3}, Julia Brangsch ¹ , Winfried Brenner ⁴ , Bernd Hamm ¹ and Marcus R. Makowski ^{1,5}

- ¹ Institute of Radiology and Nuclear Medicine, Charité—Universitätsmedizin Berlin, Corporate Member of Freie Universität Berlin, Humboldt-Universität zu Berlin, and Berlin Institute of Health, Charitéplatz 1, 10117 Berlin, Germany; avan.kader@charite.de (A.K.); dilyana.mangarova@charite.de (D.B.M.); julia.brangsch@charite.de (J.B.); bernd.hamm@charite.de (B.H.); marcus.makowski@charite.de (M.R.M.)
 - ² Department of Biology, Chemistry and Pharmacy, Institute of Biology, Freie Universität Berlin, Königin-Luise-Str. 1-3, 14195 Berlin, Germany
 - ³ Department of Veterinary Medicine, Institute of Veterinary Pathology, Freie Universität Berlin, Robert-von-Ostertag-Str. 15, Building 12, 14163 Berlin, Germany
 - ⁴ Department of Nuclear Medicine, Charité—Universitätsmedizin Berlin, Corporate Member of Freie Universität Berlin, Humboldt-Universität zu Berlin, and Berlin Institute of Health, Augustenburger Platz 1, 13353 Berlin, Germany; winfried.brenner@charite.de
 - ⁵ Department of Diagnostic and Interventional Radiology, Klinikum rechts der Isar, Technische Universität München, Ismaninger Str. 22, 81675 Munich, Germany
- * Correspondence: jing.zhao@charite.de



Citation: Zhao, J.; Kader, A.; Mangarova, D.B.; Brangsch, J.; Brenner, W.; Hamm, B.; Makowski, M.R. Dynamic Contrast-Enhanced MRI of Prostate Lesions of Simultaneous [⁶⁸Ga]Ga-PSMA-11 PET/MRI: Comparison between Intraprostatic Lesions and Correlation between Perfusion Parameters. *Cancers* **2021**, *13*, 1404. <https://doi.org/10.3390/cancers13061404>

Academic Editors: Alessio G. Morganti, Mirko D'Onofrio, Maria Antonietta Bali and Maxime Ronot

Received: 13 December 2020

Accepted: 16 March 2021

Published: 19 March 2021

Publisher's Note: MDPI stays neutral with regard to jurisdictional claims in published maps and institutional affiliations.



Copyright: © 2021 by the authors. Licensee MDPI, Basel, Switzerland. This article is an open access article distributed under the terms and conditions of the Creative Commons Attribution (CC BY) license (<https://creativecommons.org/licenses/by/4.0/>).

Simple Summary: Dynamic contrast-enhanced magnetic resonance imaging (DCE-MRI) is an important method to analyze the perfusion model of tumors, allowing noninvasive quantification of microvascular structure and function. Furthermore, simultaneous [⁶⁸Ga]Ga-prostate-specific membrane antigen (PSMA)-11 positron emission tomography (PET)/MRI is currently the most advantageous way for assessing prostate cancer staging. Therefore, combining these two examinations helps to diagnose the lesions more comprehensively. Our study analyzes perfusion parameters between intraprostatic lesions and the correlation between perfusion parameters and [⁶⁸Ga]Ga-PSMA-11 PET. This study highlights the significant effect of PSMA uptake on perfusion parameters.

Abstract: We aimed to retrospectively compare the perfusion parameters measured from dynamic contrast-enhanced (DCE) magnetic resonance imaging (MRI) of prostate benign lesions and malignant lesions to determine the relationship between perfusion parameters. DCE-MRI was performed in patients with PCa who underwent simultaneous [⁶⁸Ga]Ga-prostate-specific membrane antigen (PSMA)-11 positron emission tomography (PET)/MRI. Six perfusion parameters (arrival time (AT), time to peak (TTP), wash-in slope (W-in), wash-out slope (W-out), peak enhancement intensity (PEI), and initial area under the 60-s curve (iAUC)), and a semi-quantitative parameter, standardized uptake values maximum (SUVmax) were calculated by placing regions of interest in the largest area of the lesions. The DCE-MRI parameters between prostate benign and malignant lesions were compared. The DCE-MRI parameters in both the benign and malignant lesions subgroup with SUVmax ≤ 3.0 and SUVmax > 3.0 were compared. The correlation of DCE-MRI parameters was investigated. Malignant lesions demonstrated significantly shorter TTP and higher SUVmax than did benign lesions. In the benign and malignant lesions subgroup, perfusion parameters of lesions with SUVmax ≤ 3.0 show no significant difference to those with SUVmax > 3.0. DCE-MRI perfusion parameters show a close correlation with each other. DCE-MRI parameters reflect the perfusion characteristics of intraprostatic lesions with malignant lesions, demonstrating significantly shorter TTP. There is a moderate to strong correlation between DCE-MRI parameters. Semi-quantitative analysis reflects that malignant lesions show a significantly higher SUVmax than benign lesions.

Keywords: prostate cancer; PSMA; PET/MRI; dynamic contrast-enhanced; arrival time; time to peak; wash-in slope; wash-out slope; peak enhancement intensity; initial area under curve

1. Introduction

Prostate cancer (PCa) is one of the most common diseases in men. In the US, it accounts for 21% of new cases, and it is the second leading cause of death in men, accounting for 10% of all deaths [1].

Multiparameters magnetic resonance imaging (mpMRI) with the assessment of images using the Prostate Imaging Reporting and Data System (PI-RADS) is widely used to evaluate prostate lesions. Dynamic contrast-enhanced (DCE)-MRI is a technique used to measure the perfusion, blood flow, and tissue vascularity by analyzing the tissue's signal enhancement curve. DCE-MRI, which can assess micro-vascular properties, provides helpful additional information for characterizing lesions [2]. In many current clinical trials, DCE-MRI for a new anti-angiogenic agent is used as an early imaging biomarker to evaluate patients' response to treatment [3]. Microvessel density has been reported to be associated with tumor stage, recurrence, metastatic potential, and prognosis in patients with prostate cancer [4–6]. This signal enhancement of perfusion can be quantified with semi-quantitative analysis [7,8]. Semi-quantitative parameters can be extracted and calculated from the signal intensity curve [9,10]. The signal intensity curve reveals several parameters, including arrival time (AT), time to peak (TTP), wash-in slope (W-in), wash-out slope (W-out), peak enhancement intensity (PEI), and initial area under the 60-sec curve (iAUC). AT is arrival time, which is the time point when contrast enhancement starts. TTP is time to peak, which is the time from arrival time to the end of wash-in. A shorter TTP indicates the shorter time needed to reach the peak. Wash-in slope is the slope of the fitted line between AT and the end of wash-in. The higher W-in is, the faster the wash-in speed. W-out slope is the fitted line slope between the start of wash-out and the end of the measurement. The higher the W-out is, the faster the wash-out speed. PEI indicates the highest value of enhancement. And iAUC calculates the initial area under the curve in 60 s, reflecting the total intensity of enhancement during the first one minute.

Molecular imaging of prostate cancer is a beneficial tool for systematically evaluating tumor biology [11]. Agents targeting cell metabolism, hormone receptors, or membrane proteins have been developed to an advanced stage. Over the last few years, prostate-specific membrane antigen (PSMA) have gained much interest as specific targets for PCa imaging, which is a promising and specific target. It is a transmembrane glycoprotein related to tumor progression and disease recurrence that has been found to be overexpressed in prostate cancer cells [12,13]. PSMA-ligands as prostate cancer-specific PET tracers show and differentiate cancerous lesions within the prostate more accurately than other tracers. A whole-body hybrid PET/MRI scanner with simultaneous acquisition of PET imaging and mpMRI has enabled functional and molecular information to be combined [14–16]. Initial results suggest that [⁶⁸Ga]Ga-PSMA-11 PET/MRI is a beneficial imaging method for detecting suspicious focal prostate cancer lesions [17,18] and monitoring recurrence [19]. Combining MRI and positron emission tomography (PET) improves diagnostic accuracy [20,21]. Compared with the current standard imaging like CT, MRI, and bone scintigraphy, PSMA-PET imaging shows a higher specificity and sensitivity and is suitable for patients with primary middle-risk or high-risk prostate cancer [22].

Therefore, this study's purpose was to retrospectively compare the perfusion parameters of DCE-MRI of prostate benign lesions and malignant lesions, and determine the correlation between these perfusion parameters.

2. Results

2.1. Comparison of Parameters between Benign and Malignant Lesions

TTP and SUVmax were significantly different between benign lesions and malignant lesions ($p < 0.05$) regarding the perfusion parameters and semi-quantitative parameters. No significant differences were observed in other parameters (Table 1).

Table 1. Comparison of parameters between benign and malignant lesions.

Parameter	Benign Lesions			Malignant Lesions			p Value
	Median	Q1	Q3	Median	Q1	Q3	
SUVmax	2.3	1.5	3.7	7.0	4.2	11.5	$p < 0.05$ *
AT(min)	0.47	0.40	0.57	0.47	0.39	0.56	$p > 0.05$
TTP(min)	1.09	0.84	1.32	0.95	0.75	1.22	$p < 0.05$ *
W-in	0.13	0.07	0.18	0.12	0.08	0.22	$p > 0.05$
W-out	0.01	0.01	0.02	0.01	0.01	0.02	$p > 0.05$
PEI	0.21	0.15	0.28	0.20	0.15	0.26	$p > 0.05$
iAUC	0.08	0.05	0.11	0.08	0.05	0.12	$p > 0.05$

AT: arrival time, TTP: time to peak, W-in: wash-in slope, W-out: wash-out slope, PEI: peak enhancement intensity, iAUC: initial area under the 60-sec curve, SUVmax: standardized uptake values maximum, * $p < 0.05$.

2.2. Effect of SUVmax on DCE-MRI Parameters

All lesions were assigned into two subgroups, including benign lesions group and malignant lesions group. In both subgroups, DCE-MRI parameters between lesions with $SUV_{max} \leq 3.0$ and $SUV_{max} > 3.0$ were compared. In the benign lesions subgroup, perfusion parameters of lesions with $SUV_{max} \leq 3.0$ show no significant difference from those with $SUV_{max} > 3.0$ (Table 2). In the malignant lesions subgroup, perfusion parameters of lesions with $SUV_{max} > 3.0$ show no significant difference from those with $SUV_{max} \leq 3.0$ (Table 3).

Table 2. Comparison of parameters between benign lesions with $SUV_{max} \leq 3.0$ and $SUV_{max} > 3.0$.

Parameter	$SUV_{max} \leq 3.0$			$SUV_{max} > 3.0$			p Value
	Median	Q1	Q3	Median	Q1	Q3	
SUVmax	1.6	1.2	2.3	4.7	3.6	6.2	$p < 0.05$ *
AT(min)	0.47	0.39	0.58	0.47	0.44	0.56	$p > 0.05$
TTP(min)	1.13	0.92	1.35	0.92	0.78	1.24	$p > 0.05$
W-in	0.13	0.07	0.18	0.13	0.08	0.21	$p > 0.05$
W-out	0.01	0.01	0.02	0.01	0.01	0.02	$p > 0.05$
PEI	0.21	0.16	0.28	0.21	0.12	0.27	$p > 0.05$
iAUC	0.09	0.05	0.11	0.07	0.05	0.12	$p > 0.05$

AT: arrival time, TTP: time to peak, W-in: wash-in slope, W-out: wash-out slope, PEI: peak enhancement intensity, iAUC: initial area under the 60-sec curve, SUVmax: standardized uptake values maximum, * $p < 0.05$.

Table 3. Comparison of parameters between malignant lesions with $SUV_{max} \leq 3.0$ and $SUV_{max} > 3.0$.

Parameter	$SUV_{max} \leq 3.0$			$SUV_{max} > 3.0$			p Value
	Median	Q1	Q3	Median	Q1	Q3	
SUVmax	2.0	1.0	2.2	8.2	5.5	12.2	$p < 0.05$ *
AT(min)	0.49	0.47	0.98	0.47	0.39	0.55	$p > 0.05$
TTP(min)	0.95	0.66	1.12	0.96	0.77	1.22	$p > 0.05$
W-in	0.16	0.08	0.28	0.12	0.08	0.22	$p > 0.05$
W-out	0.01	−0.003	0.02	0.01	0.01	0.02	$p > 0.05$
PEI	0.20	0.14	0.32	0.21	0.15	0.25	$p > 0.05$
iAUC	0.08	0.05	0.19	0.08	0.05	0.12	$p > 0.05$

AT: arrival time, TTP: time to peak, W-in: wash-in slope, W-out: wash-out slope, PEI: peak enhancement intensity, iAUC: initial area under the 60-sec curve, SUVmax: standardized uptake values maximum, * $p < 0.05$.

2.3. Pearson Correlation between Perfusion Parameters of Intraprostatic Lesions

There is a moderate to strong correlation between the perfusion parameters of intraprostatic lesions (Table 4).

Table 4. Pearson correlation analysis between the perfusion parameters.

	AT	TTP	W-in	W-out	PEI	iAUC
AT	1	−0.17 *	0.18 *	−0.05	−0.004	0.18 *
TTP	-	1	−0.45 **	0.71 **	0.17 *	−0.31 **
W-in	-	-	1	−0.30 **	0.57 **	0.95 **
W-out	-	-	-	1	0.41 **	−0.18 *
PEI	-	-	-	-	1	0.70 **
iAUC	-	-	-	-	-	1

Data are Pearson correlation coefficient. AT: arrival time, TTP: time to peak, W-in: wash-in slope, W-out: wash-out slope, PEI: peak enhancement intensity, iAUC: initial area under the 60-sec curve, * $p < 0.05$, ** $p < 0.01$.

3. Discussion

DCE-MRI is an important diagnostic method in detecting focal prostate cancer lesions, which improves the accuracy of examination for detection and evaluation of intraprostatic tumor lesions [23]. It visualizes focal lesions in the prostate with varying degrees of enhancement and provides information for lesion characterization. Combining the advantages of [⁶⁸Ga]Ga-PSMA-11 PET/MRI and DCE-MRI contributes to a better differentiation of intraprostatic lesions [24]. PSMA-PET imaging can add molecular information to multiparameter MRI to describe suspicious lesions for target biopsy [25]. The clinical value of this study is the quantitative analysis of the multimodality characteristics of the lesions. DCE parameters reflect lesions' microvascular structure, while SUVmax reflects lesions' prostate-specific membrane antigen concentration. A combination of information allows for a comprehensive evaluation of tumor condition and for choosing an appropriate treatment plan.

Intraprostatic lesions perfusion parameters are investigated by several studies before [26]. Vos et al. [27] reported that quantitative parameters and semi-quantitative parameters derived from DCE-MRI at 3.0 T MRI could assess the aggressiveness of PCa in the peripheral zone. Chen et al. [28] proved that the wash-out gradient shows a significant association with Gleason score and good diagnostic performance in assessing prostate tumor aggressiveness. PCa has increased microvasculature and, therefore, can be detected by contrast-enhanced MRI techniques, as van Niekerk et al. reported [29]. These parameters provide detailed information about the aggressiveness of tumors in different prostate gland regions as, for example, in Figures 1–3. Therefore, the perfusion differences between prostate benign lesions and malignant lesions may be detected and quantified with DCE-MRI. MpmMRI of prostate scanning includes complementary and synergistic T2, diffusion, and perfusion sequences. Ren et al. [30] proved that DCE-MRI curves could differentiate benign tissue from malignant prostate tissue based on T2-weighted imaging. The omission of DCE-MRI increases the risk that some aggressive lesions will not be detected, thus discrediting prostate imaging by MRI. The sequence of contrast enhancement agents is essential in the detection of recurrence and post-treatment follow-up.

The advantage of the curve analysis method is that it is easy to calculate. Model-based measurement parameters are complex, but they provide more specific information about vascular physiology [31]. In this study, we compared perfusion parameters between benign lesions and malignant lesions. TTP was significantly different. TTP is the time that contrast enhancement reaches the peak. A shorter TTP indicates the shorter time needed to reach the peak. Then it can be explained that the blood vessels are more abundant in the corresponding lesions. We further divided the lesions into two subgroups. The lesions were divided into two groups in the benign lesion group according to SUVmax ≤ 3.0 and SUVmax > 3.0 . All perfusion parameters did not show obvious differences between SUVmax ≤ 3.0 and SUVmax > 3.0 . This indicates that SUVmax does not affect the

perfusion parameters in benign lesions. In the malignant lesions group, the same results were found.

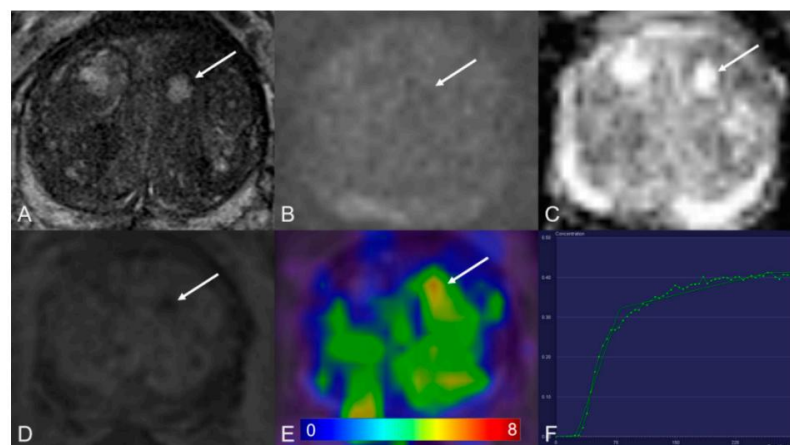


Figure 1. Transition zone with a PI-RADS 1 change. (A) Axial T2WI shows typical benign prostatic hyperplasia (BPH) change. (B) DWI ($b = 1000 \text{ s/mm}^2$) shows no lesion with a marked hyperintense signal above the background. (C) ADC map image presents no diffusion restriction. (D) Early dynamic contrast-enhanced image presents no enhancement within the typical BPH nodule. (E) [^{68}Ga]Ga-PSMA-11 PET/MRI fusion image shows moderate [^{68}Ga]Ga-PSMA-11 uptake, with SUVmax of 6.3. (F) DCE-MRI time-intensity curve demonstrates persistent increase enhancement. AT: 0.39 min; TTP: 1.09 min; W-in: 0.16; W-out: 0.02; PEI: 0.25; iAUC: 0.10.

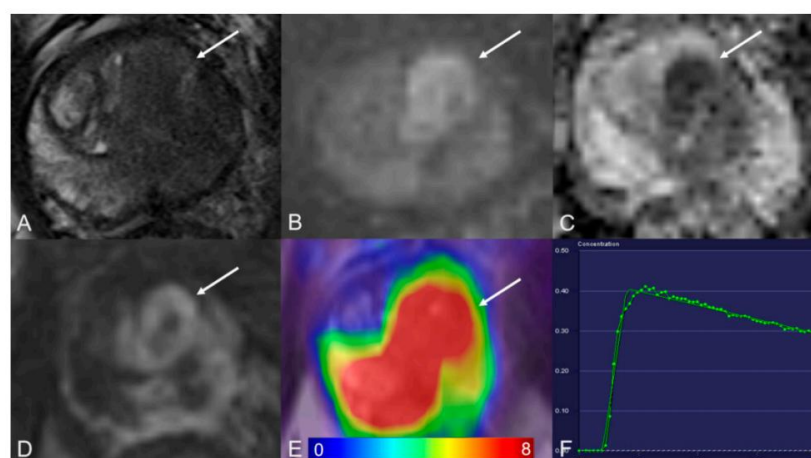


Figure 2. Transition zone with a PI-RADS 5 lesion. (A) Axial T2WI shows homogeneous hypointense. (B) DWI ($b = 1000 \text{ s/mm}^2$) shows a marked hyperintense signal above the background. (C) ADC map image presents a lesion with hypointense signal below the background. (D) Early dynamic contrast-enhanced image presents positive enhancement within the lesion. (E) [^{68}Ga]Ga-PSMA-11 PET/MRI fusion image shows avid [^{68}Ga]Ga-PSMA-11 uptake, with SUVmax of 29.2. (F) DCE-MRI time-intensity curve demonstrates a decline after initial up-slope enhancement. AT: 0.47 min; TTP: 0.50 min; W-in: 0.80; W-out: -0.03 ; PEI: 0.41; iAUC: 0.31.

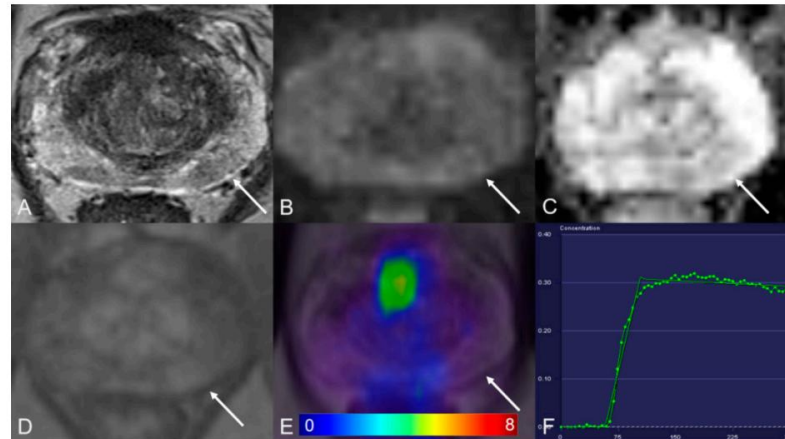


Figure 3. Peripheral zone with a PI-RADS 3 lesion. (A) Axial T2WI shows hypointense. (B) DWI ($b = 1000 \text{ s/mm}^2$) shows a mild hyperintense signal. (C) ADC map image presents a moderate hypointense signal below the background. (D) Early dynamic contrast-enhanced image presents no early enhancement within the lesion. (E) ^{68}Ga PSMA-11 PET/MRI fusion image shows no positive ^{68}Ga PSMA-11 uptake. (F) DCE-MRI time-intensity curve demonstrates plateau enhancement. AT: 0.98 min; TTP: 0.67 min; W-in: 0.26; W-out: 0.003; PEI: 0.20; iAUC: 0.13.

Moreover, we determined the correlations between perfusion parameters to understand further the physiological significance of semi-quantitative parameters in intraprostatic lesions. They may reflect gross angiogenesis within a focal lesion. AT is arrival time, the point in time when contrast enhancement starts. A shorter AT indicates that the contrast agent flows into the lesion in a shorter time. It further shows that the lesion is rich in blood vessels. W-in is the fitted line's slope between AT and the end of wash-in, reflecting the speed at which the contrast agent flows into the lesion. The slope is significantly correlated with blood flow so that it can be used to evaluate perfusion within a lesion. Another parameter, iAUC, is the initial area under the curve in 60 s. It suggests that iAUC denotes a combination of blood flow and permeability. These correlations may help select the most suitable semi-quantitative parameter to represent tumor perfusion, flow, and angiogenesis in daily practice.

Angiogenesis is an essential process in tumor growth, and a multitude of pharmacologic therapies primarily target angiogenesis by affecting vascular endothelial growth factor (VEGF) ligand binding [32]. Microvascular distribution is considered a vital sign of neovascularization, responsible for local growth and tumor metastasis [33,34]. In these applications, the potential of PSMA as an imaging biomarker is related to the exact function of PSMA in tumor-related endothelium. Conway et al. [35] demonstrated that PSMA is required for angiogenesis *in vivo* and is essential for endothelial cell invasion *in vitro*. Their results of linking PSMA with p21-activated kinase regulation suggest that PSMA is an important regulator of endothelial cell invasion and angiogenesis and may be a therapeutic target for angiogenesis-related diseases. Chang et al. [36] proved that PSMA was consistently expressed in the neovasculature of a wide variety of malignant neoplasms. More malignant lesions usually have more abundant microvascular structures [37–40]. DCE-MRI is one of the most mature imaging biomarkers of tumor microvessels. DCE-MRI and PSMA-PET can be performed simultaneously in a PET/MRI scanner so that these markers can be directly correlated.

Early research indicated that ADT causes a reduction of blood flow in the prostate gland that precedes apoptosis of the epithelium [41,42]. Another study held a different opinion. Roe et al. [43] reported that their key findings were the increased tumor vascularization following ADT. However, the above experimental conclusions are based on

animal experiments. Human studies characterizing vascular effects following ADT are limited. The long-term impact of ADT on tumor vascularization needs to be further investigated. The effects following radiotherapy of prostate measured with quantitative MRI were reported by Kershaw et al. [44] They proved that tumor blood flow decreased after treatment. Nevertheless, because of this study's relatively small sample size, a larger number of sample systematic quantitative studies are needed. Therefore, the effect of radiotherapy on the microvascular structure of the human prostate has not been conclusively established. Based on what has been discussed above, ADT and radiotherapy's effects on microvasculature were not considered in this study. There are some limitations to our study. The patient cohort is relatively small. There are only eleven patients who performed radical prostatectomy (RP) after scanning. Therefore, we were not able to take histopathology results as a gold standard.

4. Materials and Methods

4.1. Patients

This retrospective study was approved by the institutional ethics review board (EA1/060/16), and informed consent was waived for retrospective analysis.

We enrolled and excluded patients by the following criteria. Inclusion criteria: (1) patients with biopsy-proven prostate cancer who underwent [⁶⁸Ga]Ga-PSMA-11 PET/MRI between January 2017 and July 2020 in our clinic; (2) necessary information could be obtained. Exclusion criteria: (1) patients, who underwent radical prostatectomy before scanning, were excluded; (2) patients did not undergo DCE-MRI during the scan. Patients' inclusion and exclusion are summarized in the flowchart in Figure 4.

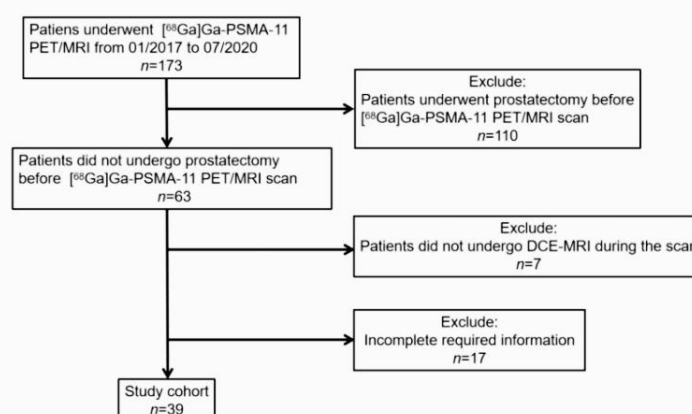


Figure 4. [⁶⁸Ga]Ga-PSMA-11 PET: gallium 68-labeled prostate-specific membrane antigen PET, DCE-MRI: Dynamic contrast-enhanced magnetic resonance imaging.

Patients who did not undergo radical prostatectomy before [⁶⁸Ga]Ga-PSMA-11 PET/MRI and performed DCE-MRI in [⁶⁸Ga]Ga-PSMA-11 PET/MRI examination were retrospectively selected from our institute's database and included in this analysis. All patients were confirmed PCa by systematic biopsy before [⁶⁸Ga]Ga-PSMA-11 PET PET/MRI scanning. Biopsy techniques included 12-core prostate biopsy and 14-core prostate biopsy. The needle biopsy technique introduced by Hodge et al. [45] has become the gold standard method for diagnosing prostate cancers. Both 12-core and 14-core prostate biopsy significantly increase the detection rate of prostate cancer and the accuracy of the biopsy Gleason score [46,47]. Clinical characteristics are compiled in Table 5.

Table 5. Summary of clinical characteristics.

Characteristics	N = 39
Age at scan (years)	69 ± 9
PSA (ng/ml) at scan time	8.70(5.18, 18.83)
Biopsy Gleason score (n)	
3 + 3	8
3 + 4	8
4 + 3	8
4 + 4	7
4 + 5	2
5 + 4	3
5 + 5	3
Treatment	
ADT prior to scan (n)	2
ADT ongoing at the time of scan (n)	3
Radiotherapy prior to scan (n)	3

ADT: Androgen deprivation therapy.

4.2. [⁶⁸Ga]Ga-PSMA-11 PET/MRI Imaging Protocol

[⁶⁸Ga]Ga-PSMA-11 was synthesized using a clinical-grade ⁶⁸Ge/⁶⁸Ga radionuclide generator (Eckert & Ziegler Radiopharma GmbH, Berlin, Germany) and PSMA-HBED-CC (ABX GmbH, Radeberg, Germany). Patients were imaged after 79 (72, 109) min after intravenous injection of a mean activity of 162.2 ± 22.1 MBq (4.4 ± 0.6 mCi) [⁶⁸Ga]Ga-PSMA-11, corresponding to activity: 1.8–2.2 MBq (0.049–0.060mCi) per kilogram bodyweight. To minimize the halo artifact caused by scattering overcorrection associated with high renal and urinary tracer activity, furosemide is injected 30 min before the start of PET acquisition. Patients were asked to void urine immediately before the start of the examination. No adverse effects were observed after [⁶⁸Ga]Ga-PSMA-11 injection.

PET and MRI were performed using the same protocol for every patient. Imaging was obtained with a 3.0 T PET/MRI system (SIEMENS MAGNETOM Biograph mMR, Erlangen, Germany). The acquisition was split into two parts. First, body PET/MRI cover from the vertex to mid-thigh was performed with 3 min of PET acquisition in each bed position, with coverage of 24 cm. Pre-contrast MRI sequences were acquired simultaneously using a combination of a dedicated mMR head-and-neck coil and phased-array mMR body surface coils. Siemens StarVIBE eliminates motion artifacts. The second part was a dedicated MRI scan of the pelvis, followed by PET data reconstruction. MRI sequence parameters are summarized in Table 6. Reconstruction was conducted with an ordered subset expectation maximization algorithm (OSEM), with 3 iterations/21 subsets, based on an x-matrix acquisition with a 4 mm Gaussian filter and relative scatter scaling. Contrast-enhanced agent gadobutrol (Gadovist[®], Bayer Pharma AG, Berlin, Germany) is intravenously administered at a clinical dose of 0.1 mmol/kg bodyweight. Following the acquisition of precontrast data, a total of 60 contrast-enhanced data were obtained, with the start of the first postcontrast acquisition corresponding with the start of the contrast injection.

4.3. Image Analysis

Post-processing of all imaging data was performed with a dedicated post-processing software, Syngo.via (Siemens Healthcare, Erlangen, Germany). Regions of interest (ROIs) were defined as regions with an abnormal signal on MRI images and manually drawn. The MRI datasets were interpreted using PI-RADS version 2.1 [48]. Lesions with PI-RADS 1 to 3 were considered benign, while those with PI-RADS 4 and 5 were considered malignant. SUVmax is measured based on ROI, which is defined as corresponding to the finding on T2-weighted imaging (T2WI). All images were read by the same double-trained doctor. All perfusion parameters extracted from time-intensity curves were generated using Syngo.via MR Tissue 4D (Siemens Healthcare; Erlangen, Germany). Perfusion parameters, including

arrival time (AT), time to peak (TTP), wash-in slope (W-in), wash-out slope (W-out), peak enhancement intensity (PEI), and initial area under the 60-sec curve (iAUC), were calculated. For the time-intensity curve, X-axis refers to time, and Y-axis refers to the ratio between baseline and post-contrast intensity. Previous publications suggested values between SUVmax 2.0 to 3.0 as appropriate cutoff values to minimize false-positive interpretation of faintly PSMA positive uptake [49,50]. A cutoff of SUVmax 3.0 was selected in this study. The definition of the above parameters is presented in Table 7.

Table 6. Imaging parameters used for MRI.

Sequence	TR/TE (msec)	FOV (mm)	Flip Angle (Degrees)	Section Thickness (mm)	Voxel Size (mm)
T2WI	1400.0/95.0	400	160	5.0	1.3 × 1.3 × 5.0
HASTE Axial	1600.0/96.0	350	160	4.0	1.1 × 1.1 × 4.0
T1WI FS VIBE	5500.0/103.0	180	150	3.0	0.5 × 0.5 × 3.0
T2WI Axial	1600.0/96.0	350	160	4.0	1.1 × 1.1 × 4.0
T2WI Sagittal	4500.0/102.0	200	173	3.0	0.4 × 0.4 × 3.0
T2WI Coronal	11,600.0/70.0	280		3.0	2.5 × 2.5 × 3.0
DWI	7.41/3.30	260	12	3.5	1.4 × 1.4 × 3.5
T1WI FS	3.71/1.77	360	9	1.2	1.1 × 1.1 × 1.2
TWIST dynamic					
T1WI STARVIBE					

Table 7. Definition of DCE-MRI Parameters.

Parameter	Definition
AT	arrival time: point in time when contrast enhancement starts
TTP	time to peak: time from arrival time to end of wash-in
W-in	wash-in: slope of the fitted line between AT and end of wash-in
W-out	wash-out: slope of the fitted line between start of wash-out and end of measurement
PEI	peak enhancement intensity: value of concentration when the contrast enhancement reaches the highest concentration
iAUC	initial area under curve in 60 s

4.4. Statistical Analysis

The DCE-MRI parameters between benign and malignant lesion groups were compared by Mann–Whitney U test. Comparison of parameters between benign lesions with SUVmax ≤ 3.0 and SUVmax > 3.0 was accessed by Mann–Whitney U test, as were malignant lesions. Pearson correlation was used to determine the correlations among various DCE-MRI parameters. All statistical analyses were performed with statistical software SPSS 25 for Windows (IBM Corp, Armonk, NY, USA). The significance level was set to two-tailed $p < 0.05$. Patient demographics and clinical characteristics are summarized using descriptive statistics. Normal distributed data are reported as mean ± standard deviation (SD), and non-normal distributed data are reported as median (interquartile range) (IQR Q1, Q3).

5. Conclusions

In conclusion, various DCE-MRI parameters can be used to quantify perfusion in intraprostatic lesions. DCE-MRI parameters reflect the perfusion characteristics of intraprostatic lesions with malignant lesions demonstrating significantly shorter TTP. There is a moderate to strong correlation between DCE-MRI parameters. Semi-quantitative analysis reflects how malignant lesions show significantly higher SUVmax than benign lesions.

Author Contributions: Conceptualization, J.Z. and M.R.M.; methodology, J.Z.; software, J.Z.; validation, A.K., D.B.M. and J.B.; formal analysis, D.B.M.; writing—original draft preparation, J.Z.; writing—review and editing, A.K.; visualization, J.B.; supervision, M.R.M.; project administra-

tion, B.H.; funding acquisition, W.B. All authors have read and agreed to the published version of the manuscript.

Funding: The PET/MRI scanner is funded in part by the German Research Foundation (INST 335/454-1). We acknowledge support from the German Research Foundation (DFG) and the Open Access Publication Fund of Charité—Universitätsmedizin Berlin.

Institutional Review Board Statement: All procedures performed in studies involving human participants were in accordance with the ethical standards of the institutional and national research committee and with the 1964 Helsinki declaration and its later amendments or comparable ethical standards. This retrospective study was approved by the institutional ethics review board (EA1/060/16), and the institutional review board waived the requirement for informed consent for this retrospective analysis.

Informed Consent Statement: Patient consent was waived due to retrospective analysis.

Data Availability Statement: The datasets analyzed and generated during this study are included in this published study.

Acknowledgments: J.Z. thanks German Research Foundation (GRK2260, BIOQIC) for the support.

Conflicts of Interest: The authors declare that they have no conflict of interest.

Abbreviations

AT	Arrival time;
BPH	Benign prostatic hyperplasia;
CT	Computed tomography;
DCE-MRI	Dynamic contrast-enhanced magnetic resonance imaging;
DWI	Diffusion-weighted imaging;
FOV	Field of view;
Ga	Gallium;
GS	Gleason score;
iAUC	initial area under curve;
MRI	Magnetic resonance imaging;
mpMRI	Multiparametric magnetic resonance imaging;
PCa	Prostate cancer;
PEI	Peak enhancement intensity;
PET/CT	Positron emission tomography / computed tomography;
PET/MR	Positron emission tomography / magnetic resonance;
PI-RADS	Prostate Imaging Reporting and Data System;
PSA	Prostate-specific antigen;
PSMA	Prostate-specific membrane antigen;
ROI	Region of interest;
SUV	Standardized uptake value;
TE	Echo time;
TR	Repetition time;
TTP	Time to peak;
T2WI	T2-weighted imaging;
W-in	Wash-in slope;
W-out	Wash-out slope.

References

1. Miller, K.D.; Siegel, R.L.; Khan, R.; Jemal, A. Cancer Statistics. *Cancer Rehabil.* **2018**, *70*, 7–30. [CrossRef]
2. Delongchamps, N.B.; Rouanne, M.; Flam, T.; Beuvon, F.; Liberatore, M.; Zerbib, M.; Cornud, F. Multiparametric magnetic resonance imaging for the detection and localization of prostate cancer: Combination of T2-weighted, dynamic contrast-enhanced and diffusion-weighted imaging. *BJU Int.* **2010**, *107*, 1411–1418. [CrossRef]
3. O'Connor, J.P.B.; Jackson, A.; Parker, G.J.M.; Roberts, C.; Jayson, G.C. Dynamic contrast-enhanced MRI in clinical trials of antivasular therapies. *Nat. Rev. Clin. Oncol.* **2012**, *9*, 167–177. [CrossRef] [PubMed]
4. Lissbrant, I.F.; Stattin, P.; Damber, J.-E.; Bergh, A. Vascular density is a predictor of cancer-specific survival in prostatic carcinoma. *Prostate* **1997**, *33*, 38–45. [CrossRef]

5. de la Taille, A.; Katz, A.E.; Bagiella, E.; Buttyan, R.; Sharir, S.; Olsson, C.A.; Burchardt, T.; Ennis, R.D.; Rubin, M.A. Microvessel density as a predictor of PSA recurrence after radical prostatectomy. A comparison of CD34 and CD31. *Am. J. Clin. Pathol.* **2000**, *113*, 555–562. [CrossRef]
6. Tan, C.H.; Hobbs, B.P.; Wei, W.; Kundra, V. Dynamic contrast-enhanced MRI for the detection of prostate cancer: Meta-analysis. *Am. J. Roentgenol.* **2015**, *204*, W439–W448. [CrossRef] [PubMed]
7. Miller, J.C.; Pien, H.H.; Sahani, D.; Sorensen, A.G.; Thrall, J.H. Imaging Angiogenesis: Applications and Potential for Drug Development. *J. Natl. Cancer Inst.* **2005**, *97*, 172–187. [CrossRef]
8. Khalifa, F.; Soliman, A.; El-Baz, A.; El-Ghar, M.A.; El-Diasty, T.; Gimel'Farb, G.; Ouseph, R.; Dwyer, A.C. Models and methods for analyzing DCE-MRI: A review. *Med. Phys.* **2014**, *41*, 124301. [CrossRef]
9. Winkel, D.J.; Heye, T.J.; Benz, M.R.; Glessgen, C.G.; Wetterauer, C.; Bubendorf, L.; Block, T.K.; Boll, D.T. Compressed Sensing Radial Sampling MRI of Prostate Perfusion: Utility for Detection of Prostate Cancer. *Radiology* **2019**, *290*, 702–708. [CrossRef] [PubMed]
10. Sung, Y.S.; Kwon, H.-J.; Park, B.-W.; Cho, G.; Lee, C.K.; Cho, K.-S.; Kim, J.K. Prostate Cancer Detection on Dynamic Contrast-Enhanced MRI: Computer-Aided Diagnosis Versus Single Perfusion Parameter Maps. *Am. J. Roentgenol.* **2011**, *197*, 1122–1129. [CrossRef] [PubMed]
11. Kader, A.; Brangsch, J.; Kaufmann, J.O.; Zhao, J.; Mangarova, D.B.; Moeckel, J.; Adams, L.C.; Sack, I.; Taupitz, M.; Hamm, B.; et al. Molecular MR Imaging of Prostate Cancer. *Biomedicines* **2020**, *9*, 1. [CrossRef] [PubMed]
12. Rahbar, K.; Weckesser, M.; Huss, S.; Semjonow, A.; Breyholz, H.-J.; Schrader, A.J.; Schäfers, M.; Bögemann, M. Correlation of Intraprostatic Tumor Extent with ⁶⁸Ga-PSMA Distribution in Patients with Prostate Cancer. *J. Nucl. Med.* **2016**, *57*, 563–567. [CrossRef]
13. Fendler, W.P.; Eiber, M.; Beheshti, M.; Bomanji, J.; Ceci, F.; Cho, S.; Giesel, F.; Haberkorn, U.; Hope, T.A.; Kopka, K.; et al. ⁶⁸Ga-PSMA PET/CT: Joint EANM and SNMMI procedure guideline for prostate cancer imaging: Version 1.0. *Eur. J. Nucl. Med. Mol. Imaging* **2017**, *44*, 1014–1024. [CrossRef] [PubMed]
14. Souvatzoglou, M.; Eiber, M.; Martinez-Moeller, A.; Fürst, S.; Holzapfel, K.; Maurer, T.; Ziegler, S.; Nekolla, S.; Schwaiger, M.; Beer, A.J. PET/MR in prostate cancer: Technical aspects and potential diagnostic value. *Eur. J. Nucl. Med. Mol. Imaging* **2013**, *40*, 79–88. [CrossRef]
15. Zhao, J.; Hamm, B.; Brenner, W.; Makowski, M.R. Lesion-to-background ratio threshold value of SUVmax of simultaneous [⁶⁸Ga]Ga-PSMA-11 PET/MRI imaging in patients with prostate cancer. *Insights Imaging* **2020**, *11*, 1–11. [CrossRef]
16. Souvatzoglou, M.; Eiber, M.; Takei, T.; Fürst, S.; Maurer, T.; Gaertner, F.; Geinitz, H.; Drzezga, A.; Ziegler, S.; Nekolla, S.G.; et al. Comparison of integrated whole-body [¹¹C]choline PET/MR with PET/CT in patients with prostate cancer. *Eur. J. Nucl. Med. Mol. Imaging* **2013**, *40*, 1486–1499. [CrossRef]
17. Guberina, N.; Hetkamp, P.; Ruebben, H.; Fendler, W.; Grueneisen, J.; Suntharalingam, S.; Kirchner, J.; Puellen, L.; Harke, N.; Radtke, J.P.; et al. Whole-Body Integrated [⁶⁸Ga]PSMA-11-PET/MR Imaging in Patients with Recurrent Prostate Cancer: Comparison with Whole-Body PET/CT as the Standard of Reference. *Mol. Imaging Biol.* **2019**, *22*, 788–796. [CrossRef] [PubMed]
18. Mansbridge, M.; Chung, E.; Rhee, H. The Use of MRI and PET Imaging Studies for Prostate Cancer Management: Brief Update, Clinical Recommendations, and Technological Limitations. *Med. Sci.* **2019**, *7*, 85. [CrossRef]
19. Kranzbühler, B.; Müller, J.; Becker, A.S.; Schüler, H.I.G.; Muehlemaier, U.J.; Fankhauser, C.D.; Kedzia, S.; Guckenberger, M.; Kaufmann, P.A.; Eberli, D.; et al. Detection Rate and Localization of Prostate Cancer Recurrence Using ⁶⁸Ga-PSMA-11 PET/MRI in Patients with Low PSA Values ≤ 0.5 ng/mL. *J. Nucl. Med.* **2019**, *61*, 194–201. [CrossRef] [PubMed]
20. Afshar-Oromieh, A.; Haberkorn, U.; Schlemmer, H.P.; Fenchel, M.; Eder, M.; Eisenhut, M.; Hadaschik, B.A.; Kopp-Schneider, A.; Röthke, M. Comparison of PET/CT and PET/MRI hybrid systems using a ⁶⁸Ga-labelled PSMA ligand for the diagnosis of recurrent prostate cancer: Initial experience. *Eur. J. Nucl. Med. Mol. Imaging* **2014**, *41*, 887–897. [CrossRef]
21. Zhao, J.; Mangarova, D.B.; Brangsch, J.; Kader, A.; Hamm, B.; Brenner, W.; Makowski, M.R. Correlation between Intraprostatic PSMA Uptake and MRI PI-RADS of [⁶⁸Ga]Ga-PSMA-11 PET/MRI in Patients with Prostate Cancer: Comparison of PI-RADS Version 2.0 and PI-RADS Version 2.1. *Cancers* **2020**, *12*, 3523. [CrossRef] [PubMed]
22. Lecouvet, F.E.; El Mouedden, J.; Collette, L.; Coche, E.; Danse, E.; Jamar, F.; Machiels, J.P.; Berg, B.V.; Omoumi, P.; Tombal, B. Can whole-body magnetic resonance imaging with diffusion-weighted imaging replace Tc 99m bone scanning and computed tomography for single-step detection of metastases in patients with high-risk prostate cancer? *Eur. Urol.* **2012**, *62*, 68–75. [CrossRef]
23. Hara, N.; Okuizumi, M.; Koike, H.; Kawaguchi, M.; Bilim, V. Dynamic contrast-enhanced magnetic resonance imaging (DCE-MRI) is a useful modality for the precise detection and staging of early prostate cancer. *Prostate* **2004**, *62*, 140–147. [CrossRef] [PubMed]
24. Hamm, B.; Asbach, P. Magnetic Resonance Imaging of the Prostate in the PI-RADS Era. *Dis. Abdomen Pelvis* **2018**, *2018–2021*, 99–115.
25. Maurer, T.; Eiber, M.; Schwaiger, M.E.M.; Gschwend, T.M.J.E. Current use of PSMA-PET in prostate cancer management. *Nat. Rev. Urol.* **2016**, *13*, 226–235. [CrossRef]
26. Berman, R.M.; Brown, A.M.; Chang, S.D.; Sankineni, S.; Kadakia, M.; Wood, B.J.; Pinto, P.A.; Choyke, P.L.; Turkbey, B. DCE MRI of prostate cancer. *Abdom. Radiol.* **2016**, *41*, 844–853. [CrossRef]
27. Vos, E.K.; Litjens, G.J.; Kobus, T.; Hambrock, T.; de Kaa, C.A.H.-V.; Barentsz, J.O.; Huisman, H.J.; Scheenen, T.W. Assessment of Prostate Cancer Aggressiveness Using Dynamic Contrast-enhanced Magnetic Resonance Imaging at 3 T. *Eur. Urol.* **2013**, *64*, 448–455. [CrossRef] [PubMed]

28. Chen, Y.-J.; Chu, W.-C.; Pu, Y.-S.; Chueh, S.-C.; Shun, C.-T.; Tseng, W.-Y.I. Washout gradient in dynamic contrast-enhanced MRI is associated with tumor aggressiveness of prostate cancer. *J. Magn. Reson. Imaging* **2012**, *36*, 912–919. [CrossRef]
29. van Niekerk, C.G.; van der Laak, J.A.; Hambroek, T.; Huisman, H.J.; Witjes, J.A.; Barentsz, J.O.; de Kaa, C.A.H. Correlation between dynamic contrast-enhanced MRI and quantitative histopathologic microvascular parameters in organ-confined prostate cancer. *Eur. Radiol.* **2014**, *24*, 2597–2605. [CrossRef]
30. Ren, J.; Huan, Y.; Wang, H.; Chang, Y.-J.; Zhao, H.-T.; Ge, Y.-L.; Liu, Y.; Yang, Y. Dynamic contrast-enhanced MRI of benign prostatic hyperplasia and prostatic carcinoma: Correlation with angiogenesis. *Clin. Radiol.* **2008**, *63*, 153–159. [CrossRef] [PubMed]
31. Yi, B.; Kang, D.K.; Yoon, D.; Jung, Y.S.; Kim, K.S.; Yim, H.; Kim, T.H. Is there any correlation between model-based perfusion parameters and model-free parameters of time-signal intensity curve on dynamic contrast enhanced MRI in breast cancer patients? *Eur. Radiol.* **2014**, *24*, 1089–1096. [CrossRef] [PubMed]
32. Jayson, G.C.; Kerbel, R.; Ellis, L.M.; Harris, A.L. Antiangiogenic therapy in oncology: Current status and future directions. *Lancet* **2016**, *388*, 518–529. [CrossRef]
33. Folkman, J. The role of angiogenesis in tumor growth. *Semin. Cancer Biol.* **1992**, *3*, 45–71.
34. Borre, M.; Offerens, B.V.; Nerström, B.; Overgaard, J. Microvessel density predicts survival in prostate cancer patients subjected to watchful waiting. *Br. J. Cancer* **1998**, *78*, 940–944. [CrossRef]
35. Conway, R.E.; Petrovic, N.; Li, Z.; Heston, W.; Wu, D.; Shapiro, L.H. Prostate-Specific Membrane Antigen Regulates Angiogenesis by Modulating Integrin Signal Transduction. *Mol. Cell. Biol.* **2006**, *26*, 5310–5324. [CrossRef]
36. Chang, S.S.; Reuter, V.E.; Heston, W.D.; Bander, N.H.; Grauer, L.S.; Gaudin, P.B. Five different anti-prostate-specific membrane antigen (PSMA) antibodies confirm PSMA expression in tumor-associated neovasculature. *Cancer Res.* **1999**, *59*, 3192–3198. [PubMed]
37. Singanamalli, A.; Rusu, M.; Sparks, R.E.; Shih, N.N.; Ziober, A.; Wang, L.-P.; Tomaszewski, J.; Rosen, M.; Feldman, M.; Madabhushi, A. Identifying in vivo DCE MRI markers associated with microvessel architecture and gleason grades of prostate cancer. *J. Magn. Reson. Imaging* **2015**, *43*, 149–158. [CrossRef] [PubMed]
38. van den Ouden, D.; Kranse, R.; Hop, W.C.; van der Kwast, T.H.; Schroder, F.H. Microvascular invasion in prostate cancer: Prognostic significance in patients treated by radical prostatectomy for clinically localized carcinoma. *Urol. Int.* **1998**, *60*, 17–24. [CrossRef]
39. Antunes, A.A.; Srougi, M.; Dall'Oglio, M.F.; Crippa, A.; Paranhos, M.; Cury, J.; Nesrallah, L.J.; Leite, K.R. Microvascular invasion is an independent prognostic factor in patients with prostate cancer treated with radical prostatectomy. *Int. Braz. J. Urol.* **2006**, *32*, 668–677. [CrossRef]
40. Salomao, D.R.; Graham, S.D.; Bostwick, D.G. Microvascular invasion in prostate cancer correlates with pathologic stage. *Arch. Pathol. Lab. Med.* **1995**, *119*, 1050–1054.
41. Shabsigh, A.; Chang, D.T.; Heitjan, D.F.; Kiss, A.; Olsson, C.A.; Puchner, P.J.; Buttyan, R. Rapid reduction in blood flow to the rat ventral prostate gland after castration: Preliminary evidence that androgens influence prostate size by regulating blood flow to the prostate gland and prostatic endothelial cell survival. *Prostate* **1998**, *36*, 201–206. [CrossRef]
42. Shabsigh, A.; Lee, B.; Buttyan, R. Unique morphological aspects of the rat ventral prostate gland revealed by vascular corrosion casting. *Prostate* **1999**, *39*, 240–245. [CrossRef]
43. Røe, K.; Mikalsen, L.T.; Van Der Kogel, A.J.; Bussink, J.; Lyng, H.; Ree, A.H.; Marignol, L.; Olsen, D.R. Vascular responses to radiotherapy and androgen-deprivation therapy in experimental prostate cancer. *Radiat. Oncol.* **2012**, *7*, 75. [CrossRef] [PubMed]
44. Kershaw, L.E.; Logue, J.P.; Hutchinson, C.E.; Clarke, N.W.; Buckley, D.L. Late tissue effects following radiotherapy and neoadjuvant hormone therapy of the prostate measured with quantitative magnetic resonance imaging. *Radiother. Oncol.* **2008**, *88*, 127–134. [CrossRef]
45. Hodge, K.K.; McNeal, J.E.; Terris, M.K.; Stamey, T.A. Random Systematic Versus Directed Ultrasound Guided Transrectal Core Biopsies of the Prostate. *J. Urol.* **1989**, *142*, 71–74. [CrossRef]
46. Elabbady, A.A.; Khedr, M.M. Extended 12-Core Prostate Biopsy Increases Both the Detection of Prostate Cancer and the Accuracy of Gleason Score. *Eur. Urol.* **2006**, *49*, 49–53. [CrossRef]
47. Uno, H.; Nakano, M.; Ehara, H.; Deguchi, T. Indications for Extended 14-Core Transrectal Ultrasound-Guided Prostate Biopsy. *Urology* **2008**, *71*, 23–27. [CrossRef]
48. Turkbey, B.; Rosenkrantz, A.B.; Haider, M.A.; Padhani, A.R.; Villeirs, G.; Macura, K.J.; Tempany, C.M.; Choyke, P.L.; Cornud, F.; Margolis, D.J.; et al. Prostate Imaging Reporting and Data System Version 2.1: 2019 Update of Prostate Imaging Reporting and Data System Version 2. *Eur. Urol.* **2019**, *76*, 340–351. [CrossRef] [PubMed]
49. Giesel, F.L.; Fiedler, H.; Stefanova, M.; Sterzing, F.; Rius, M.; Kopka, K.; Moltz, J.H.; Afshar-Oromieh, A.; Choyke, P.L.; Haberkorn, U.; et al. PSMA PET/CT with Glu-urea-Lys-(Ahx)-[68Ga(HBED-CC)] versus 3D CT volumetric lymph node assessment in recurrent prostate cancer. *Eur. J. Nucl. Med. Mol. Imaging* **2015**, *42*, 1794–1800. [CrossRef]
50. Woythal, N.; Arsenic, R.; Kempkensteffen, C.; Miller, K.; Janssen, J.-C.; Huang, K.; Makowski, M.R.; Brenner, W.; Prasad, V. Immunohistochemical Validation of PSMA Expression Measured by 68Ga-PSMA PET/CT in Primary Prostate Cancer. *J. Nucl. Med.* **2018**, *59*, 238–243. [CrossRef] [PubMed]

Curriculum Vitae

My curriculum vitae does not appear in the electronic version of my paper for reasons of data protection.

Publication list

First Author

1: Zhao J, Hamm B, Brenner W, Makowski MR: Lesion-to-background ratio threshold value of SUVmax of simultaneous [⁶⁸Ga]Ga-PSMA-11 PET/MRI imaging in patients with prostate cancer. *Insights into Imaging* 2020;11:137.

IF: 3.579 JCR: Q1 Category: Radiology, Nuclear Medicine, and Medical Imaging

2: Zhao J, Mangarova DB, Brangsch J, Kader A, Hamm B, Brenner W, Makowski MR: Correlation between Intraprostatic PSMA Uptake and MRI PI-RADS of [⁶⁸Ga]Ga-PSMA-11 PET/MRI in Patients with Prostate Cancer: Comparison of PI-RADS Version 2.0 and PI-RADS Version 2.1. *CANCERS* 2020;12:3523.

IF: 6.126 JCR: Q1 Category: Oncology

3: Zhao J, Kader A, Mangarova DB, Brangsch J, Brenner W, Hamm B, Makowski MR: Dynamic Contrast-Enhanced MRI of Prostate Lesions of Simultaneous [⁶⁸Ga]Ga-PSMA-11 PET/MRI: Comparison between Intraprostatic Lesions and Correlation between Perfusion Parameters. *CANCERS* 2021;13:1404.

IF: 6.126 JCR: Q1 Category: Oncology

Coauthor

4: Kader A, Brangsch J, Kaufmann JO, **Zhao J**, Mangarova DB, Moeckel J, Adams LC, Sack I, Taupitz M, Hamm B, Makowski MR: Molecular MR imaging of prostate cancer. *Biomedicines* 2021;9:1.

IF: 4.717 JCR: Q1 Category: Pharmacology & Pharmacy

5: Molwitz I, Yamamura J, Ozga A, Wedekind I, Nguyen T, Wolf L, Kamo M, **Zhao J**, Can E, Keller S: Gender trends in authorships and publication impact in Academic Radiology—a 10-year perspective. *EUR RADIOL* 2021

IF: 4.101 JCR: Q1 Category: Radiology, Nuclear Medicine, and Medical Imaging

6: Kader A, Brangsch J, Reimann C, Kaufmann JO, Mangarova DB, Moeckel J, Adams

LC, **Zhao J**, Saatz J, Traub H, Buchholz R, Karst U, Hamm B, Makowski MR: Visualization and quantification of the extracellular matrix in prostate cancer using an elastin specific molecular probe. *Biology* 2021;10:1217.

IF: 5.079 JCR: Q1 Category: Biology

7: Kader A, Kaufmann JO, Mangarova DB, Moeckel J, Brangsch J, Adams LC, **Zhao J**, Reimann C, Saatz J, Traub H, Buchholz R, Karst U, Hamm B, Makowski MR: Iron oxide nanoparticles for visualization of prostate cancer in MRI. *CANCERS* 2022;14

IF: 6.639 JCR: Q1 Category: Oncology

8: Kader A, Kaufmann JO, Mangarova DB, Moeckel J, Adams LC, Brangsch J, Heyl JL, **Zhao J**, Verlemann C, Karst U, Collettini F, Auer TA, Hamm B, Makowski MR: Collagen-Specific molecular magnetic resonance imaging of prostate cancer. *International Journal of Molecular Sciences* 2023;24:711.

IF: 6.208 JCR: Q1 Category: Biochemistry & Molecular Biology

9: Yamamura J, Molwitz I, Ozga A, Nguyen T, Wedekind I, Wolf-Baldauf L, Kamo M, **Zhao J**, Can E, Keller S: Gender differences and cooperation in medical authorships - an analysis of the recent ten years in five key medical disciplines. *BMC MED EDUC* 2023;23:68.

IF: 3.263 JCR: Q1 Category: Education & Educational research

Acknowledgement

First of all, I wish to express my deepest gratitude and appreciation to my supervisor, Univ. Prof. Dr. med Marcus R. Makowski. Thank you immensely for providing me with the opportunity to be a part of your esteemed research group. This experience has not only enabled me to come to this beautiful country but also allowed me to immerse myself in a completely different culture. Your continuous support and encouragement have been the driving force behind my work.

I extend my heartfelt gratitude to Univ. Prof. Dr. Bernd Hamm, Prof. Dr. med. Winfried Brenner, and Prof. Dr. med. Tobias Penzkofer for their invaluable assistance in my research. I am also deeply thankful for the support from the German Research Foundation (DFG), GRK2260, and the research training group BIOQIC, along with our coordinator, Dr. Judith Bergs, who provided substantial aid during my training program.

A special note of appreciation goes to my colleagues from AG Makowski - Avan Kader, Jan Ole Kaufmann, Jana Möckel, Julia Brangsch, Carolin Reimann, Dilyana B. Mangarova and Matteo Ippoliti. Your camaraderie made my time in Berlin truly enjoyable, offering me a deeper understanding of the culture of this country and instilling in me a positive attitude towards research.

Furthermore, I would like to express my thanks to Ms. Bettina Herwig for her invaluable help in enhancing my manuscript for publication, as well as to the German Research Foundation and the Open Access Publication Fund of Charité—Universitätsmedizin Berlin for funding my publications. I am genuinely appreciative of Dr. Martina Kaufmann for her guidance and support with my dissertation.

I extend my deepest gratitude to my parents for their unwavering love, encouragement, and support throughout my doctoral journey. Lastly, I acknowledge and commend my own efforts and perseverance. Overcoming the challenges of acclimating to a new country and the demands of research. I devoted all my energy and time to research, resulting in significant achievements. My determination and perseverance were my guiding lights, leading me through the challenges and triumphs of the doctoral pursuit. This journey has provided me with a profound understanding of the essence of life and the importance of medical science and research. Doctoral research, beyond being a training ground for academic skills, has been a transformative experience that will resonate throughout my life.